"Solar Cells Based on Electrodeposited CdS and CdTe Films"

By

Stéphen Mark Mc Gregor

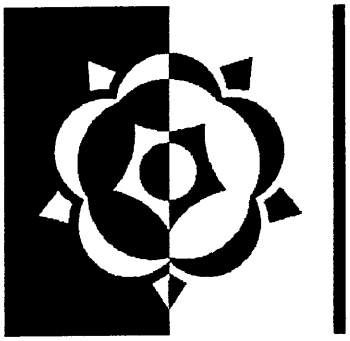

Thesis Submitted in Partial Fulfilment of the Requirements of Sheffield Hallam University for the Degree of Doctor of Philosophy

September 1999

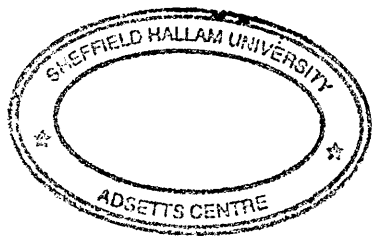
SHEFFIELD HALLAM UNIVERSITY
ADSETTS CENTRE

Abstract

The aim of this study was to understand the properties of glass/TCO/CdS/CdTe/metal solar cells, the CdS and CdTe being grown by aqueous electrodeposition. Deposited films and completed cells were characterised using electrical, structural and optical techniques. This report describes the production of well-formed polycrystalline CdS and CdTe with well defined XRD peaks and band gap. Experiments were performed to investigate the pre-conditioning of the CdTe bath on the overall cell performance. Pre-conditioning the CdTe deposition bath was found to improve the V_{OC} value of the completed devices.

It has been known for some time that treating the CdTe layer of a CdS/CdTe solar cell with chlorine brings about significant improvements in the efficiency of these devices. This report presents results on a systematic variation of the chlorine concentration within a CdTe deposition bath. Solar simulated I-V measurements of completed devices clearly show that the addition of $CdCl_2$ to the CdTe deposition bath significantly improved the efficiency values for the glass/TCO/CdS/CdTe/metal devices. The electrical parameter most significantly affected by the addition of chlorine is the J_{SC} value. In terms of the V_{OC} performance of the device, this investigation showed that there was a trend of improving V_{OC} with increasing chlorine concentration. Addition of chlorine also produces improvements in the preferred orientation of CdTe films as measured by XRD. Optical absorption results showed a correlation that the minima of the band gap vs. chlorine concentration graph for annealed samples matches up with the maximum in the efficiency and J_{SC} graphs.

To investigate whether this phenomenon was specific to chlorine or was displayed by other elements, similar experiments were performed with no chlorine inclusion but varying the indium concentration in the deposition bath. Solar simulated I-V measurements of completed devices clearly show that the addition of $In_2(SO_4)_3$ to the CdTe deposition bath significantly reduced the efficiency values for the glass/TCO/CdS/CdTe/metal devices. The electrical parameter most significantly affected by the addition of indium is the J_{SC} value. The addition of indium also had a detrimental effect on the preferred orientation measured by XRD.

TABLE OF CONTENTS

List of Symbols and Abbreviations

A	Diode Quality Factor
ALE	Atomic Layer Epitaxy
AM	Air Mass
AR	Antireflecting
CIGS	Copper Indium Gallium Diselenide ($CuIn_{1-x}Ga_xSe_2$)
CIS	Copper Indium Diselenide ($CuInSe_2$)
CSS	Close Spaced Sublimation
CSVT	Close Spaced Vapour Transport
DCM	Dichloromethane
DLTS	Deep Level Transient Spectroscopy
E_A	Activation Energy (eV)
EBIC	Electron Beam Induced Current
E_g	Semiconductor Band Gap (eV)
E_M^0	Standard Reduction Potential (V)
E_{OVER}	Over Potential (V)
F	Frequency of Incident Radiation (Hz)
FF	Solar Cell Fill Factor
FWHM	Full Width at Half Maximum
G(x)	Rate of Free Carrier Generation
ΔG	Gibbs Free Energy ($Jmole^{-1}$)
I_0	Reverse Saturation Current (A)
I_L	Light Generated Current (A)
I_{SC}	Short Circuit Current (A)
J_{SC}	Short Circuit Current Density ($mAcm^{-2}$)
K	Boltzman Constant
MBE	Molecular Beam Epitaxy
MOCVD	Metal-Organic Chemical Vapour Deposition

NREL	National Renewable Energy Laboratory
P_{hkl}	Harris Probability for the (hkl) Plane
PL	Photoluminescence
P_m	Solar Cell Maximum Power Output
PPE	Periodic Pulse Electrodeposition
PVD	Physical Vapour Deposition
QRP	Quasi Rest Potential
R_S	Series Resistance (Ω)
S	Surface Recombination velocity (cms^{-1})
SCE	Saturated Calomel Electrode
SHE	Standard Hydrogen Electrode
SIMS	Secondary Ion Mass Spectroscopy
TCJF	Type Conversion-Junction Formation
TCO	Transparent Conducting Oxide
TCS	Transparent Conducting Semiconductor
V_{OC}	Open Circuit Voltage (V)
w	Depletion Width (μm)
XPS	X-ray Photoelectron Spectroscopy
Γ	Photon Flux ($mWcm^{-2}$)
α	Optical Absorption Coefficient (cm^{-1})
η	Solar Cell Efficiency (%)
τ	Minority Carrier Lifetime (s)

Chapter 1.0: Introduction

It is known that the solar radiation reaching the earth's surface in less than one hour is sufficient to satisfy the global demand for energy for a whole year. Harnessing this energy presents society with an opportunity on an unequalled scale. Photovoltaics is a technology which actively addresses the challenge by transforming the sun's energy directly into a more convenient and widely usable form i.e. electricity. Theoretically the conversion is simple; practically the major goal is to carry out the conversion process at a cost approaching that of extracting energy from fossil fuels. Comparing the costs of a renewable source of energy with fossil fuels is not straightforward. This is because of the difficulty of putting a figure on the benefit of renewables such as, for example, those stemming from reduction in carbon dioxide emissions.

The key features of photovoltaic technology can be summarised as: -

- Totally renewable resource

- Direct conversion

  This is important because it alleviates the need for an intermediate electrical generator. Compare this with wind or wave energy, which typically require a turbine to transfer kinetic energy into electricity.

- Environmentally very acceptable

  There are no waste products or pollution and systems are perfectly quiet. Locating systems is less of a problem than for some other forms of renewable energy, which are associated with their own particular environmental problems, for example, tidal barrages (effects on marine and bird life) and windmills (unsightly and noisy).

- Good reliability and long life.

  Based on solid state technology, systems have no moving parts, resulting in relatively low maintenance demands over long periods approximately 25-30 years.

- Mass produceable and modular

  The technology is suited to mass production and is flexible being readily adapted to provide "milliwatt to megawatt" quantities of electricity. The solar "module" is the basic building block of larger-scale systems. Working installations of a specified output can easily be built by putting a number of these modules together.

1.1 Context

Solar cells based on the CdS/CdTe heterostructure have been proposed as a suitable candidate for terrestrial energy production [Farenbruch et al 1974]. In order to produce low cost solar cell modules, thin film technology is utilised. One cost effective method of producing thin films is electrodeposition [Fulop et al 1985, Lokhande et al 1989, Rajeshwar 1992], and it is attractive because it can be adapted for large scale production. Electrodeposition is widely used in industry, which uses relatively cheap equipment. The electrodeposition technique minimises material usage, clean up from spent solutions is readily accomplished and it reduces the health hazards of the toxic components used. Furthermore, solutions can be used for long periods.

High efficiency (>10%) thin film CdTe based solar cells have been prepared using CdTe deposited by a variety of methods such as sintering [Park et al 1992, Kim 1994] Metalorganic Chemical Vapour Deposition (MOCVD) [Sudharsanan et al 1991], Molecular Beam Epitaxy (MBE) [Ringel et al 1991], screen printing [Yoshida 1992], Physical Vapour Deposition (PVD) [McCandles et al 1991] and Close-Spaced Sublimation (CSS) [Britt et al 1993]. The highest efficiency achieved by these groups is for the Close-Spaced Sublimation [Britt et al 1993] technique which quotes a total area conversion efficiency of 15.8% under AM 1.5 illumination, although it should be noted that this device did have an Antireflecting (AR) coating which gives improved efficiency over devices which do not have AR coatings. In the case of electrodeposited films Das and Morris [Das et al 1992, Das et al 1993] have reported CdS/CdTe solar cells with an efficiency of 11.5% and Dennison 1994 has reported cells with 11.6% efficiency.

CdTe is a II-VI semiconductor with direct band gap of 1.45eV at room temperature which is almost optimum for the effective absorption of the solar spectrum. A direct band gap transition gives a good absorption coefficient, which leads to a short absorption length when compared to grain sizes typically encountered. This property reduces recombination at grain boundaries, a major problem with other polycrystalline materials. As a result, a large fraction of the photogenerated carriers are created within the depletion layer allowing more efficient collection. CdTe can be obtained in either p-type or n-type depending on growth conditions, doping and heat treatment.

CdS is an II-VI semiconductor with n-type conduction and a band gap of 2.4eV at room temperature. The wide band gap CdS acts as a window admitting photons of energy less than 2.4eV and creating charge carriers with photons of energy greater than 2.4eV. The photons with energy between 2.4eV and 1.45eV will create carriers in the CdTe layer.

1.2 Aims and Objectives

The aims and objectives of this project are to investigate fundamental properties of the CdS/CdTe solar cell leading to a better understanding of this device to achieve the commercial goal of a low cost, high efficiency and stable solar cell. An ideal device would have efficiences exceeding the best solar cells based on CdS/CdTe structures or better than those outlined by the US Department of Energy. Their aim is to make flatplate modules of 15% solar conversion efficiency at a cost below US$180 m^{-2} and a lifetime of 20 years [US Department of Energy 1987, US Department of Energy 1989]. In order to achieve large area module (of the order of m^2) efficiencies of 15%, small area module (of the order of mm^2) efficiencies should be at least 18%.

1.3 Approach

The approach to achieve the aims of this project is to use electrodeposition, which was a low cost technique of producing semiconductors. The two semiconductors used, CdTe and CdS, are well suited as solar cell absorber material and solar cell window material respectively. Strict control of deposition conditions and better understanding of the semiconductor characteristics of elecrodeposited materials should lead to the improved efficiency of these devices. It has been shown that chlorine treatment of the CdTe can bring about significant improvements in device performance [Ringel et al 1991, Sudharsanan et al 1991, Birkmire et al 1992, Al-Allak et al 1996, Loginov et al 1996]. In the case of the electrodeposition technique chlorine treatment is readily achieved by the addition of $CdCl_2$ to the deposition solution. Chlorine is a well known and regularly used n-type dopant in CdTe. In order to investigate whether this could be a factor in the significant improvement of these devices, another n-type dopant, indium was added to the CdTe deposition bath to observe whether similar improvments in device performance were obtained. Films were characterised electrically, optically, and structurally.

Chapter 2.0: Theory of CdS/CdTe Solar Cells

2.1 History of Solar Cells

The first photovoltaic cell can be traced back to the work of Becquerel (1839) who was involved in a series of experiments investigating electricity; the subject of intense research interest in those times. His studies centred on the behaviour of solids in contact with electrolyte solutions. He observed that when metal plates immersed in a suitable electrolyte were exposed to the sun, a small voltage and current were produced; the photovoltaic effect. Adams and Day (1877) observed a similar effect in the solid material selenium, the first report directly attributed to the photovoltaic effect in a solid, shortly after Smith (1873) had demonstrated the phenomenon of photoconductivity in selenium. Subsequent work on photovoltaic effects in selenium and cuprous oxide led to the development of the selenium photovoltaic cell used for many years in photographic exposure meters. By 1914, solar conversion efficiencies of approximately 1% were achieved with the selenium cell. It was finally realised that an energy barrier was involved in this cell and in the copper/copper oxide cell.

Significant developments in photovoltaic technology began when Chapin et al (1954) reported a solar conversion efficiency of 6% for a silicon single crystal cell. With improved technology, silicon cell efficiency under terrestrial sunlight had reached 14% by 1958. Then in 1954 Reynolds et al, reported 6% solar conversion efficiency from a cuprous sulphide/cadmium sulphide heterojunction. This served as the beginning for intense research on thin film photovoltaic devices. By taking advantage of new cell technology researchers have rapidly raised the efficiency of the gallium arsenide (GaAs) based cell reported by Jenny et al (1956) with 4% efficiency to present efficiencies of approximately 25 % for crystalline GaAs [Eisgruber 1993].

The current state of technology is that crystalline Si solar cells achieve efficiencies of 24% [Eisgruber 1993], copper indium diselenide (CIS) solar cells achieve 15.4% [Eisgruber 1993] and copper indium gallium diseleninde (CIGS) solar cells achieve 16.9% [Eisgruber 1993].

2.2 Introductory Theory of Solar Cells

Photovoltaic (PV) solar cells convert solar radiation directly into direct current (d.c.) electricity, using sunlight, a universally available inexhaustible source of energy. Solar cells are not based on thermomechanical conversion and, hence, are free from noise and pollution, need minimum maintenance and are modular.

There are essentially three elements in converting solar energy to useful power. The first is absorption of the solar energy in a semiconductor to create electron-hole pairs and hence current. The second is the semiconductor junction, which effectively separates the electron-hole pairs and generates voltage. The third is the electrical contact to the front and rear faces which collect the current and allows connection to an external load.

2.2.1 Solar Cell Potential Energy Barriers

A solar cell consists of a potential energy barrier within a semiconductor material that is capable of separating the electrons and holes that are generated by the absorption of light within the semiconductor. The three most common types of barriers are:

(i) *Homojunctions*: p/n junctions within the same semiconductor material

(ii) *Heterojunctions*: p/n junctions between two different semiconductor materials. Normally with a window layer of a larger band-gap semiconductor added to reduce surface recombination loss.

(iii) *Schottky Barriers*: metal/semiconductor junctions

The rest of this discussion concentrates on the p/n heterojunction as this is the barrier type in the CdS/CdTe solar cell.

Five domains can distinguish the various electronic processes occurring in a solar cell:

(1) The contact (front contact) to the n-type semiconductor which allows sunlight to pass through and introduces a contact resistance.
(2) The bulk of the wide band gap n-type region, which converts high energy photons into electricity and contributes mainly a series resistance.
(3) The junction itself with the associated depletion region, where carriers are separated by the junction electric field.
(4) The bulk of the p-type region, where most of the electron-hole pairs are generated by absorption of the light and where the minority carriers (electrons) are transported by diffusion and are partially lost by recombination.
(5) The metal contact (back contact) to the p-type semiconductor which introduces a contact resistance.

2.2.2 The p/n Heterojunction Solar Cell

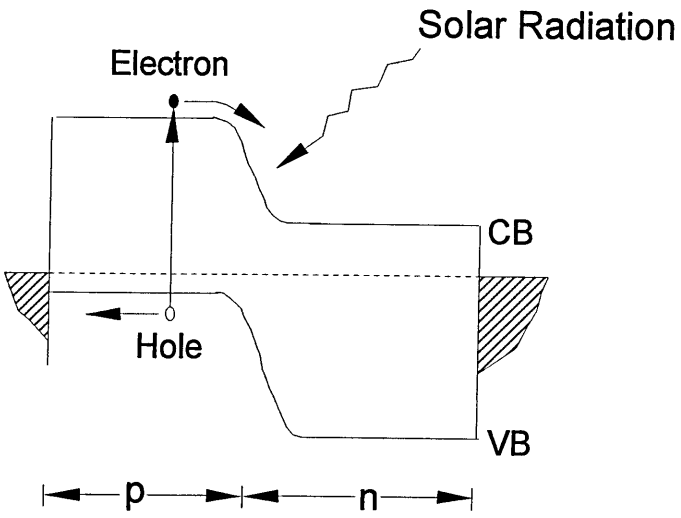

Figure 2.1. Idealised Band Structure for a p/n Heterojunction Solar Cell.

Figure 2.1 shows an idealised band structure for a p/n heterojunction solar cell with no energy spike i.e. the band bending is continuous with no discontinuities in the bands at the junction. The generation rate for electron-hole pairs in the bulk p-type region is determined by the illumination flux and the optical absorption constant, $\alpha(\lambda)$, of the semiconductor. The diffusion transport process is controlled by the mobility of the photogenerated minority electrons in the p-type region. The recombination loss can be described in terms of a lifetime, τ, for bulk recombination, as well as the surface recombination velocity, S, for recombination of carriers generated near the free surfaces of the device.

The idealised junction current in the dark for the junction region of Figure 2.1 is given by the diode equation

$$I = I_0(\exp[q\{V - IR_S\}/AkT] - 1) \qquad (2.1)$$

Where the reverse saturation current, I_0, and the diode quality factor, A, are determined by the specific current transport processes occurring at the junction. R_S is the total series resistance, T is the Temperature and K is the Boltzman Constant. Under illumination, Equation 2.1 becomes

$$I = I_0(\exp[q\{V - IR_S\}/AkT] - 1) - I_L \qquad (2.2)$$

Where I_L is the light-generated current determined by the processes mainly in the bulk p-type depletion region. For an ideal cell, I_0 and A are not functions of illumination and any parallel shunting resistance across the junction is effectively infinite. As the band gap, E_g, of the absorbing region is increased, the diode quality factor generally decreases strongly, which in turn increases the voltage obtainable from the cell. Increasing E_g also decreases the photogenerated current available since less and less of the solar spectrum is absorbed. The compromise between these two effects produces a maximum in the solar efficiency at band gap energies of 1.4 - 1.5 eV [Loferski 1956].

When a solar cell is exposed to the solar spectrum, a photon that has an energy less than the band gap, E_g, makes no contribution to the cell output i.e. does not generate any electron-hole pairs. A photon that has energy greater than E_g contributes to the cell output by creating one electron-hole pair. Excess energy ($hf-E_g$) is wasted as heat.

2.2.3 Solar Cell Current-Voltage Characteristics

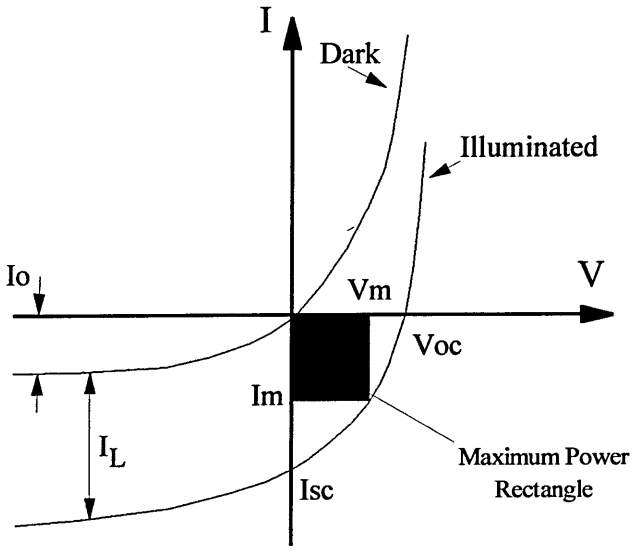

Figure 2.2. A schematic illustration of the I-V characteristic of a simple p-n junction solar cell both in the dark and under illumination. The open-circuit voltage, V_{oc}, short circuit current, I_{sc}, and maximum voltage and current, V_m and I_m, are defined in the figure.

The I-V characteristic [Grovenor 1989, Sze 1985] of the device under illumination (Figure 2.2) shows the curve passes through the fourth quadrant and, therefore, power can be extracted from the device. The behaviour of the cell can be described in terms of the four parameters I_{SC}, V_{OC}, FF and P_m where:

> V_{OC}, the open circuit voltage, is the output measured with a load whose impedance is much larger (ideally infinity) than the device impedance.
>
> I_{SC}, the short circuit current, is the current output when the load impedance is much smaller (ideally zero) than the device impedance. When a comparison between the performance of various cells is of concern, the short circuit current density J_{SC}, i.e. I_{SC} per unit area, is a more suitable parameter.

FF, the fill factor, is the ratio between the maximum power output, P_m, and the product $V_{OC}I_{SC}$. The Fill Factor is a measure of the "squareness" of the I-V characteristic.

The voltage and current that correspond to P_m are called V_m and I_m respectively thus:

$$P_m = V_m I_m \qquad (2.3)$$

Therefore:

$$FF = \frac{V_m I_m}{I_{sc} V_{oc}} = \frac{P_m}{I_{sc} V_{oc}} \qquad (2.4)$$

The conversion efficiency (η) of the solar cell, is equal to P_{out}/P_{in} simply follows from the previously defined quantities:

$$Efficiency = \frac{V_m I_m}{P_{in}} = \frac{FF V_{oc} I_{sc}}{P_{in}} \qquad (2.5)$$

Where P_{in} is the power impinging on the cell in the form of optical radiation. Two cases can be defined.

P_{in} is referred to the whole area of the device (i.e. including the surface of the semiconductor layers shaded by the front metallization or other inactive materials). In this case the practical efficiency, $\eta=\eta_p$.

P_{in} is referred to the active area (the surface of the heterojunction exposed to optical radiation). This is the intrinsic conversion efficiency, $\eta=\eta_i$.

The open circuit voltage, V_{OC}, is usually the parameter that depends most heavily on the crystalline perfection and purity of the materials used in the solar cells. This is important because the power generated by the cell depends directly on V_{OC}. From Equation 2.2, V_{OC} is given by:

$$V_{OC} \sim \frac{AkT}{q} \ln\left(\frac{J_L}{J_0} + 1\right) \qquad (2.6)$$

It is clear that V_{OC} can be increased by decreasing the dark current density, J_0, across the p-n junction or by increasing the diode factor A. The simplest way of reducing J_0 is to increase E_g but this has detrimental consequences for the fraction of the solar spectrum absorbed.

The open circuit voltage, V_{OC}, is directly related to the energy barrier height at the junction but the short circuit current is also determined by the spectrum of the light source and the spectral response of the cell. The latter in turn depends on the optical absorption coefficient, α, also the properties of the charge carrier (lifetime and diffusion length) and of the junction width of the depleted zone and electric field strength.

2.3 Solar Radiation

The sun is a complex radiator whose spectrum can be approximated by a 6050 K black body. This black body spectrum is modified by the variation in temperature across the sun, effect of the solar atmosphere and the Fraunhofer absorption lines. 98% of the total energy radiated by the sun lies between 0.25 and 3.0 μm. A quantity called the solar constant is defined as the rate at which energy is received on a unit space, perpendicular to the suns direction, in free space at the earth's mean distance from the sun, which has a value of approximately 1.353 kWm^{-2}. The value of solar radiation actually reaching the earth at any time of year depends on the distance between the earth and the sun.

Both the intensity and the spectral distribution of the radiation arriving at the earth's surface depend on the composition of the atmosphere as well as the path length of the radiation through the atmosphere. The most important parameters of the atmosphere are the water content, the turbidity coefficient (expressing the effect of haze and related scattering), the ozone content, the cloudiness of the sky and the effect of ground reflection.

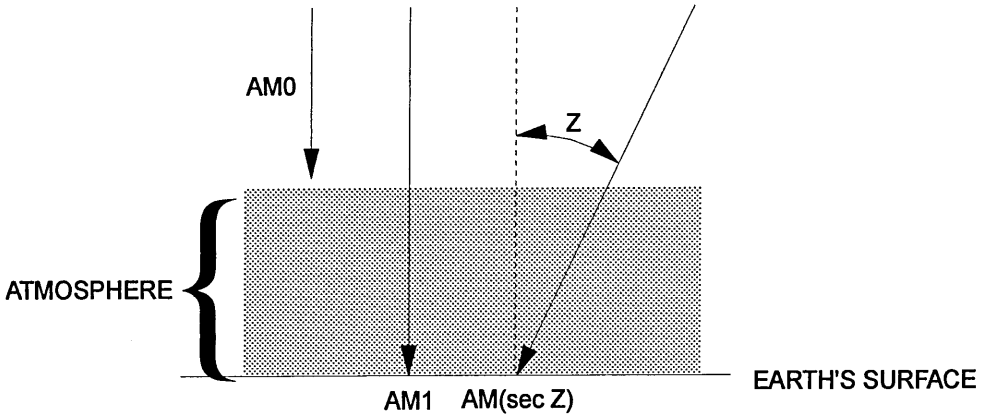

Figure 2.3. Illustration of the solar radiation labelled AM0 in space, AM1 at the earth's surface for normal incidence and AMm at the earth's surface with m= sec Z, where Z is the deviation from normal incidence.

Since the radiation reaching the periphery of the earth's atmosphere, normal to the sun's direction, depends only on the earth-sun distance other geometrical effects such as the sun's declination angle are manifested mainly by varying the path length through the atmosphere. "Air mass" is defined as the thickness of the air layer around the earth which sunlight passes through. Air mass 1, AM1, as shown in Figure 2.3, is the solar spectrum at the earth surface for optimum weather conditions at sea level with the sun just above. AM1.5 is that with the sun at an angle of 48° from the zenith.

2.3.1 The Solar Spectrum

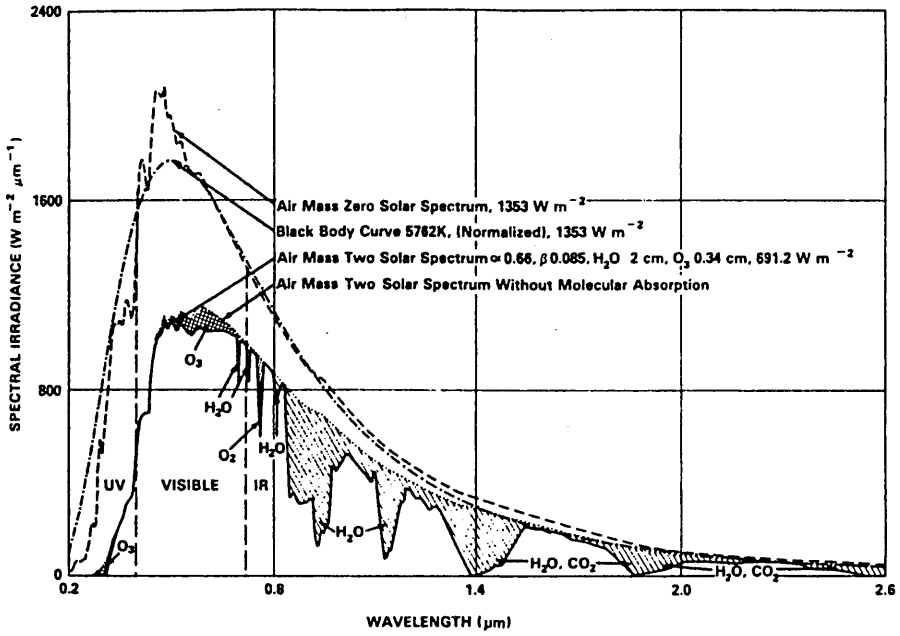

Figure 2.4. Comparison of AM0 and AM2 solar spectra, showing the various atmospheric absorbtion bands in AM2. The α and β for the AM2 spectrum are turbidity coefficients.

Figure 2.4 shows a comparison of the AM0 and AM2 spectra [Farenbruch 1983, p29], AM0 corresponds to the solar spectrum in outer space and AM2 correspond approximately with the average solar spectrum at the earth's surface. The atmosphere modifies the AM0 spectrum by Rayliegh scattering, which is responsible for the blue colour of the sky. In addition electronic absorption bands, primarily in oxygen and ozone (nearly all radiation with $\lambda > 0.29$ μm is absorbed by ozone), molecular rotational and vibrational absorption bands in H_2O and CO_2 (nearly all radiation with $\lambda > 3.0$ μm is absorbed by H_2O and CO_2) and scattering by aerosols and particulate matter which is greater for the shorter wavelengths.

2.4 History of CdTe

The history of CdTe [Wald 1977] began over 100 years ago in 1879 when the French chemist Margottet first prepared it with many other tellurides when he reacted tellurium with the metals at red heat. Fabre 1888 determined the heat of formation and reported that the process lead to well crystallised material, indicating that ease of preparation has been a hallmark of CdTe from the very beginning. Modern interest in CdTe arose from Frerichs 1947 who grew single crystals of CdTe from the vapour phase reaction of Cadmium and Tellurium in the presence of H_2. Fundamental investigations by De Nobel 1959 led to the preparation of crystals with well-defined conductivity, by growth from the melt. Its promise as a solar cell material was suggested in the classical papers of Rappaport 1959 and Loferski 1956 who, on the basis of idealised models, predicted that the optimum band gap for solar energy conversion was about 1.5 eV, the band gap of CdTe.

2.5 Properties of CdTe

Wald 1977 and Strauss 1977 have reviewed the properties of CdTe. CdTe has the largest lattice constant of the II-VI semiconductors, a = 6.481 Å. It crystallises in the cubic zinc blende structure, belongs to space group $F\bar{4}3m$ and shows cleavage along the (110) planes. It has a linear thermal expansion coefficient at room temperature of $4.9 \times 10^{-6}\ K^{-1}$ and a thermal conductivity of 0.075 $W(cmK)^{-1}$. The energy band gap of CdTe is direct with both conduction and valance band extrema located at $\underline{k} = 0$ [Chadi et al 1972]; the variation of absorption constant with photon energy near the absorption edge has been measured by Mitchell et al 1977 using photovoltaic techniques. At 4 K the band gap is 1.606 eV [Zanio 1978], at around room temperature [Strauss 1977] it can be described by

$$E_g = 1.622 - 3.5 \times 10^{-4} T \text{ eV} \quad (2.7)$$

The defect structure has been thoroughly analysed by Kröger 1964. It is difficult to obtain very high conductivity p-type material ($p > 10^{17}$ cm^{-3}), which is probably due to self-compensation effects.

2.6 History of CdS

Polycrystalline CdS films have been used as heterojunction partners in several types of thin film solar cells; CdS/Cu_2S, CdS/$CuInSe_2$ and CdS/CdTe. The CdS/Cu_2S solar cell was first developed in 1954 and was the first polycrystalline thin film cell intended for space and terrestrial applications [Reynolds et al 1954]. The CdS/Cu_2S solar cell was commonly of the backwall or substrate configuration and appeared to have low cost potential for terrestrial applications. By 1978, the CdS/Cu_2S cell had achieved efficiencies of 9.14 % [Barnett et al 1978] (J_{SC} = 21.8 $mAcm^{-2}$, V_{OC} = 0.52 V and FF = 0.71) under 87.9 $mWcm^{-2}$, AM1 illumination. However, the CdS/Cu_2S solar cells showed degradation in J_{SC} and FF under illumination due to the electrochemical decomposition of Cu_2S at operating voltages of higher than 0.33 V and the rapid diffusion of Cu through the junction structure [Chu 1995]. Since the late 1970's, CdS has been used in CdS/$CuInSe_2$ and CdS/CdTe solar cells with the aim of large-scale terrestrial energy production [Chu 1995].

2.7 Properties of CdS

CdS is an n-type semiconductor with a direct band gap of 2.4 eV. Its stable structure is wurtzite (a_0 = 4.295 Å and c_0 = 7.01 Å) [Chu 1995]. It has a melting point of 1475°C and a thermal expansion coefficient at room temperature of 4.7 x 10^{-6} K^{-1}.

CdS is readily doped n-type with In, Al, Cl or Br, all of which form shallow donors. Sulphur vacancies, induced by the presence of excess Cd during film or crystal growth, act as donors and resistivities below 0.1 Ωcm can be achieved with no intentional impurity introduction. Deep acceptor states are formed by Cu, Ag and Au impurities that readily compensate the native donors [Farenbruch 1983].

2.8 Development of CdTe Heterojunction Solar Cells

The first thin film CdTe heterojunction solar cell had the configuration Cu_2Te/CdTe prepared in a manner similar to Cu_2S/CdS solar cells i.e. an n-type film of resistivity about 10 Ωcm, vapour-deposited on a molybdenum or glass substrate, was treated with a cuprous salt solution to form the heterojunction [Cusano 1963]. The main difference exists in the fact that Cu_2Te is not photoelectrically active, being used only as a transparent contact to the n-type films. Solar radiation is incident on the Cu_2Te side and is nearly all absorbed by the CdTe. Conversion efficiencies of about 6% have been obtained [Cusano 1963].

The deposition of relatively low resistivity n-CdTe films and the formation of low-resistance ohmic contacts to these films are relatively simple. However, the Cu_2Te/CdTe solar cells are unstable due to the high diffusivity of copper in CdTe. Subsequent work was directed to the use of a large band gap high conductivity semiconductor, referred to as transparent conducting semiconductor (TCS) or window layer, as the heterojunction partner. Since essentially all known TCSs are n-type, p-type CdTe must be used as the absorber. The problems associated with the use of p-CdTe films are well known. These are the difficulty of depositing high conductivity films, owing to self-compensation and the difficulty of forming low resistance ohmic contacts owing to the large work function of p-CdTe.

2.9 Theory of CdS/CdTe Solar Cells

A desirable II-VI heterojunction photovoltaic cell [Farenbruch et al 1974] should have a band gap near 1.4 eV, a large difference in band gaps, ΔE_g, to permit front wall illumination through the large band gap component and small difference in linear expansion coefficients to minimise the density of interface recombination states. Five of the most interesting II-VI heterojunction systems are summarised in Table 2.1.

System	Smaller Eg (eV)	ΔEg (eV)	Carriers injected	Energy Spike[a] (eV)	Diffusion Voltage[b]	Lattice mismatch[c] (%)	Maximum theoretical solar efficiency[d] (%)
p-ZnTe/n-CdSe	1.7	0.56	Holes	None	0.61	(33)	6
p-ZnTe/n-CdTe	1.44	0.82	Holes	0.04	1.28	(30)	14
p-CdTe/n-CdS	1.44	0.98	Electrons	None	1.02	9	17
p-CdTe/n-ZnSe	1.44	1.23	Electrons	0.19	1.43	21	21
p-CdTe/n-$Zn_{0.35}Cd_{0.65}S$	1.44	1.39	Electrons	None	1.22	2	23

[a] Data For these calculations taken from Table 1.2 of A G Milnes and D L Feucht, Heterojunctions and Metal Semiconductor Junctions (Academic, New York 1972), p8.

[b] Diffusion voltage calculated assuming that the Fermi level lies 0.1 eV from the appropriate band edge in both p- and n-type materials.

[c] Approximate values. Parentheses indicate estimated values from extrapolation.

[d] Calculated assuming (i) no reflection loss, (ii) no series resistance loss, (iii) unity quantum efficiency, (iv) complete utilisation of cell area and reverse saturation current controlled by generation-recombination processes.

Table 2.1. Characteristics of Several II-VI Heterojuctions

The p-CdTe/n-CdS system seems to have the least handicaps of any of the simple binary junctions and has a theoretical efficiency of 17%. CdTe has an optimum value of E_g of 1.44 eV and the difference in band gaps between CdTe and CdS, ΔE_g, is relatively large. The p-CdTe/n-CdS system has no energy spike at the junction. This is advantageous because spikes and notches can be formed at some heterojunctions and can interfere with the separation of photoexcited carriers across the junction. The lattice mismatch is also small at 9% minimising the density of interface recombination states.

2.9.1 Structure of the CdS/CdTe Solar Cell

The form of the CdS/CdTe solar cell is of the superstrate geometry where the thin films are grown on glass through which incident light passes, as shown on Figure 2.5. This is the structure used in almost all-high efficiency CdS/CdTe solar cells. This geometry allows the layered structure to be easily built up and allows encapsulation for modulisation.

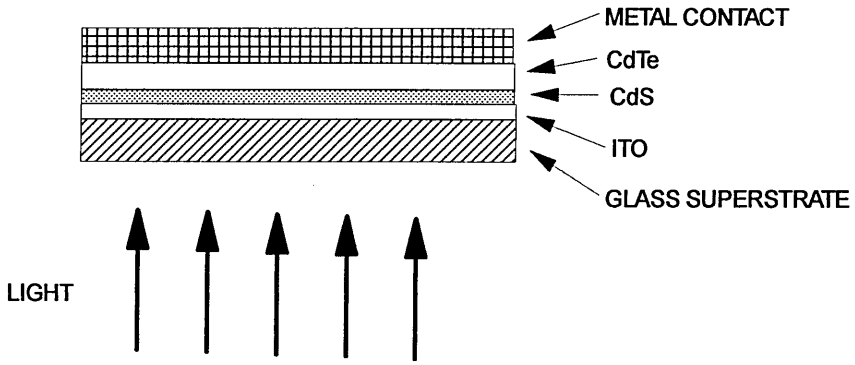

Figure 2.5. Schematic of Superstrate Structure CdS/CdTe Solar Cell

2.9.1.1 Glass Superstrate

To date borosilicate glasses have been used as substrates to produce high efficiency solar cells but interest has been expressed in the use of soda-lime silicate glass substrates due to their low cost [Ramathan et al 1993, Dhere et al 1993]. Although solar energy conversion efficiencies of approximately 10 % have been achieved [Ramathan et al 1993] on soda lime substrates, they are lower than those produced on borosilicate substrates.

2.9.1.2 Transparent Conducting Oxide

Thin film solar cells built in the superstrate geometry rely on Transparent Conducting Oxides (TCOs) to make the front contact [Das 1993a, Niles et al 1993]. Several different TCOs have been used as the superstrates for the production of high efficiency solar cells e.g. Indium Tin Oxide (ITO, In_2O_3:Sn) and Fluorine Tin Oxide (FTO, SnO_2:F). Taking the example of SnO_2, a crystalline, defect free SnO_2 film would be a highly resistive, wide band gap semiconductor (hence doping with fluorine). SnO_2 is quoted as having a direct optical band gap in the range $3.6 \leq E_g\,(SnO_2) \leq 4.3$ eV, although in contrast, oxygen vacancies render SnO_2 degenerately n-type conductive, with the Fermi level near or even in the conduction band [Niles et al 1993]. Commercially available TCOs have sheet resistivities of 8-15 Ω/□. It is important to use a low resistivity TCO as resistance from the TCO contributes to the series resistance of the solar cell.

2.9.1.3 Semiconducting Layers

The thickness of the two semiconductor layers is critical to the performance of the device. The CdS window layer is normally 500 - 1000 Å. This is thick enough to utilise high-energy photons (>2.4 eV) but not thick enough to prevent lower energy photons reaching the CdTe layer. This preserves the blue response of the cell [Sites 1988, Sasala et al 1992]. A CdS layer, 0.1 μm thick, absorbs approximately 63% of the incident radiation with photon energy greater than the band gap energy [Chu 1995].

The CdTe layer is normally 1.5-2.0 μm thick to ensure absorption of a large number of photons but not so thick as to encourage recombination in the bulk or at grain boundaries. Due to the high absorption coefficient, α, of CdTe, a 1 μm thick film of CdTe should absorb 90% of incident photons. Ideally the depletion width, w, should encompass the total thickness of both semiconductors to enable collection of all electron hole pairs within the device.

2.9.1.4 Metal Contacts

One of the major problems associated with solar cells involving p-type CdTe is the difficulty of forming a low resistance and stable electrical contact. This is particularly crucial for thin film cells in which a back contact to the polycrystalline CdTe is needed. Two approaches have been used to overcome this problem. In the first method another semiconducting layer is introduced between the CdTe and the metal. Ohmic back contacts are achieved by introducing semiconducting p-type ZnTe or HgTe between the CdTe and the back metal contact [Chu et al 1988, Meyer 1988, Gessert 1993].

The other method of producing low resistance contacts to CdTe is to use chemical etching to modify the semiconductor surface prior to metallisation. Anthony et al 1982 reported CuAu alloy contacts on a K_2CrO_7:H_2SO_4 etched surface of p-type CdTe. On 0.5 Ωcm^{-1} CdTe the contact resistivity was between 0.1 and 0.5 Ωcm^{-2} and varied approximately linearly with the bulk resistivity. It is stable at room temperature for at least several months, but did increase if subjected to a heat treatment. Danaher et al 1986 reported the chemical etching of single crystal p-CdTe and electrodeposited thin film p-CdTe using a 0.1 % bromine/methanol solution and a K_2CrO_7:H_2SO_4 solution. Etched surfaces were investigated using XPS and SIMS. It was found that the bromine/methanol solution left the surface rich in Te^0 and depleted in cadmium. The K_2CrO_7:H_2SO_4 etch left the surface rich in Te^0 (Cd:Te approximately 0.2). No TeO_2 was present if the etch was sufficiently acidic.

The most commonly used etching procedure for thin film CdTe is a K_2CrO_7:H_2SO_4 etch followed by a hydrazine hydrate etch [Basol et al 1986, Das 1992]. The hydrazine hydrate etch is used to remove any residual layers formed on the CdTe surface. A range of CdTe surface preparation methods and their effects on metal contacts to CdTe have been investigated [Dharmadasa et al 1989] using XPS. Due to the toxic nature of hydrazine hydrate it was proposed that the hydrazine hydrate etch was replaced with a sodium hydroxide/sodium thiosulphate aqueous solution etch in order to remove surface oxides [Blomfield 1995].

2.10 Development of CdS/CdTe Solar Cells

The first thin film CdS/CdTe heterojunction solar cell was fabricated by Adirovich et al 1969, 1971, who reported an efficiency of 1%. This cell had superstrate configuration and was fabricated by evaporating an undoped CdTe film over a CdS/SnO_2/glass substrate.

Bonnet and Rabhenhorst 1972 reported the first efficient all thin film CdS/CdTe solar cell. Their large grain (5-20 μm) CdTe films were deposited onto molybdenum foil substrates at 500-700°C by high temperature gas transport. Evaporating thin CdS layers over the CdTe films (substrate structure) completed the devices. An efficiency of approximately 5% was reported for these cells under 50 $mWcm^{-2}$ illumination.

Fahrenbruch et al 1975 investigated five II-VI heterojunction systems concentrating on the CdS/CdTe system. Cells of n-CdS/p-CdTe were prepared by depositing p-CdTe by Close Spaced Vapour Transport (CSVT) on single crystal n-CdS, and by evaporating n-CdS on single crystal p-CdTe. These cells exhibited quantum efficiencies between 0.5 and 0.8, V_{OC} between 0.50 and 0.66 V, and solar cell efficiencies of 3-4 %. Values of solar efficiencies were limited by contact resistance to the p-CdTe and larger than desirable forward leakage currents. By 1977 [Mitchell et al 1977a] this group produced CdS/CdTe devices with an efficiency of 7.9 % under 85 $mWcm^{-2}$ solar simulator illumination (V_{OC} = 0.63 V, J_{SC} = 16.1 $mAcm^{-2}$, FF = 65.8%). This device was produced by evaporating n-CdS films on p-CdTe single crystal substrates. ITO was then deposited onto the CdS by rf sputtering to act as a transparent electrode to the CdS.

Yamaguchi et al 1975, 1976, 1977 obtained 12% efficiency (active area) by the vacuum evaporation of CdS on (111) p-doped CdTe grown by the Bridgeman technique. An analysis of this cell shows the structure to be n-CdS/n-CdTe/p-CdTe and, therefore, contains some elements of the homojunction.

Using the screen-printing method, Nakayama et al 1976 obtained 8.1% power conversion efficiency (total area) for an all-thin film cell. The structure is a backwall cell and had the elements of both the CdS/CdTe and Cu_2Te/CdTe heteropairs. A 20 μm CdS film with a resistivity of 0.2 Ωcm was deposited by screen-printing. A 10 μm thick CdTe paste of about the same resistivity was prepared by mixing indium doped n-CdTe and $CdCl_2$ with a binder in a mixer and was applied by screen printing. The structure was dipped into a hot aqueous cuprous ion solution to form Cu_2Te. It was thought copper diffusion along the CdTe grains promoted the formation of p-n junction near the CdS/CdTe interface.

CdS/CdTe heterojunction cells have also been prepared by deposition of CdS by spray pyrolysis [Chamberlin 1966] onto single crystal CdTe [Ma et al 1977, 1977a]. The highest efficiency cell had an almost ideal quantum efficiency, with V_{oc} of 0.53 V, J_{sc} of 16.4 $mAcm^{-2}$ and a solar efficiency of 6.5%.

CdS/CdTe heterojunctions formed by e-beam evaporation of CdS on single crystal p-type CdTe substrates [Werthen et al 1983] showed an efficiency of 7.5 %. Values of V_{OC} of 0.63 V and J_{SC} of 17 $mAcm^{-2}$ were obtained for the best cells.

Tyan 1980, 1982 and his co-workers at Kodak achieved a major improvement in CdS/CdTe solar cells. Both CdS and CdTe were grown by CSVT to form a cell with the structure glass/0.3 μm, In_2O_3/0.1 μm, CdS/4 μm, CdTe/0.05 μm, gold contact. It was reported that a small concentration of oxygen introduced during the deposition enhanced the p-type character of the CdTe film and ensured a shallow junction between the CdS and the CdTe rather than a less desirable buried junction in the CdTe. The thin CdS layer enhanced the blue response of the cell. Kodak reported 75 $mWcm^{-2}$ simulated AM2 efficiencies of 10.5 % (V_{OC} = 0.75 V, J_{SC} = 17 $mAcm^{-2}$) for 0.1 cm^2 CdS/CdTe cells deposited at about 1 Torr pressure [Tyan 1982].

The first efficient electroplated CdS/CdTe heterojunction solar cell was reported by Basol et al 1982a that gave an efficiency of 8% under 80 $mWcm^{-2}$ AM1.5 illumination. Solar cells with over 10% efficiency were fabricated using electrodeposition with both CdTe and HgCdTe films by the mid-1980's [Basol 1988]. The intellectual property to Monosolar's work was purchased by British Petroleum Solar and pursued in the late 1980's and early 1990's producing impressive results [Woodcock et al 1991] (For full discussion of this work see chapter 3, Electrodeposition of Semiconductors).

The first high efficiency solar cell by screen-printing was reported by the Matsushita group in 1982 having a conversion efficiency of 10% [Uda et al 1982]. These cells, which were produced by sintering at high temperature (at approximately 600°C), showed a poor response in the short wavelength due to the formation of a CdS_xTe_{1-x} solid solution layer at the CdS/CdTe interface. It should be noted that Matsushita's devices did not use TCO electrodes. Front contacts were made directly to the CdS layer and, therefore, CdS films of these devices often needed to be doped to obtain low sheet resistance.

The late 1980's and early 1990's has seen significant improvement in small area efficiencies approaching 16% and the pursuit of large scale manufacturing capability for CdS/CdTe modules. To date, ten processes have yielded cell efficiencies of 10% to 16%, although only five techniques have been used for module fabrication. These are electrodeposition, high rate evaporation, spraying, screen printing/sintering [Zwiebel et al 1993] and CSS [Bonnet et al 1995].

2.11 Current State of CdS/CdTe Solar Cell Technology

2.11.1 Close Spaced Sublimation (CSS)

Table 2.2 summarises a league table of the highest efficiency CdS/CdTe solar cells to date. This table clearly shows it is possible to produce high efficiency (>10%) CdS/CdTe solar cells by a wide variety of techniques. The University of South Florida (USF) [Britt et al 1993] has achieved the best conversion efficiency of 15.8%. This investigation emerged from the initial work of Ting and Shirley Chu at USF [Chu 1988, Chu et al 1988a]. Ting and Shirley Chu retired from USF in 1992, after producing a world record 14.6% efficient CdS/CdTe cell [Chu et al 1992, 1992a]. They left there students, Chris Ferekides and Jeff Britt, to carry on their work subsequently producing the 15.8% cell, the first non-single-crystal thin film cell to surpass 15%. The deposition techniques used in this device are Chemical Bath Deposition (CBD) for the n-type CdS and Close Spaced Sublimation (CSS) for the CdTe layer. This device had a MgF_2 AR coating giving it efficiency advantage over other cells in Table 2.2 that do not have an AR coating.

CSS can produce CdTe films at extremely high rates and in that respect is attractive for high throughput manufacturing. There are challenges to be met in large-scale production environments. These include maintaining a uniform temperature gradient and uniform gap between source and substrate. Solar Cells Inc. of Toledo, Ohio is presently pursuing a large area module production facility. This group is using a modified CSS system, differing from CSS in that the superstrate is inserted into and removed from the deposition zone hot rather than being both heated and cooled while in close proximity to the source material. This is a high rate evaporation process that produces the active semiconductor layers in about one minute. Large area modules of 7200 cm^2 were produced. These consisted of 116 cells connected in series, with each cell having dimensions of 1 cm by 60 cm. The best characteristics for these modules were 17.7 $mAcm^{-2}$ J_{SC}, 0.80 V per cell V_{OC}, 0.61 FF, 8.6% active area efficiency, 0.86 area ratio and 53 watts power output [Nolan 1993, Meyers 1993]. Work is currently under way to move from the initial pilot production plant to a full manufacturing plant, producing modules at a rate of 20 MW/year [Meyers 1993a].

2.11.2 Electrodeposition

Electrodeposition occupies the second place in Table 2.2 with 14.2% [Woodcock et al 1991]. As is shown in the table, this is for an area of 0.02 cm^2. This group has reported devices with active areas of 706 cm^2 with 10.1% efficiency and good outdoor stability and performance [Barker et al 1992].

The group from the University of Queensland [Morris et al 1993] occupies fourth position, again using electrodeposition. Their device has a very high value of J_{SC} of 27.9 $mAcm^{-2}$ that is described as being due to the devices having good diffusion lengths (approximately 0.6μm as measured by EBIC) and it was thought that loss mechanisms were interface controlled rather than bulk processes.

2.11.3 Atomic Layer Epitaxy (ALE)

The third highest efficiency was achieved using Atomic Layer Epitaxy (ALE) [Skape et al 1992]. The growth of ZnS for electroluminescent thin film display devices has shown that ALE is an advantageous technique in commercial production, but the technology is not proven for the production of low cost, large-area solar cells.

2.11.4 Spray Pyrolysis

The Photon Energy Group has pioneered fabrication of high efficiency CdS/CdTe devices by the spraying technique [Albright et al 1990, 1992]. Slurry spraying is a low cost, large-area deposition technique. Due to commercial confidentiality, this process has not been widely reported but it is reported that the CdS thickness was of the order of 0.8 μm [Jordan 1988] and the CdTe was of the order of approximately 6 μm. As shown in Table 2.2 small-area devices of 12.7% efficiency have been produced, in addition, modules with areas of 929 cm^2 have achieved over 8% aperture area efficiency (active area efficiency up to approximately 10%). Modules with areas of 3716 cm^2 have been tested at NREL at 23.1 W. Photon Energy has new owners and is now called Golden Photon and has a new facility in Golden Colarado [Zweibel et al 1993]. This new facility has an estimated production capacity of approximately 80000 modules, producing approximately two megawatts of total power output capacity, at current average module efficiencies of 6.5% [Johnson 1993].

2.11.5 Screen Printing/Sintering

The group at the Korea Advanced Institute of Science and Technology (KAIST) have produced 12.5% efficiency devices by the screen printing/sintering technique although these devices are not strictly CdS/CdTe devices but have the structure $Cd_{1-x}Zn_xS$/CdTe [Seol 1989]. ZnS with a band gap of 3.68 eV can be substituted into CdS (2.42 eV) to increase the band gap of the window material.

Screen-printed CdS/CdTe junctions have been developed by the Matsushita Battery Group from Japan. The first high efficiency device with around 10% conversion efficiency was reported in 1982 and cells with over 11% conversion efficiency by 1990 [Suyama et al 1990, Matsumoto et al 1984]. Matsushita Battery is presently the only company producing commercially available CdS/CdTe solar cell modules and produces about 1 MW/year for Texas Instruments calculators and other consumer applications [Ikegami 1988, Suyama et al 1990a]. A large-area (1200 cm^2) device has shown a total area conversion efficiency of 6.2% (which corresponds to 8.7% active area efficiency) under AM1.5 100 $mWcm^{-2}$ illumination.

2.11.6 Metal-Organic Chemical Vapour Deposition (MOCVD)

Metal-organic chemical vapour deposition (MOCVD), widely used for the epitaxial growth of compound semiconductors, has been applied to the deposition of polycrystalline CdTe films [Chu et al 1990, 1991, 1992b]. CdTe films can be deposited at rates of up to 4 μm/h at a temperature of 350-400°C by the reaction between dimethylcadmium (DMCd) and diisopropyltelluride (DIPTe). The group at Georgia Institute of Technology [Rohatgi 1992] showed the highest efficiency CdS/CdTe cells produced by MOCVD. Problems with degradation of Au/Cu contacts were observed so these were replaced with ZnTe/Ni contacts [Rohatgi 1992].

Table 2.2. Characteristics of Thin-Film CdS/CdTe Solar Cells Produced by Various Groups

CdTe Deposition Process	Area (cm^2)	Efficiency (%)	J_{SC} ($mAcm^{-2}$)	V_{OC} mV	FF	Organisation	Reference
CSS	1.05	15.8*	25.09	843	0.745	USF	Britt et al 1993
ELECTRODEPOSITION	0.02	14.2	23.5	819	0.74	BP SOLAR	Woodcock et al 1991
ALE	0.12	14.0	23.8	804	0.73	MICROCHEMISTRY	Skape et al 1992
ELECTRODEPOSITION	0.02	13.1	27.9	720	0.65	UNIV. OF QUEENSLAND	Morris et al 1990
SPRAY	0.30	12.7*	26.21	799	0.605	PHOTON ENERGY	Albright et al 1992
SCREEN PRINTING	0.30	12.5	17.8	870	0.61	KAIST	Seol 1989
MOCVD	0.08	11.9	24.5	756	0.64	GEORGIA INST. TECH.	Rohatgi 1992
CSS	0.388	11.6*	22.16	797	0.654	BATTELLE EUROPE	Bonnet et al 1992
CSS	1.08	11.3	22.57	833	0.60	NREL	Ramanathan et al 1993
SCREEN PRINTING	1.02	11.3	21.1	797	0.67	MATSUSHITA	Suyama et al 1990
ELECTRODEPOSITION	1.068	11.2*	22.36	767	0.696	AMETEK	Meyers 1989
PVD	0.191	11.0*	20.09	789	0.692	IEC	Shafaraman et al 1991

* Measured by NREL.

Chapter 3.0: Electrodeposition of Semiconductors

3.1 History of Electrodeposition of Semiconductors

The electrodeposition of semiconductors has been reviewed by several authors [Fulop et al 1985, Lokhande et al 1989, Hodes 1995]. First attempts to electrodeposit semiconductors date back to the mid 1800's when St. Claire De Ville 1854 claimed he had produced silicon as a result of the electrolysis of impure molten $NaAlCl_4$. Since the material did not oxidise at white heat the claim was probably not true. Ullik 1865 was probably the first to deposit elemental silicon when he electrolysed a solution containing K_2SiF_6 in KF. More systematic studies of silicon electrodeposition began in the 1930's, with Dodero's 1934, 1939 investigation of the electrolysis of molten silicates at temperatures of 800 to 1250°C. The very high potentials used in these studies would be expected to liberate not only silicon, but also alkali and alkaline earth metals. Several investigators have studied silicate or SiO_2 melts in an effort to develop a commercial process for electrodepositing silicon [Monnier et al 1957, 1964]. The molten solutions studied contained SiO_2 in cryolite, (Na_3AlF_6).

Cuombo and Gambino 1968 were the first to electrochemically synthesise a III-V compound gallium phosphide (GaP). GaP is an important electroluminesent material. By molten salt electrolysis, they prepared up to 100 μm thick layers of GaP on silicon substrates. GaAs (the next most commercially important material after silicon) growth was reported by DeMattei et al 1978, using a molten salt solution which contained $NaAsO_2$ and Ga_2O_3 in a B_2O_3-NaF solvent at 720-760 °C. GaAs layers 10 μm thick were deposited on (100) n-type GaAs Substrates.

3.1.1 Electrodeposition of II-VI Compounds

The first reports of the aqueous electrodeposition of II-VI compounds were published in 1976. Hodes et al 1976 reported the growth of a polycrystalline layer of CdSe on titanium. Miller et al 1976 produced layers of CdS and Bi_2S_3 by the anodization of cadmium and bismuth in polysulfide solutions. Peter 1978 studied the mechanism for the formation of sulphide films on cadmium. The anodization was performed on polished 5N polycrystalline cadmium rods in a solution of 0.1 M Na_2S and 1.0 M $NaHCO_3$.

Monosolar Inc. initiated research on the cathodic electrodeposition of CdTe for solar cell applications in 1976, under contract from the Energy Research and Development Administration (ERDA). The initial work at Monosolar and its subcontractor, the University of Southern California (USC), concentrated on the development and the understanding of the cathodic electrodeposition technique for CdTe. Kröger 1978 published the most significant piece of work in this field. This work set down the theoretical basis for the cathodic deposition of semiconductors. Kröger defined two classes of co-deposition defined by whether the difference in electrode potential of the individual components is larger (Class 1) or smaller (Class 2) than the shift in electrode potential of either component as a result of compound or alloy formation. In the case of Class 1 the potential of the deposit is determined by the less noble component over the entire composition range, the deposition potential shifting monotonically with composition. In Class 2 the role of the potential determining species may shift from one component to the other at an intermediate composition, the deposition potential at this composition being more positive than that of either of the components when deposited individually.

Kröger described the use of quasi rest potentials (QRP) to determine the electrode potentials. The QRP is defined as the potential of the deposit relative to the electrolyte with activities of the potential-determining species as at the solid-electrolyte interface during deposition. The polarisation is established with relaxation time, τ, $\leq 10^{-3}$ seconds. Therefore, the QRP can be determined experimentally [Dennison 1995] by measuring the electrode potential approximately equal to 10^{-3} seconds after interruption of the deposition current. The QRP is a more accurate measure of what is happening at the solid electrolyte interface in respect of the movement of the ions to the deposition surface. Further changes of potential occur when the composition of the electrolyte at the interface changes back to the bulk value, a process with a relaxation time of seconds.

Panicker et al 1978 produced the first experimental work on the aqueous electrodeposition of CdTe. CdTe was deposited cathodically from an aqueous solution of $CdSO_4$ and TeO_2. Films were deposited at potentials of -0.20 to -0.75 against a Standard Calomel Electrode (SCE). The rate of deposition was found to increase with stirring rate and was proportional to the concentration of TeO_2 but independent of the $CdSO_4$ concentration. Films deposited at room temperature were amorphous and films deposited at higher temperatures were crystalline, the degree of crystallinity increasing with deposition temperature. Grain sizes were found to be in the range 500-1000 Å. Annealing the films at 350°C caused the grain size to increase to ≥ 0.5 μm.

In addition in 1978 Danaher et al reported the cathodic aqueous electrodeposition of CdTe onto titanium substrates. The deposition solution consisted of 0.01 M H_2TeO_3, 1.5 M H_2SO_4 and 0.27 M $CdSO_4$. The films were heat treated for 16 hours at 250°C and tested in a photoelectrochemical cell. A power conversion efficiency of 0.4% was observed.

The Monosolar and USC team started to work on a joint program in 1979 supported by the Solar Energy Research Institute (SERI). This project was aimed at the identification and evaluation of the mechanisms, limiting the efficiency of the electroplated CdTe cells.

Hokkaido University, Japan reported the aqueous deposition of CdTe from a solution of pH 1.4, containing 1M $CdSO_4$, 1 mM TeO_2 and 0.05 M H_2SO_4 on Titanium or Nickel sheets [Takahashi et al 1984, 1984a]. A three-electrode cell was used for the preparation of CdTe and for photoelectrochemical measurements. A platinum sheet and an Ag/AgCl electrode were used as a counter and a reference electrode, respectively. Photocurrents were found to be small when compared with those of CdTe single crystals. It was suggested the major reasons for this low efficiency were the effective recombination of hole-electron pairs at grain boundaries and at the surface. Photocurrents were increased by heat treating the films in a helium atmosphere and the removal of surface tellurium by an etching treatment.

3.2 Theory of Electrodeposition of Semiconductors

Many of the key parameters in the electrodeposition of semiconductors are similar to those encountered in electroplating. The electrodeposition of semiconductor compounds like any other chemical reaction is governed by thermodynamic considerations. In the case of electrodeposition, the reactions are thermodynamically unfavourable. The overall free energy change (ΔG) for the reaction is positive and the electrical energy needs to be supplied to obtain the energy to drive the reaction. Following the argument of Fulop et al 1985, the Nernst equation for the potential, E_M, of a metal electrode in a given solution is a suitable starting point

$$E_M = E^0_M + (RT / mF) \ln[(a_M{}^{m+}) / a_M] \qquad (3.1)$$

Where E^0_M is the standard potential for the reduction to form the metal (M), R is the gas constant and T is the absolute temperature, m is the number of electrons required for the reduction, F is the Faraday constant, and $a_M{}^{m+}$ and a_M are the activities of M^{m+} in the electrolyte and M in the deposit, respectively. Electrodeposition of M can occur at potentials more negative than the equilibrium potential; this difference in potential is the overpotential (or overvoltage), E_{OVER}.

When considering alloy or compound electrodeposition of semiconductors the important factors are the equilibrium potentials of the alloy or compound components, the stability of the resultant deposit and the activities of the ions in solution. For a compound M_rN_s, for which deposition of component M involves m electrons and component N involves n electrons, the equilibrium potentials of M and N are:

$$E_M = E^0_M + (RT / mF) \ln[(a_M{}^{m+}) / a_M] \qquad (3.2)$$

and

$$E_N = E^0_N + (RT / nF) \ln[(a_N{}^{n+}) / a_N] \qquad (3.3)$$

The conditions necessary to obtain the simultaneous deposition of two different kinds of ions at the cathode can be written as:

$$E_M + E^m_{OVER} = E_N + E^n_{OVER} \qquad (3.4)$$

The activities of the metals M and N in the compound or alloy are determined by their concentrations and by the thermodynamic stability of the deposit. The reversible potential of a metal M alloyed with a component should be more positive than that of the pure metal. That is due to the free energy of formation of the alloy or compound, ΔG, with a shift of potential of:

$$E = -\Delta G / rmF \qquad (3.5)$$

The shift of potential is a constant value for the formation of a compound. This often makes it very difficult to control deposit stoichiometry since significant variation of electrochemical potential can be expected.

Thermodynamics is concerned with the equilibrium aspect of deposition. Once the potential between the electrodes is raised above the deposition potential, the system is in a non-equilibrium condition and kinetics must be considered. While it is possible to determine some aspects of the deposition process, such as the electron transfer processes occurring at the electrodes and the rate-controlling step for deposition (i.e. tellurium diffusion in the case of CdTe). From a practical point of view, it is more important to determine those conditions that yield a smooth deposit and what the expected growth rate will be under those conditions.

In order to determine the rate of growth of the depositing layer, the amount of material deposited per unit time must be determined. Faraday's law of electrolysis gives the mass of material deposited by a given amount of charge, q, as:

$$\text{Mass} = (M\, q\, \varepsilon) / (n\, F) \qquad (3.6)$$

Where M is the molecular weight of the material, n is the number of electrons transferred and ε is the deposition efficiency. The volume is given by

$$v = (M\, q\, \varepsilon) / (\rho\, n\, F) = A\, y \qquad (3.7)$$

Where ρ is the density of the material, A is the area of deposition and y is the deposition thickness. The rate of growth (dy/dt) is given by

$$\frac{dy}{dt} = \frac{M\varepsilon}{\rho n F A}\frac{dq}{dt} = \frac{M\varepsilon}{\rho n F}\frac{I}{A} = \frac{M\varepsilon}{\rho n F}J \qquad (3.8)$$

The term $M/\rho nF$ is a constant for any given deposition process and the current density J is measured in $mAcm^{-2}$. Practically, ε is usually less than one.

3.3 Theory of Electrodeposition of CdTe

The detailed mechanism to explain the electrodeposition of CdTe from an aqueous electrolyte has been investigated by Danaher 1984 and Saraby-Reintjes 1993. In general terms two steps can represent the overall deposition process:

(a) Tellurium reduction

$$HTeO_{2(aq)}^{+} + 3H_{(aq)}^{+} + 4e^{-} \rightarrow Te_{(s)} + 2H_2O \quad (3.9)$$

(b) The tellurium deposited reacts rapidly with the Cd^{2+} ions in solution

$$Te_{(s)} + Cd_{(aq)}^{2+} + 2e^{-} \rightarrow CdTe_{(s)} \quad (3.10)$$

The overall cathode reaction can be generalised as

$$Cd_{(aq)}^{2+} + HTeO_{2(aq)}^{+} + 3H_{(aq)}^{+} + 6e^{-} \rightarrow CdTe_{(s)} + 2H_2O \quad (3.11)$$

The anode reaction can be generalised as

$$4OH^{-} \rightarrow O_2 + 4e^{-} + 2H_2O \quad (3.12)$$

The cathode reaction is the formation of the compound CdTe.

A large negative value of ΔG, of 9.97×10^4 $Jmole^{-1}$, for CdTe formation favours a compound rather than alloy deposition. The reaction can be performed at virtually 100% current efficiency in water. The anode reaction at the inert surface is oxygen evolution.

There are five main deposition parameters,

(i) Concentration of TeO_2.

(ii) Concentration of $CdSO_4$.

(iii) Solution pH.

(iv) The deposition potential or deposition current density.

(v) The temperature of the deposition solution.

Taking each of these parameters in turn, (i) and (ii), the bath composition has cadmium concentration in the molar range and tellurium concentration in the millimolar range due to its low solubility. At high $CdSO_4$ concentrations there is no effect of the concentration of Cd^{2+} on the deposition rate.

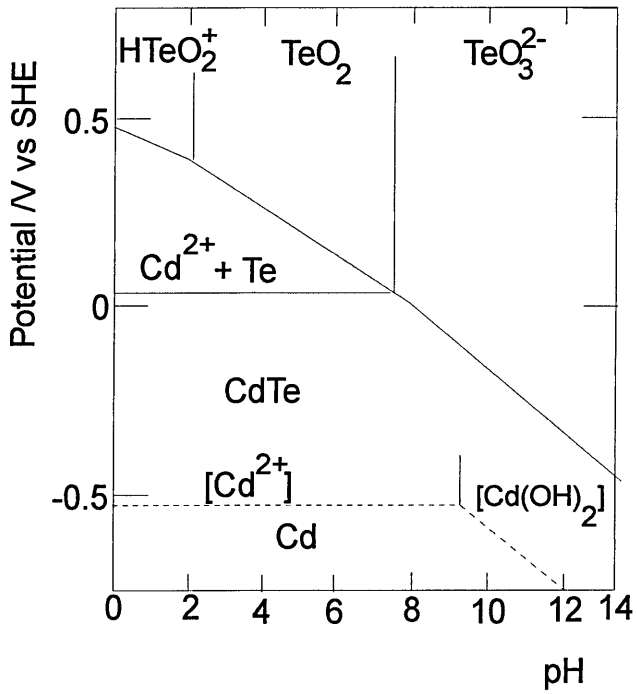

Figure 3.1. Pourbaix Diagram of CdTe in Aqueous Solution

Parameter (iii) solution pH can be understood with the help of a Pourbaix diagram [Pourbaix 1963], which shows the dependence of the deposition potential on the pH value of an electrolyte. A Pourbaix diagram is an isothermal phase diagram, which represents metal-ion-oxide equilibria plotted with deposition potential and pH as co-ordinates. The Pourbaix diagram for CdTe in aqueous solution is shown in Figure 3.1. Tellurium is introduced as the dioxide, which, at the pH of approximately 1.7, dissolves to give the $HTeO_2^+$ species shown in the cathode reaction.

Parameter (iv) is the deposition potential and current. The current density is low and it has been established in previous studies that the steady state limiting current is controlled by the diffusion of soluble tellurium species ($HTeO_2^+$ ions) to the electrode [Takahashi et al 1984, Sella et al 1986, Danher 1994].

Control has to be potentiostatic, the more usual practice in electroplating of current control (Galvanostatic Deposition) is not suitable for this reaction, which follows from the thermodynamics of compound formation. The standard reduction potentials for tellurium and cadmium are +0.551 V and -0.403 V against a Standard Hydrogen Electrode (SHE), respectively. Cadmium telluride is formed at potentials positive of the standard potential for cadmium ion reduction, that is to say it is an underpotential deposition with regard to cadmium. This is possible through the free energy change and high cadmium activity in the bath. The standard tellurium reduction potential is shifted somewhat towards cadmium due to its low activity but, at potentials approaching cadmium reduction, tellurium reduction is very fast.

Cadmium telluride can be formed anywhere in the 200 mV region leading up to the cadmium reduction potential but, despite being formed over a range of potentials the stiochiometry, it will not necessarily be single valued. This is shown through calculation by Engelken and Van Doren 1985, 1985a, 1987, 1988, from thermodynamic data. This work has shown that, theoretically at least, only one potential exists where pure cadmium telluride can be formed, the Point of Perfect Stoichiometry (PPS). This work was supported experimentally by Dennison 1995. Either side of this PPS potential the resulting electroplate will be a mixture of tellurium or cadmium corrupted material with a kind of flip-flop instability between these two states. This underlines the requirement for close potential control of the reaction.

Parameter (v) is the temperature of the deposition solution. Films deposited at room temperature are amorphous or only slightly crystalline, whilst those deposited at higher temperature are crystalline and exhibit orientation effects [Panicker 1978, Lyons et al 1984]. The limit of deposition temperature is the boiling point of the aqueous electrolyte. Practically most depositions are performed at temperatures of 85 - 95°C. Oxygen removal methods are often used such as bubbling Argon through the electrolyte.

3.4 Theory of Electrodeposition of CdS

Peter 1978 reported the anodic growth of CdS on cadmium substrates. The disadvantage of anodic growth is that growth becomes hindered by the barrier nature of the n-type semiconducting film leading to a porous layer of CdS.

Following the early theoretical work of Kröger 1978, the first cathodic growth experimental work came from the groups of Power et al 1981 and Jackowska et al 1986. The CdS film was cathodically deposited from a solution containing cadmium and thiosulphate ions [McCann et al 1981, Jackowska et al 1986, Dennison 1993,]. The cathodic reactions leading to CdS formation are:

$$Cd^{2+}_{(aq)} + 2e^- \Leftrightarrow Cd_{(s)} \qquad (E_0 = -0.403V \text{ vs } SHE) \qquad (3.13)$$

$$2Na^+_{(aq)} + S_2O^{2-}_{3(aq)} + 6H^+_{(aq)} + 4e^- \Leftrightarrow 2S_{(s)} + 3H_2O \qquad (E_0 = +0.50V \text{ vs } SHE) \qquad (3.14)$$

An electrochemical system with sufficient potential to reduce cadmium will also easily reduce sulphur since its reduction potential is much more positive. Other reactions can contribute to sulphur reduction and to homogeneous CdS formation. Acidification of sodium thiosulphate solution produces unstable thiosulphuric acid, which can spontaneously decompose into sulphurous acid, and sulphur, which precipitates [Nebergall 1963]. Such precipitation is expected to occur at lower pH values. The thiosulphate ions disproportion, depending on the pH, according to:

$$S_2O_3^{2-}{}_{(aq)} \Leftrightarrow S_{(aq)} + SO_3^{2-}{}_{(aq)} \qquad (3.15)$$

Sulphonous acid can also be electrochemically reduced to sulphur [Dean 1973], although the reduction potential is more negative than that for cadmium, making this unlikely,

$$SO^{2-}_{3(aq)} + 3H_2O + 4e^- \Leftrightarrow S_{(s)} + 6OH^-_{(aq)} \qquad (E_0 = -0.66\,V \text{ vs } SHE) \qquad (3.16)$$

Thiosulphuric acid can also slowly dissociate freely in solution independent of pH as follows:

$$H_2S_2O_{2(aq)} \Leftrightarrow S_{(s)} + H_2O + SO_{2(g)} \qquad (3.17)$$

Depending on conditions, other compounds such as H_2S, H_2SO_4 and polythionates can be formed [Schmidt 1957, Foerster 1934]. The solubility product of CdS (6×10^{-28} moles/litre at 298 K) is very small [Kröger 1978] so that an extremely low concentration of sulphur would lead to CdS formation given the high concentration of cadmium ions.

Thus the overall electrode reaction is:

$$Cd^{2+}_{(aq)} + S_2O_3^{2-}{}_{(aq)} + 2e^- \Leftrightarrow CdS_{(s)} + SO_3^{2-}{}_{(aq)} \qquad (3.18)$$

Power et al 1981 showed that reaction 3.16 does not run with any significant efficiency under normal conditions, so a decrease in pH is necessary to cause decomposition of $S_2O_3^{2-}$ ions to produce colloidal sulphur.

The source of the Cd^{2+} ions has been found to be an important factor in this system. In this case, $CdCl_2$ is used rather than $CdSO_4$, as is the case for CdTe, as the use of $CdCl_2$ in the deposition bath tends to form a hexagonal structure of CdS as shown by XRD. If $CdSO_4$ is used the structure is found to be cubic. The hexagonal structure has much better optical properties than the cubic structure of CdS [Farenbruch 1983].

The source of thiosulphate ions in the electrolyte is normally sodium thiosulphate and the pH of the electrolyte is normally adjusted using HCl. The temperature of the electrolyte for deposition is normally 80°C.

Dennison 1993 reported, "CdS deposition from $S_2O_3^{2-}$ containing solutions has been shown to require the deposition of cadmium to initiate compound formation and does not involve an underpotential deposition process as is the case with CdTe. This indicates a fundamental difference between the growth of these two semiconductors that does not become apparent from the theoretical treatments of compound semiconductor electrodeposition."

3.5 Electrodeposition of CdS/CdTe Solar Cells

3.5.1 BP Solar Apollo Project

BP Solar's Apollo (Apollo is a trademark of The British Petroleum Company plc) thin film photovoltaic module fabrication process is based on the deposition of the thin film semiconductor CdS either by Chemical Bath Deposition (CBD) or electrodeposition and the electrodeposition of CdTe thin films. BP Solar has produced the highest efficiency CdS/CdTe solar cell by electrodeposition with an efficiency of 14.2% and an area of 0.02 cm^2. This is the second highest efficiency for a CdS/CdTe device grown by any method [Woodcock et al 1991].

Aperture area efficiencies of more than 10% have been reported for devices of area 706 cm^2 [Barker et al 1992] and, by incorporating six plates in a 3 x 2 format under a monolithic cover glass aperture, areas up to 4540 cm^2 and efficiencies up to 8.4% have been achieved [Woodcock et al 1994]. The process has been demonstrated with greater than a 90% yield of modules having efficiencies greater than 8%. External testing of modules in Spain has shown stable module efficiencies above 6% [Woodcock et al 1991]. The current focus of this research is based in Fairfield, California, USA [Cunnigham 1999]. A pilot production facility is being developed based on 0.55 m^2 superstrates. The main production system consists of deposition tank capable of taking 40 of the 0.55 m^2 plates simultaneously, this tank is then repeated eight times. An outdoor testing program is being carried out on a 2kW ground mounted system consisting of 72, 0.43 m^2 Apollo module interconnects. In the future it is planned to move to 0.94 m^2 plates.

3.5.1.1 Electrodeposition of CdTe

Figure 3.2 shows the essential features of a multiplate bath. Parallel processing is essential due to the low reaction rate. The optimum space-time yield or compactness of these channels is determined by a practical compromise between mass transport and potential control requirements. The essential features are a common electrolyte for all plates fed from a holding tank that serves to condition the electrolyte solution via heating, filtration and tellurium addition. Tellurium addition is achieved by flow of electrolyte through a packed bed of tellurium oxide. A single cadmium/cadmium sulphate ($Cd/CdSO_4$) reference electrode is common to a multichannel potentiostat designed for this task. The anode profile, shown as dots, needs to be small so as not to impinge on the electrolyte flow regime and the essentially parallel electrolyte potential compensation.

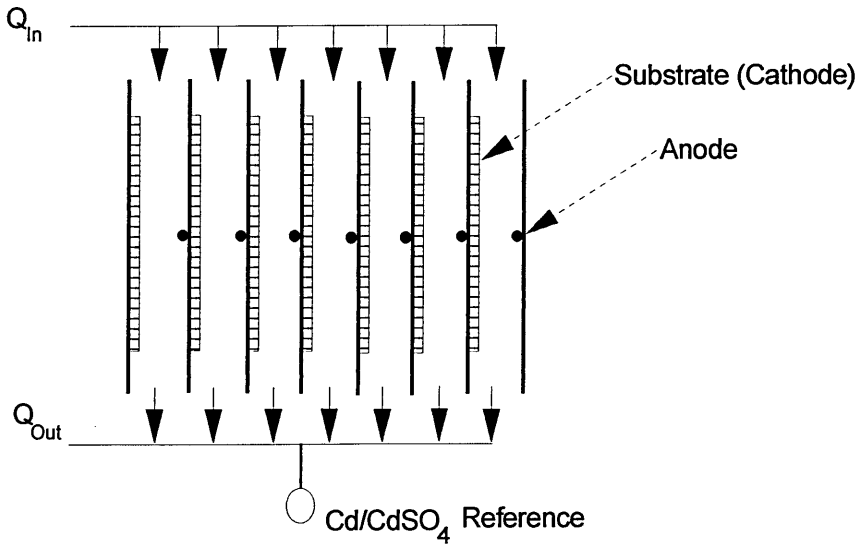

Figure 3.2. Schematic Diagram of BP Solar Multiplate Electrodeposition System.

Baths are made up from Analar Grade cadmium sulphate, Aristar grade sulphuric acid and Puratonic tellurium dioxide. New baths after a period of self-purification were producing high-grade material within a few days. The deionised water used for topping up and the preparation of solutions was 18 MΩ millipore water. Bath lifetime can be affected by impurity control i.e. a decline in product quality is observed as a particular impurity poisons a bath. Careful control of impurities led to bath lifetime measuring in years and, barring accidents, bath lifetimes should be indefinite.

3.5.1.2 Electrodeposition of CdS

Dennison 1993 has described the cathodic electrodeposition of CdS from aqueous solutions containing Cd^{2+} and $S_2O_3^{2}$ onto transparent conducting oxides. Solutions were made up of 0.2 M Cd^{2+} and 0.009 M $S_2O_3^{2-}$ using deionised water and either $CdCl_2$ or $CdSO_4$ and $Na_2S_2O_3$. The optimum conditions for CdS deposition from a Cd^{2+}/ $S_2O_3^{2-}$ solution were found to be at a potential of -0.69 ± 0.01 V against SCE at 90°C. Under these conditions, CdS films of thickness 60-100 nm can be grown in approximately 60 minutes. Dennnison 1993 describes that at 90°C decomposition of the electrolyte occurs with the formation of CdS in the bulk of solution. The decomposition is accompanied by a trend towards increasingly poor performance during the subsequent electrodeposition of CdTe, as the CdS bath aged over a period of two to three days. This led to the peeling of both the CdTe and CdS films from the TCO substrate when CdS films deposited from a CdS bath more than two days old were used. As a result, CdS deposition baths were discarded after a maximum of two days of use. For the electrodeposition of CdS thin films to become economically feasible, a longer bath-life and more reliable performance is required.

3.5.2 Monosolar Inc. and the University of California

The first efficient electroplated CdS/CdTe heterojunction solar cell was reported by the groups working at Monosolar Incorporated and the University of California, Los Angeles (UCLA) in 1982 [Basol et al 1982, 1982a]. Initial device efficiencies were 7-8% for 0.02 cm^2 area devices. By the late 1980's devices with efficiencies of 10.3% were being produced with areas of 0.16 cm^2 [Basol 1988].

3.5.2.1 Electrodeposition of CdTe

The CdTe electrodeposition system used by Monosolar/UCLA is shown in Figure 3.3, this consisted of a 0.5M $CdSO_4$ electrolyte, a calomel reference electrode, two anodes (one tellurium and one inert) and a potentiostat that controlled the plating potential. The use of two anodes allowed the tellurium ion concentration to be kept constant (in this case approximately 30 ppm). The system allowed the switching of the current through either anode. Passing the current through the tellurium anode lead to anodic dissolution of the anode and introduction of tellurium ions into the plating solution. When the required tellurium ion concentration was reached, as determined by atomic absorption, the current was switched to the inert anode. This switching was performed periodically during deposition so to maintain constant tellurium ion concentration.

This group was the first to demonstrate the importance of Cl^- ions in the formation of high efficiency CdTe solar cells [Basol et al 1986]. The inclusion of Cl^- ions improved the J_{SC} from 11.2 $mAcm^{-2}$ with no Cl^- ions to 19 $mAcm^{-2}$ with 0.015 M Cl^- ions. The pH of the solution was adjusted to 1.5-2.0 using H_2SO_4. A deposition temperature of 90°C and magnetic stirring was used to achieve circulation of the solution.

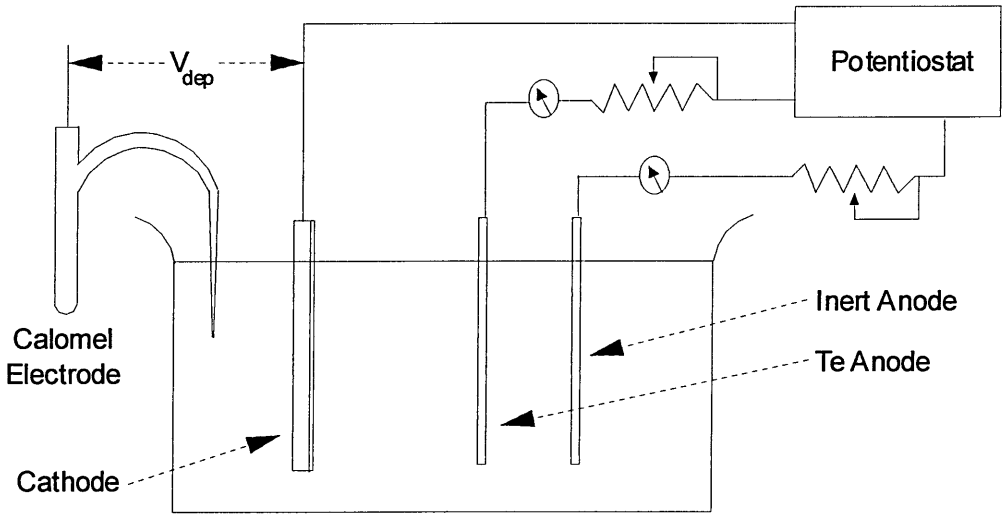

Figure 3.3. Dual Anode Electrodeposition System

Basol described the key step in the fabrication process of high efficiency electrodeposited CdS/CdTe solar cell which he called the "Type Conversion-Junction Formation" (TCJF) procedure that involved heating the as deposited CdTe layers in air at around 400°C [Basol et al 1983, 1985, Basol 1984]. Without this step the CdS/CdTe structures indicated a rectifying junction close to the metal/CdTe interface rather than at the CdS/CdTe interface. It is thought that the annealing step converted the originally n-type CdTe films into p-type and thus a rectifying junction was formed between the type converted CdTe layer and the CdS film.

3.5.2.2 Electrodeposition of CdS

The CdS electrodeposition bath consisted of a $CdCl_2$ solution (0.1 - 0.5 M) containing sodium thiosulphate (0.01 M) [Basol 1988]. The deposition potential was kept at -0.65 V against SCE. The electrolyte was stirred and heated to 85-90°C. The typical plating current density was about 0.03 $mAcm^{-2}$, giving a deposition rate of 15 $Åmin^{-1}$. Well-adhering CdS films 500 - 1000 Å were deposited onto TCO substrates.

3.5.3 University of Queensland

The initial work of Danaher 1978 on the aqueous deposition of CdTe led to the development of CdS/CdTe solar cell by the mid 1980's, both the CdS and CdTe being formed by aqueous electrodeposition [Danaher et al 1985]. By the early 1990's, an efficiency of 13.1% had been achieved, the second highest efficiency for a CdS/CdTe device produced by electrodeposition [Morris et al 1990].

3.3.5.1 Electrodeposition of CdTe

The CdTe deposition system consisted of a bath solution of pH 2.0, made up as 2.5 M Cd^{2+} and 120 ppm tellurium concentration using $3CdSO_4 \cdot 8H_2O$ (Analytical grade reagent), H_2SO_4, Milli-Q water and tellurium ions which were injected from a specpure tellurium rod.

The anode used was a slit anode system of a tellurium and carbon rod. The anode was produced by melting tellurium crystal pieces in a reducing hydrogen atmosphere in a tapered silica tube mould and a carbon rod was slid into the melt [Morris 1992]. To avoid cracks in the tellurium anode it was brought down to room temperature over a 12-hour period. The reference electrode used in this work comprised cadmium wires immersed in saturated cadmium sulphate solution, a combination chosen to avoid the introduction of different materials in contact with the solution.

Electrolysis of acidified cadmium sulphate solution was used to purify the solution. In this step, a platinum cathode was used at such a potential that some cadmium was being plated out. Electropurification was carried out for two to three hours generally but, when longer periods were needed, the preferred cathode was a platinum wire contacting a mercury pool separated by a glass frit from the main bath solution. This mercury pool dissolved the discharged cadmium whereas in similar conditions with a platinum cathode, long strings of cadmium crystals grew out from the platinum.

The CdTe films of around 2 μm thickness were deposited in approximately two hours at quasi-rest potentials of + 25 ± 5 mV relative to the measured cadmium deposition potential (approximately -620 mV with respect to the SCE) using a split anode system (tellurium and carbon) [Das 1993].

3.5.3.2 Electrodeposition of CdS

CdS deposition solution was made with $CdCl_2 \cdot H_2O$ dissolved in Milli-Q water (18 MΩ) to make the solution 0.2 M Cd^{2+} [Das 1992]. The solution was kept at 90°C and stirred. A small platinum wire was used as the cathode (approximately -620 mV with respect to SCE) to measure the cadmium potential. The bath solution was then electropurified for 12 hours at 5 mV more positive than the measured cadmium potential. Sodium thiosulphate was added to the purified solution to make 0.01 M $S_2O_3^{2-}$. The pH was adjusted to 2.5 using HCl. A CdS deposition potential 40 mV more positive than the measured cadmium potential was used. The counter electrode was a spectroscopic grade carbon rod. In about two hours a 80-100 nm thick CdS film yellowish in colour was deposited.

This group reported a comparison of CdS/CdTe cells having CdS produced by either electrodeposition or vacuum evaporation [Morris et al 1991]. This work showed those CdS/CdTe solar cells having efficiencies greater than 10% could be achieved using both techniques, although it was discussed that electrodeposition has a number of advantages when large-scale commercial development was to be pursued.

3.5.3.3 Periodic Pulse Electrodeposition of CdS and CdTe

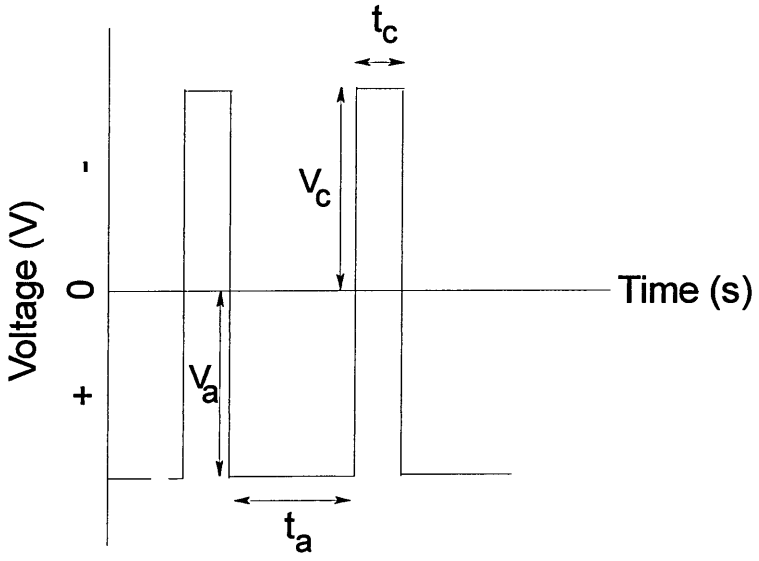

Figure 3.4. Periodic Pulse Waveform Used to Electrodeposit CdS.

Work has been performed on the Periodic Pulse Electrodeposition (PPE) of both CdS [Morris 1992a] and CdTe [Morris 1993, Morris 1996]. PPE may have the advantages of possible beneficial effects on the morphology, coverage and compositional uniformity. It is possible with PPE to initiate a variety of transport processes, enhance the rate of nucleation and provide different electrocrystallization conditions with several adsorption and desorbtion phenomena occurring during the different pulses. The waveform for the PPE of CdS is shown in Figure 3.4. It is a square wave with four variables: anodic voltage (V_a) and anodic on time (t_a), cathodic voltage (V_c) and cathodic on time (t_c). The preferred deposition conditions were: V_a = +0.6 V, V_c = -0.95 V (SCE), t_a = 2 s and t_c = 1 s, with a solution whose composition was 0.2 M Cd^{2+}, 0.01 M $S_2O_3^{2-}$ and pH = 2 at a temperature of 90°C. It was found that CdS prepared by PPE adhered more strongly to FTO than to ITO and better to either substrate than films prepared by DC methods. The PPE CdS films were preferable for the production of larger area CdS/CdTe devices.

3.5.4 AMETEK

AMETEK's early work concentrated on solar cells using the MIS design i.e. using metal-insulator-semiconductor structures [Fulop et al 1981, So et al 1984]. The CdTe was electroplated onto a cadmium film 1000 Å thick on nickel-clad stainless steel. After a heat treatment for one hour at 310°C in air, a 25 Å layer of aluminium oxide (the I layer) was deposited followed by a 200 Å layer of nickel (the M layer). The most efficient MIS device produced had a V_{OC} of 0.723 V, a J_{SC} of 18.7 $mAcm^{-2}$ and an efficiency of 8.6% [Fulop et al 1982]. Two primary problems associated with the MIS devices were that (a) the built in voltage is limited by interface states to a value of approximately 0.9 V and (b) the optical transmission of the nickel layer is approximately 70%. These limitations can be overcome using the CdS/CdTe heterojunction structure.

The AMETEK CdS/CdTe device was produced as follows, CdS was deposited onto ITO coated glass substrates by pyrolysis at a temperature of 450°C from an aqueous mist containing dissolved $CdCl_2$ and thiouria, a typical film thickness was 0.15 μm. CdTe was electroplated, as in the MIS design, to thickness of 2 μm. A 4 cm^2 cell produced a J_{SC} of 22 $mAcm^{-2}$, a V_{OC} of 740 mV and an efficiency of 10.4% [Meyers 1988].

3.5.4.1 n-i-p Solar Cells

AMETEK describe the main problems associated with p-CdTe heterojunctions as being

(a) Difficulty of preparing high conductivity films
(b) Difficulty of making low resistivity contacts
(c) Low minority carrier lifetimes

To overcome these problems AMETEK proposed to use a p-i-n structure to accommodate the innate properties of CdTe rather than overcome them [Meyers 1986, 1988, 1988a]. The structure chosen was CdS/CdTe/ZnTe. An idealised energy band diagram for the CdS/CdTe/ZnTe is shown in Figure 3.5. High resistivity rather than low resistivity films are desired and the collection of charge carriers is assisted by the field in the I layer.

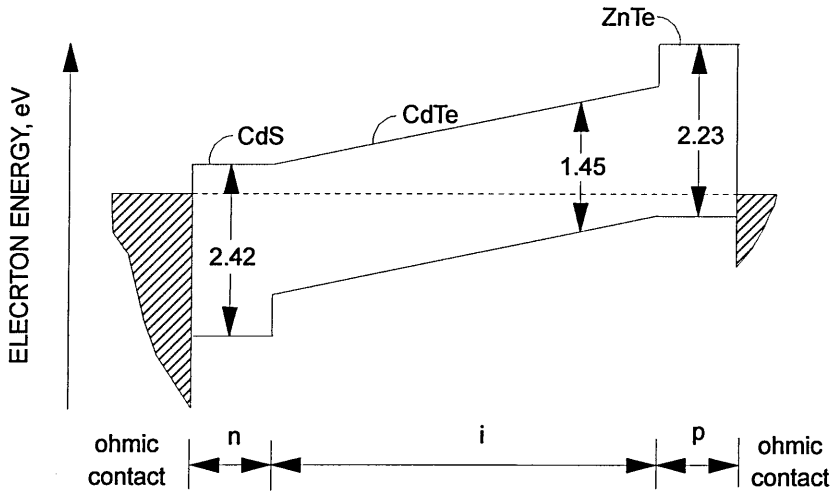

Figure 3.5. Idealised Energy Band Diagram of the CdS/CdTe/ZnTe n-i-p Solar Cell.

Fabrication procedures for the n-i-p solar cell were similar to those for CdS/CdTe heterojunctions except that a 0.06 μm layer of ZnTe was vacuum evaporated onto a 250°C surface of CdTe. Small area (1 cm^2) devices have been produced with efficiencies of 11% (J_{SC} = 20.1 $mAcm^{-2}$, V_{OC} = 763 mV and FF = 0.72) [Meyers 1989]. A submodule consisting of ten solar cells, each with an area of 5.1 cm^2, was constructed using nickel for the back contact metal. This module had an active area efficiency of 9.3% (total area efficiency of 6.1%), a J_{SC} of 24.5 $mAcm^{-2}$, a V_{OC} of 0.7 V and FF of 0.54 [Meyers 1988]. It is now believed that AMETEK has left the field of thin film CdTe production [Zweibel et al 1993].

3.5.5 The University of Texas at Arlington, Texas

This group performed some of the pioneering work on the electrodeposition of CdTe in the early 1980's. CdS layers were grown by either vacuum deposition or solution growth. The CdTe electrodeposition system [Bhattacharya 1984] consisted of an aqueous solution of 1M $CdSO_4$ and 10^{-5}-10^{-3} M TeO_2, the pH being adjusted to 2.5-3.0 using H_2SO_4. Initially, the TeO_2 was speciated with NaOH (approximately pH 9-10) and then the solution was brought into the acidic pH range (approximately pH 1-3) by the slow addition of H_2SO_4. The initial solution in NaOH allows the introduction of higher TeO_2 concentrations in the bath. Nominal deposition potentials ranging from -0.65 to -0.85 V vs SCE and current densities in the range 0.3-0.5 $mAcm^{-2}$ were used. A conventional three-electrode cell was employed, the counter electrode being either a Pt spiral or a glassy C electrode. All depositions were carried out at temperatures above ambient (40-60°C).

A device with structure ITO/CdS/CdTe/Au consisting of a vacuum deposited CdS layer 0.3 μm thick, an Arsenic doped CdTe layer approximately 2 μm thick gave an AM1 efficiency of 4.5% (V_{OC} = 0.436 V, J_{SC} = 23 $mAcm^{-2}$, FF = 0.44) [Bhattacharya 1985].

3.5.6 Laboratoire "Physique des Liquides et Electrochimie" Paris and Laboratoire d'Electrochimie et de Chimie Analytique, Paris

These two groups have produced individual and collaborative papers on the electrodeposition of CdTe and are therefore, described in a single section. One group has produced CdS/CdTe structures on tin oxide coated glass [Kampmann et al 1995]. CdS was prepared by CBD [Ortega-Borges 1993]. The electrodeposition of CdTe was carried out in an aqueous solution of sulphuric acid, pH 2.5, containing 0.8 M $CdSO_4$ and 3 x 10^{-4} M $HTeO_2^+$. The reference electrode was a cadmium electrode immersed in a 0.8M $CdSO_4$ solution and placed in a compartment separated from the deposition solution by a fritted glass junction. The electrodeposition temperature was 85°C. The constant potential applied to the tin oxide contact for the electrodeposition of CdTe was varied within the region of 65 mV positive to the Cd/Cd^{2+} potential in the same solution. The Cd/Cd^{2+} potential at the deposition temperature (85°C) lies at about -0.4 V SHE. Structural and optical results were presented but no solar cell characteristics were provided.

This group has claimed to produce epitaxial (111) CdTe films on $(\bar{1}\,\bar{1}\,\bar{1})$ InP single crystals by a one step electrodeposition process [Lincot et al 1995]. It was found that the epitaxy was markedly improved when the InP substrate was covered with a thin film (20-30 nm) of epitaxial CdS grown by chemical bath deposition which acts as an interfacial buffer layer. The electrochemical deposition of CdTe was performed under the same conditions described above. Layers of CdTe approximately 0.1 μm thick were deposited. Structural characterisation of the films and determination of the epitaxial relations with the substrate were carried out using RHEED and XRD using a five-circle goniometer. The epitaxy of CdTe took place with a direct continuation of the InP lattice.

3.5.7 Charles University Prague

A group at the Charles University, Prague has produced devices with the structure glass/SnO_2/CdS/CdTe/Au where the CdTe was grown by electrodeposition [Touskova et al 1992, Valvoda et al 1986]. Polycrystalline layers of CdS were prepared by spray pyrolysis using a solution of cadmium chloride and thiourea with equal concentrations of Cd^{2+} and S^{2-} ions. The thickness of the CdS layers was 0.2 - 0.7 μm.

Layers of CdTe with thickness of 1.0 - 1.5 μm were electrochemically deposited from an aqueous solution containing $CdSO_4$, TeO_2 and $CdCl_2$ at deposition potentials from -500 to -600 mV against SCE. Structural, optical and electrical (I-V and C-V) characteristics are presented but no I-V characteristics under illumination were presented. It is not possible therefore, to determine the solar energy conversion efficiency of these devices.

3.5.8 Colorado School of Mines

Colorado School of Mines is the most recent group to come into the field of electrodeposition of CdTe [Qi et al 1996]. CdS layers were deposited onto SnO_2 coated glass by spray pyrolysis. Cadmium telluride was deposited from a plating solution containing 1.2 M $CdCl_2$ with 16 - 20 ppm tellurium and occupied a total volume of 30 litres. The solution was adjusted to a pH of 2 by addition of HCl or KOH. The solution temperature was maintained at 80°C. A dual anode system consisting of a tellurium and a cadmium anode were employed. The current ratio between these two anodes was adjusted between 2:1 and 3:1 during the film deposition. The sample potential was set at -600 mV against Ag/AgCl reference electrode. A current density of 0.35-0.40 $mAcm^{-2}$ was passed between the cathode (sample) and the anodes yielded a typical growth rate of 1 μm/hour. XRD and SEM results were presented but no solar cell characteristics were given.

3.6 Doping of CdTe

A key factor in making semiconductor devices, including photovoltaic devices, is the ability to incorporate controlled amounts of dopant elements in various regions of the devices. It is well understood that dopant elements can determine the conductivity characteristics of a semiconductor i.e. whether it is n-type or p-type. The concentration of dopants present can control the concentration of charge carriers, i.e. the resistivity of the semiconductor. In thin film semiconductor devices it is generally necessary to incorporate a dopant element during the deposition process since bulk semiconductor doping techniques, such as diffusion, cannot be carried out without damaging the device structure. Zanio 1978 has described the influence of dopants on the electrical characteristics of CdTe.

3.6.1 Doping of CdTe Grown by Non-Aqueous Electrodeposition

Balakrishnan et al 1991 reported in-situ phosphorous doping of electrodeposited CdTe films grown from organic electrolyte. Anhydrous phosphorous in the range 1×10^{-5} M - 4×10^{-4} M where introduced into the dimethyl sulphoxide electrolyte. A phosphorus concentration of 6×10^{-5} M - 6×10^{-4} M was found to produce a reduction in the CdTe resistivity. Electrical measurements under illumination were not reported on these films so no indication of the solar cell performance of these films was given.

Von Windheim et al 1990 doped CdTe grown from non-aqueous solvents with indium, copper, silver, Cadmium, Tellurium, and oxygen by codeposition, electromigration [Talasek et al 1986] and diffusion. CdTe samples were prepared as described by Darkowski 1985. The deposition solution contained 2-10 mM cadmium perchlorate or trifluoromethane sulfonate, 120 mM lithium perchlorate or sodium trifluoromethane sulfonate and 7-26 mM phosphine telluride. Current density ranged from 0.1 to 0.5 $mAcm^{-2}$ for constant current deposition, and potential ranged from -650 to -1600 mV vs Ag/AgCl for constant potential deposition. Deposition temperatures of 50-120 °C were used.

The different dopants and methods of doping for these experiments are outlined in table 3.1. For electrical characterisation, films were removed from the conductive substrate by attaching a plate to the surface of the film using a non-shrink epoxy. After the epoxy was dried overnight, the epoxy and the cadmium telluride film came away with the plate when force was applied between the plate and the substrate. Crack and pinhole free samples with areas as large as 3 cm^2 could be removed from ITO coated glass with a success rate greater than 90%.

Dopant	Dopant Source	Doping Conditions	Heat Treatment
Electromigration [Von Windheim et al 1990]			
Ag	0.1 M silver triflouromethanesulfonate	In water with lithium perchlorate as supporting electrolyte	10 min at 400°C under argon
Cd	0.05M cadmium perchlorate	In propylene carbonate with lithium perchlorate as supporting electrolyte	10 min at 400°C under argon
In	0.006 M indium chloride	In propylene carbonate with lithium perchlorate as supporting electrolyte	10 min at 400°C under argon
Co-electrodeposition			
In	0.6 μmol indium chloride	Added to standard CdTe deposition solution [Darkowski 1985]	1 h at 200°C followed by 10 min at 400°C under argon
Diffusion [Von Windheim et al 1990]			
Te	0.5g of tellurium powder	Evacuated in sample chamber of stainless steel tube	10 min at 400°C
O_2	Air	Heat treated in air	10 min at 400°C

Table 3.1. Method and Conditions for Doping Experiments of Electrodeposited CdTe.

Von Windhiem et al summarises the results as follows. The resistivity and activation energy (E_A) are affected by the nature (donor or acceptor) and density of dopant. Thus, acceptors lower the values of the two parameters above, but low densities of a donor increase them. Oxygen has little effect on E_A but decreases the resistivity somewhat. In addition, the photoresponse (i.e. the decrease in resistivity due to 120 mW insolation of white light) appears to mirror the decrease in E_A and resistivity. While air exposure of the films has little effect on E_A and the resistivity, it causes a marked decrease in the photoresponse.

This work was not used for the production of solar cells, although earlier [Darkowski 1987] this group had produced CdS/CdTe solar cells by non-aqueous electrodeposition. CdS was deposited from a solution containing 20 ml diethylene glycol, 2 ml H_2O, 0.1 g sulphur, 0.4 g lithium perchlorate and 0.3 g cadmium perchlorate [Baranski et al 1981, Baranski 1984]. Constant current (1 $mAcm^{-2}$) deposition at 120°C was carried out under nitrogen in a two-electrode cell consisting of an ITO cathode and a cadmium anode. A deposition period of 90 seconds gave CdS films having thicknesses around 500 Å. CdTe was deposited as described above. 1.0 μm of CdTe was deposited in about 30 minutes. A 0.07 cm^2 device under 40 $mWcm^{-2}$ illumination gave an efficiency of 5.2% (V_{OC} = 400 mV, J_{SC} = 11.2 $mAcm^{-2}$, FF = 0.43).

3.6.2 Doping of CdTe Grown by Aqueous Electrodeposition

Although the field of aqueous electrodeposition of CdS/CdTe solar cells has been widely reviewed the effect of impurities on these devices has not been widely reported. It has been shown that electrodeposited CdTe films contain fewer impurities than CdTe single crystal supplied as 5N pure as measured by SIMS [Lyons et al 1984]. This indicates that the electrodeposition process is acting to purify the nominally unpure (AR Grade) chemicals used to prepare electrolytes to better than 5N grade. The same group [Lyons et al 1989] reported on an investigation into sources and identification of impurities in electrodeposited CdTe films. The techniques of ICP-OES and atomic absorption were used to investigate electrolytes. SIMS was used to investigate the CdTe films. It was shown that electrodeposition of $CdSO_4$ solution removed a number of impurities prior to the introduction of tellurium ions, although the introduction of tellurium ions also introduced impurities. An Ag/AgCl/KCl (1M) reference electrode was noted as being a source of K^+ ions in the bath solution even when separated from the bath by a porous frit.

Attempts to intentionally dope electrodeposited CdTe have not been widely reported in the literature. Valvoda et al 1986 tried to introduce indium and copper as dopants into cathodically deposited CdTe on nickel substrates from an aqueous solution of $CdSO_4$ and TeO_2. To dope the films with indium 10^{-2} % $In_3(SO_4)_3$ was added to the electrolyte and deposition potentials of -680 to -720 mV against Ag/AgCl were used. To dope the films with copper 10^{-2} % $CuSO_4$ was added to the electrolyte and a deposition potential of -640 mV against Ag/AgCl was used. Indium doped CdTe produced rectifying gold contacts indicating n-type conductivity. Copper doped CdTe showed no rectification with gold contacts indicating p-type conductivity. The resistivity of the copper doped samples was approximately100 Ωcm that is an order of magnitude greater than for undoped samples.

Initial attempts to dope electrodeposited CdTe with copper [Bhattacharya et al 1985a] showed increased copper inclusion in the films with increased copper ions in the deposition bath. No reports of solar cell parameters such as V_{OC} or I_{SC} were quoted for this device. Copper doping was found to cause problems due to copper diffusion and short circuiting effects. Subsequently, arsenic was used in an attempt to produce as-grown (i.e. not requiring heat treatment in air) p-type films [Bhattacharya et al 1985]. A small area device (0.2 cm^2) gave an AM1 efficiency of 4.5% (V_{OC} = 0.436V, J_{SC} = 23 $mAcm^{-2}$, FF = 0.44) although no correlation was made between the degree of As doping and the efficiency of the device.

Ondris 1989 produced a patent that included the use of copper and silver ions as dopants in the CdTe electrodeposition bath. Copper and silver ions were added in the range 6 to 24 ppb to the solution. With no added copper or silver an efficiency of 5.66% was achieved, addition of copper ions in the range 6-12 ppb gave an efficiency of 9.18% and addition of silver ions in the range 6-12 ppb achieved an efficiency of 9.82% (under AM 1.5 conditions).

Dennison 1994 carried out the most comprehensive work on the intentional doping of electrodeposited CdTe. His work observed the effect of deliberately adding Cl^-, Cu^{2+} and Ag^+ ions into the deposition bath. Again, atomic absorption and ICP-AES were used to measure impurities and SIMS was used to measure impurities in the films. This was the first significant work to study the effect of deliberately added impurities on the performance of the CdS/CdTe solar cell.

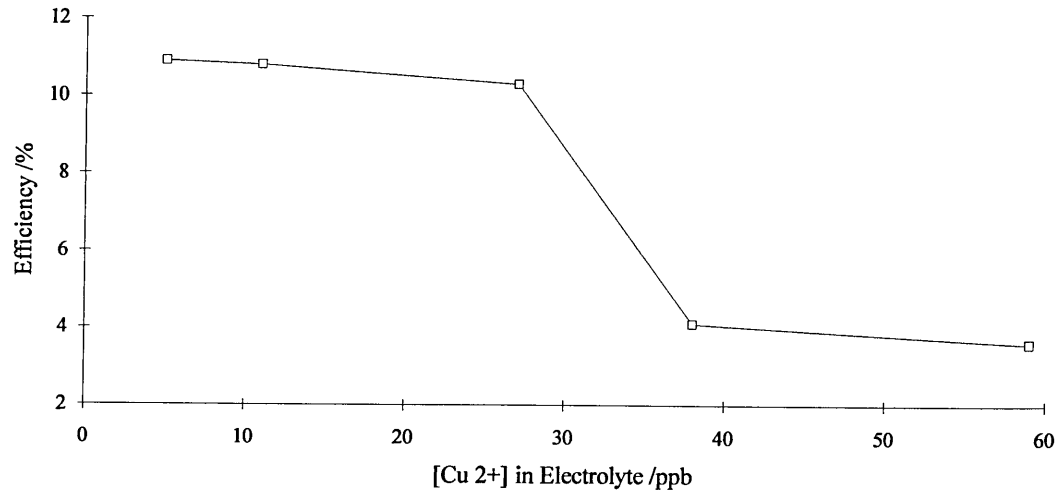

Figure 3.6. Graph Showing Device Efficiency as a Function of [Cu^{2+}] in the CdTe Electrolyte [Dennison 1994].

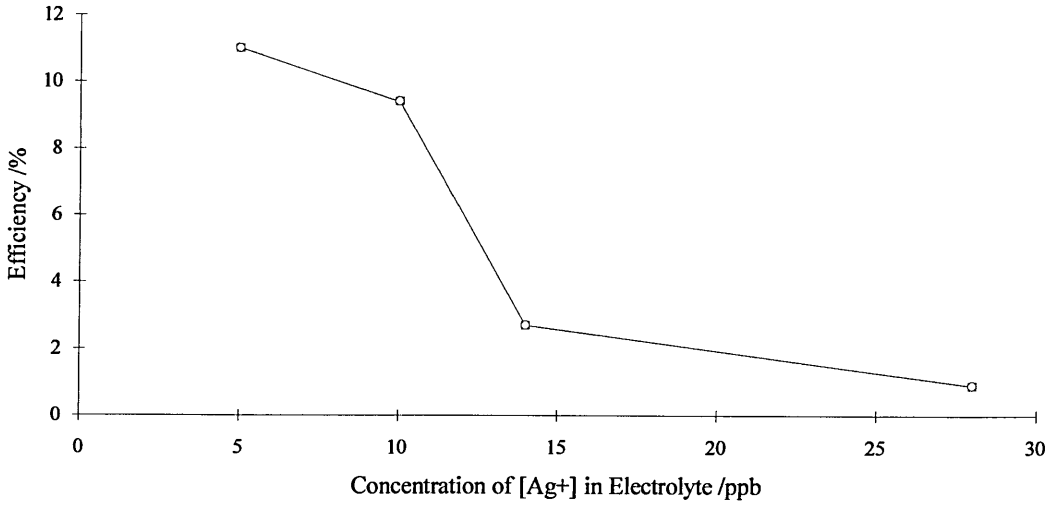

Figure 3.7. Graph Showing Device Efficiency as a Function of [Ag^+] in the CdTe Electrolyte. [Dennison 1994].

Dennison 1994 found that levels of Cu^{2+} of greater than 30 ppb in the deposition bath led to dramatically reduce device efficiencies as shown in Figure 3.6. At a Cu^{2+} concentration of 59 ppb, both efficiency and V_{OC} showed large reductions compared to the Cu^{2+} free case. Other device parameters also showed substantial changes due to Cu^{2+} addition. In particular the shunt resistance of the device decreased from approximately 500 kΩ at 5 ppb to less than 100 kΩ at approximately 60 ppb, which is likely to have caused a reduction in FF. Dennison describes the transition from good to bad performance at 30 ppb Cu^{2+} in the electrolyte as possibly due to copper being incorporated substitutionally into the host lattice and acting as an acceptor in the CdTe, or at least as an inactive species, below 30 ppb Cu^{2+} in the electrolyte. Above 30 ppb Dennison suggests the copper is incorporated interstitially and behaves as a donor species[Dennison 1994].

Levels of Ag^+ of greater than 10 ppb in the deposition bath led to reduced device efficiencies, as shown in Figure 3.7, and reduced V_{OC} as shown in Table 3.3. The effect of silver is more severe than the case of copper, at an Ag^+ concentration of 28 ppb, when both efficiency and V_{OC} show large decreases compared to the Ag^+ free case. The data in Table 3.3 shows that even at concentrations as low as 10 ppb, Ag^+ has a detrimental affect on the CdS/CdTe device. No indication of other solar cell performance parameters such as J_{SC} or FF is given.

Chlorine was found to have a beneficial effect on device performance, the optimum value being of the order of 300 ppm Cl^- ions in the deposition bath. Dennison points out that at the potentials used in his experiments there is no direct electrochemical reaction for Cl^- at the operating potentials used. He suggests chlorine incorporation may occur by association of Cl^- with the Cd^{2+} ion.

3.7 Chlorine Treatment of CdTe Films

The presence of $CdCl_2$ at some stage of device fabrication appears to be important for CdS/CdTe solar cells made by a variety of different methods [Abou-Elfotouh et al 1993]. $CdCl_2$ has a melting point of 568°C and is a well-established fluxing agent for both CdS and CdTe [Ikegami 1988]. Dipping CdTe films into $CdCl_2$/methanol solution and thus forming a thin layer of $CdCl_2$ on their surfaces before heat treatment is now commonly used to induce grain growth in those films grown by different techniques such as vacuum evaporation [Birkmire et al 1992], MBE [Ringel et al 1991], MOVCD [Sudharsanan et al 1991] and CSS [Loginov et al 1996, Al-Allak et al 1996].

The actual physical processes taking place in this beneficial procedure are still a matter for discussion. Grain growth (recrystallisation) is sometimes observed, but often grain boundary passivation seems to be important. CdS/CdTe interdiffusion [Birkmire et al 1992], reduction of interface recombination [Rohatgi 1992] and reduction of recombination and generation centres in the space charge region [Rohatgi 1992] have been observed.

High efficiency (10-11%) CdTe/CdS solar cells have been produced by electrodeposition without the use of $CdCl_2$ surface treatment [Dennison 1994, Das et al 1993]. The plating solution used for the deposition of these films however, contained Cl^- ions as an additive. The use of Cl^- ions in the deposition bath was first described by Basol et al 1986. He showed the inclusion of Cl^- ions brought about a significant improvement of the short circuit current of these devices.

In addition to the effects of $CdCl_2$ on the structural properties of CdTe, the possible influence of chlorine on the electronic properties of the $CdCl_2$ treatment of CdTe films needs to be considered. Several investigators have studied the effects of chlorine in single crystal CdTe by PL and DLTS measurements [Ringel et al 1991, Cotal et al 1990, Das et al 1990, and Figueroa 1986]. Chlorine is a donor in CdTe and is also known to form defect complexes with cadmium vacancies, which are produced during heat treatment. Chlorine-cadmium vacancy complexes are acceptor type and give rise to shallow and deep energy levels depending on the type of defect complex. According to the literature, the chlorine-cadmium defect complexes have energies in the range $E_v + 0.15$ to $E_v + 0.9$ eV [Ringel et al 1991].

Chapter 4.0: Experimental Techniques

4.1 Introduction

Experimental techniques employed in this study can be divided into those employed in the production of the thin film glass/TCO/CdS/CdTe/metal devices and those used for the characterisation of the resulting thin film devices. The general techniques used were electrical, structural and optical techniques. Semiconducting layers were deposited by electrodeposition, the metal layer being deposited by vacuum evaporation. The choice of electrodeposition for the production of the semiconducting layers is primarily an experimental one. The advantages of using this technique are that electrodeposition equipment is relatively inexpensive (c.f. vacuum deposition equipment), it is readily scaleable for large area, large-scale industrial production and the chemicals used are relatively inexpensive and can be recycled.

Electrical characterisation was performed using solar simulated and dark current-voltage (I-V) measurements. This indicated how well produced devices work as solar cells and how various treatments performed on the devices affected the solar cell characteristics. Optical characterisation was performed using the optical absorption technique. This indicated how the semiconducting layers perform as absorbers of light and gives a value for the band gap of the material. Structural characterisation was performed using X-Ray Diffraction (XRD) and Scanning Electron Microscopy (SEM). XRD gave information on the composition and degree of crystallinity of the deposited films. SEM enabled the determination of the morphology of the deposited films.

4.2 Electrodeposition

4.2.1 Potentiostatic Electrodeposition

Cathodic deposition is preferred to anodic deposition due to the self-limiting effects observed with anodic methods. The aim of using the cathodic electrodeposition method employed was to measure the potential of the working electrode (the cathode) against a third electrode whose potential in the solution was known and was a constant. This electrode is known as the reference electrode. The potential impressed across the working electrode and its counter electrode (the anode) could then be adjusted to the level that would impart the desired potential to the cathode with respect to the reference electrode, as shown in Figure 4.1. This is known as potentiostatic electrodeposition.

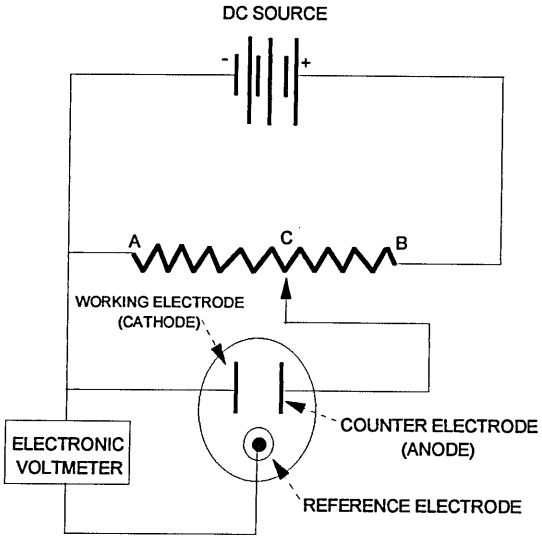

Figure 4.1. Circuit Diagram for Apparatus used in Electrolysis at a controlled Cathode Potential. Contact C is Continuously Adjusted to Maintain the Cathode Potential at the desired level.

The preferred reference electrode system for this work was the silver/silver chloride (Ag/AgCl) electrode. The Ag/AgCl electrode [Ives et al 1961] consisted of a silver electrode in contact with solid silver chloride immersed in a solution of potassium chloride that has been saturated with silver chloride. Ag/AgCl electrodes have the advantage that they can be used at temperatures greater than 60°C.

4.2.2 CdTe Electrodeposition Cell

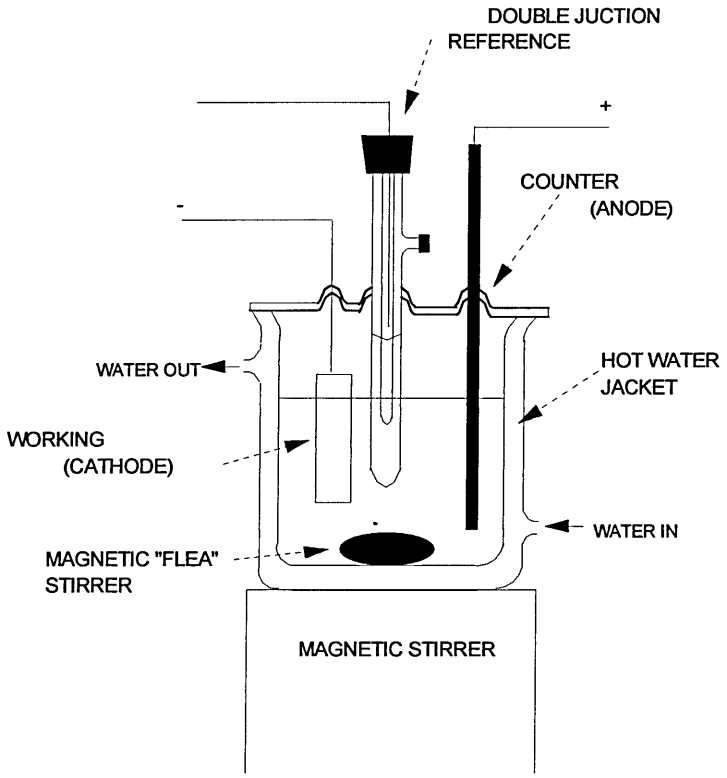

Figure 4.2. Schematic Diagram of Electrodeposition Cell.

The CdTe electrodeposition cell (Figure 4.2) was a 1-litre water-jacketed glass beaker. The water jacket is connected to a hot water bath to enable the cell to be maintained at a constant 90°C. The cell is totally enclosed so as to avoid excessive evaporation of electrolyte. This is particularly important as evaporation leads to composition variations within the electrolyte, which can lead to variation in deposition conditions. In addition variations in electrolyte volume affect experiments involving need for the inclusion of additional elements. A refluxer (not shown in Figure 4.2) was used to prevent pressure build up within the vessel. Stirring was achieved using a stirrer/hot plate with a magnetic "flea" stirrer in the electrolyte solution. Strict stirring control is vital, as stirring aids electrolyte transport between electrodes and, hence, deposition current. Excessive stirring leads to high deposition currents, which lead to unstable growth and insufficient stirring leads to low film growth rates.

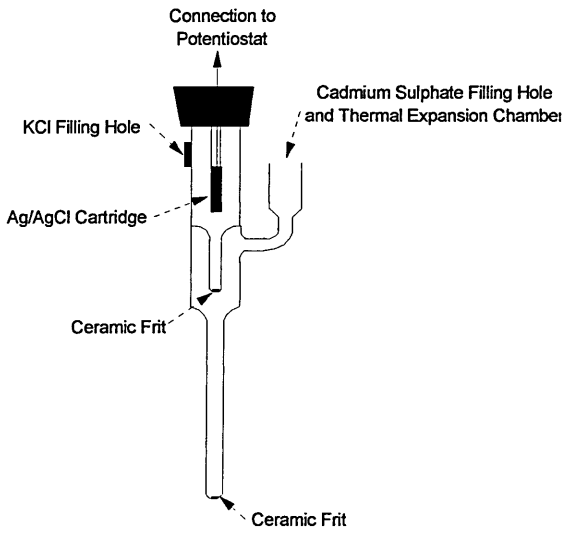

Figure 4.3. Schematic Diagram of the Double Junction Ag/AgCl Reference Electrode used for CdTe Deposition.

The reference electrode (Figure 4.3) used was a double junction Ag/AgCl electrode (constructed for this project by Russell pH Ltd). This electrode had two compartments, the inner compartment contains the Ag/AgCl reference. The outer compartment was filled with the same concentration of purified $CdSO_4$ electrolyte as that in the deposition electrolyte. This electrode system was used to reduce contamination by KCl of the deposition electrolyte from the Ag/AgCl reference. The length of the bottom compartment was 240 mm, to prevent diffusion of KCl from the top compartment through the $CdSO_4$ solution in the bottom compartment into the deposition solution. This design also ensured that the KCl compartment and KCl filling hole were outside the electrodeposition cell. The $CdSO_4$ in the bottom compartment was changed daily to avoid excessive contamination by KCl. The top compartment being outside the electrodeposition cell was at room temperature. This resulted in a temperature gradient down the cell to the point of contact with the electrolyte. Removing the Ag/AgCl reference form the electrodeposition cell had the advantage of reducing the temperature at which the reference operated. It is not advisable to operate Ag/AgCl reference electrodes at temperatures greater than 65°C.

The counter electrode used was either platinum gauze or a specroscopically pure carbon rod. The working electrode was CdS coated Glass/TCO and the working area of glass/TCO/CdS used to deposit CdTe was 2 cm^2. The connection of the TCO to the external circuit was achieved using a Pt, wire held in position using a PTFE pressure clip. The atmosphere within the deposition cell contained acidic electrolyte vapour, which attacks all non inert materials within the cell. To combat this problem all components within the cell were made either from glass, PTFE, platinum or carbon.

Deposition potentials were maintained using a EG+G Par Model 362 Scanning Potentiostat. QRP measurement and control was performed using the method described by Panicker et al 1978. After initiating deposition, the current flow in the electrochemical cell was interrupted for approximately 0.3 seconds and the decay of the working electrode (Glass/TCO/CdS/CdTe) during the interrupt period was monitored. The potential decay was monitored directly on an X-Y plotter. When the current was switched off, the potential dropped rapidly, followed by a characteristically slower decay. The QRP could then be estimated and the applied potential adjusted as necessary to move the QRP into the range required.

4.2.2.1 CdTe Deposition Solution

The CdTe deposition solution was made with $3CdSO_4 \cdot 8H_2O$ (AR Grade) dissolved in Millipore water (18 MΩ Resistance) to make a solution of 0.5 M Cd^{2+}. This solution was then electropurified, as described in section 4.4. TeO_2 (5N Purity) was then added to the solution to make 150 ppm $HTeO_2^+$. The pH of the solution was adjusted to 1.8 ± 0.1 using H_2SO_4 (AR Grade). To ensure thorough dissolution of the added TeO_2 the solution was heated to 90°C and stirred for eight hours prior to commencing deposition of CdTe. Adjusting the solution pH prior to the addition of the TeO_2 aids the dissolution of the TeO_2 as dissolution is increased at lower pH. The $HTeO_2^+$ concentration in the solution was measured by an atomic absorption spectrometer.

4.2.3 CdS Electrodeposition Cell

The CdS electrodeposition cell is essentially the same as the CdTe deposition cell. The counter electrode used was platinum gauze and the reference electrode used was a double junction Ag/AgCl electrode. The working electrode was TCO coated glass, with a working area of 10 cm^2. Deposition potentials were maintained using an EG+G Par Model 362 Scanning Potentiostat.

4.2.3.1 CdS Deposition Solution

The CdS deposition solution was made with $CdCl_2 \cdot H_2O$ (Puratonic Grade) dissolved in Millipore water (18 MΩ Resistance) to make a solution of 0.2 M Cd^{2+}. This solution was then electropurified, as described in section 4.4. $Na_2S_2O_3$ (AR Grade) was added to the purified solution to make it 0.01 M $S_2O_3^{2-}$. The pH of the Cd^{2+} + $S_2O_3^{2-}$ solution was 4.5 ± 0.2. Deposition was performed at this pH or the pH was adjusted using HCl (AR Grade).

4.2.4 Voltametry

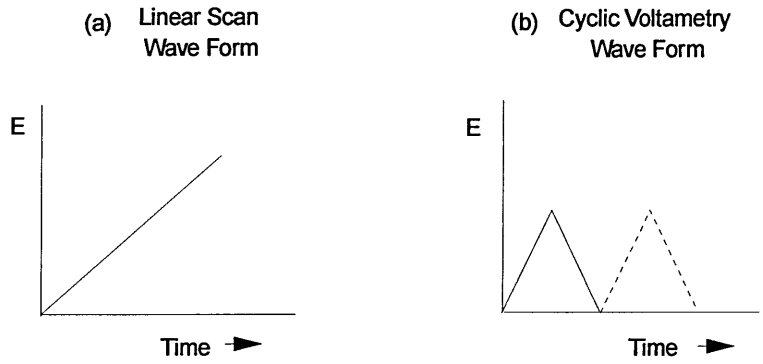

Figure 4.4. Potential Excitation Signals Used in Voltametry.

In voltametry, a variable potential excitation signal is impressed upon an electrochemical cell. The excitation signal elicits a characteristic current response upon which the method is based. The classical voltametric excitation signal is the linear scan shown in Figure 4.4a, in which the dc potential applied to the cell increases linearly as a function of time. The current that develops in the cell is then recorded as a function of time (and thus as a function of applied potential).

In the case of the triangular wave form, shown in figure 4.4b, the potential is cycled between two values, first increasing linearly to a maximum and then decreasing linearly, with the same numerical slope, to its original value. This process can be repeated numerous times, with the current being recorded as a function of time, to monitor initial deposition and subsequent growth of films.

Voltametry is used as a practical way of determining suitable deposition conditions for elements or compounds from the electrolyte. Ideally, there is no current flow until the deposition potential of the element is exceeded. In most practical cases, some extrapolation of both the baseline and rising portion of a current against voltage (I-V) plot is necessary to determine the deposition potential. A series of I-V plots with different solution concentrations will give the variation of deposition potential with concentration. Repeating this procedure for each element in the semiconductor will give the range of solution conditions under which co-deposition of the elements is possible. Danaher 1984 gives an example of this procedure for CdTe. Fatas et al 1984 and Jackowska 1986 give an example for CdS.

4.3 Glass/TCO Cleaning Procedure

Prior to deposition of films, the Glass/TCO superstates were thoroughly cleaned. The TCO's used were either SnO_2:F supplied by BP Solar or In_2O_3:F Supplied by Pilkington Glass. The superstrates were rinsed in Millipore water (18 MΩ Resistance) to remove any particles remaining from the cutting operations. The superstrates were cleaned in acetone, methanol and, isopropanol, respectively for 15 minutes in an ultrasonic bath, rinsing in Millipore water (18 MΩ Resistance) between each solvent clean. The superstrates were placed in a soxlet which was placed in a refluxer, and refluxed in dichloromethane (DCM) for 30 minutes. On removal from the refluxer, the superstrates were thoroughly rinsed in Millipore water (18 MΩ Resistance) before being placed in the deposition bath. This cleaning procedure removed any dirt or grease contamination from the superstrates.

4.4 Electropurification of Deposition Solutions

In order to reduce impurities in the depositions, pre-electrolysis of the solutions was performed. It has been shown that electrodeposited CdTe films had fewer impurities, as revealed by secondary ion mass spectrometry, than crystal CdTe purchased as 99.999% pure from commercial suppliers [Lyons et al 1984]. Impurities remain in the electrodeposited film, but do not have a significant impact upon the solar conversion efficiency.

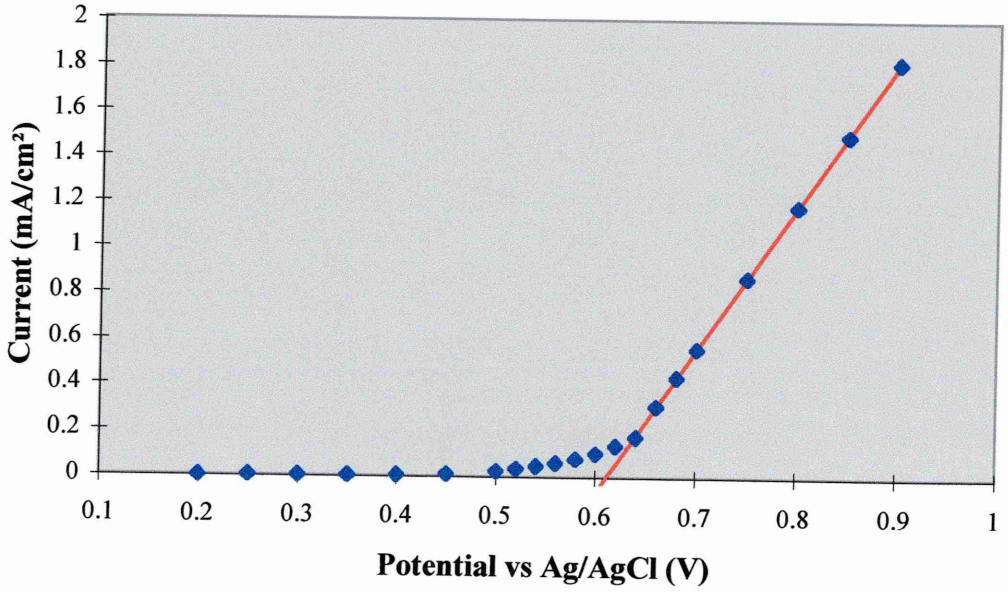

Figure 4.5. Determination of Cd^{2+} Potential for 0.5 M Solution of $CdSO_4$. Temperature 90 ± 2°C. Scan Rate 5 mVs^{-1}. Solution pH of 3.83.

Pre-electrolysis is an important method in impurity reduction, and was performed as follows: The cadmium salt (normally Analytical Reagent grade) was dissolved in Millipore water (18 MΩ Resistance). The solution was then heated to the deposition temperature (90 ± 2°C) and the Cd^{2+} deposition potential determined. This was done using linear scan voltametry, as shown in Figure 4.5. The points shown in Figure 4.5 are the experimental measurements. The solid line is a regression best fit of the experimental points on the rising section of the current against voltage plot beyond the Cd^{2+} potential. The Cd^{2+} potential was determined at the intercept of the potential axis. In this case the Cd^{2+} potential was determined as 0.61 ± 0.01 V against Ag/AgCl. The experimental arrangement was the same as for semiconductor deposition, the substrate being a cleaned TCO coated glass (Area 4 cm^2). The pre-electrolysis deposition potential was then set at +20 mV from the determined Cd^{2+} potential and electropurified for a period of approximately 12 hours, so that a small amount of cadmium was plated out on to the glass/TCO substrate.

4.5 Solar Cell Completion.

4.5.1 Heat Treatment

As described in section 2.10, a heat treatment is a vital process in producing high efficiency CdS/CdTe solar cells by electrodeposition [Basol et al 1983, 1985, Basol 1984]. Samples were heat treated in a Biorad Contact Making Furnace. This furnace had a very rapid thermal ramp rate of temperature in automatic mode. Samples subjected to this rapid temperature ramp rate may undergo thermal shock. Thermal shock was observed as grains of CdTe jumping off the surface of the sample leaving small pin holes and rendering the cell useless for solar cell fabrication. To avoid thermal shock of the samples, they were heated up slowly, using a temperature ramp of 10°C every 30 seconds from 80 to 300°C, then 5°C every 30 seconds from 300-400°C. Samples were annealed in air normally for 8 to 15 minutes and then allowed to cool slowly.

4.5.2 Etching of Semiconductor Surfaces

Etchant	Etchant Composition	Etching Time (seconds)
Dichromate Etch	1.2g $Na_2Cr_2O_7$, 75 ml conc H_2SO_4, 150 ml conc H_3PO_4	60
Polysulphide Etch	20g NaOH, 100 ml H_2O, 16g S (Diluted 10x)	120

Table 4.1. CdTe Surface Etchant Composition and Etching Time.

Following heat treatment, the samples were washed in millipore water and then etched in the dichromate etch followed by the polysulphide etch [Dennison 1996], as shown in Table 4.1. After each etch, the samples were thoroughly washed in running millipore water. Once etching was complete, the samples were stored in acetone before being transferred to the back contact forming mask.

4.5.3 Back Metal Contact Formation

After etching, samples were transferred to an Edwards metaliser, equipped with rotary and diffusion pumps, quartz crystal oscillator thickness monitor and a d.c. evaporation source. Samples were mounted on to a shadow mask with holes of 1.0 mm in diameter. The samples and mask arrangement were placed in the vacuum chamber immediately after the etching procedure leading to exposure of the sample surface to the atmosphere for approximately 5 minutes. The gold, silver or antimony contacts were evaporated from twisted W wire baskets, from either wire or shot 99.999% (5N) pure sources. Evaporation of the metal was performed at a vacuum of approximately 10^{-6} mbar. Typical contacts were approximately 5000 Å thick, as measured by the quartz thickness monitor.

4.5.4 TCO Contact Completion

To form the electrical contact to the TCO, conducting silver paint was used. The silver paint was applied directly to the TCO and allowed to dry for several hours before electrical measurements were made. Figure 4.6 shows the completed cell structure with an electrical probe on the metal contact forming the back electrical contact. An electrical probe contacts the dried silver paint to form the front electrical contact.

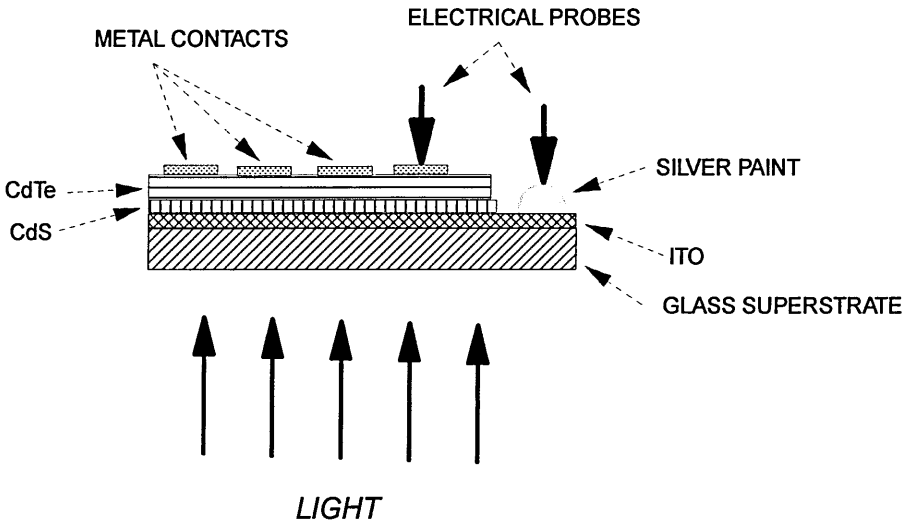

Figure 4.6. Schematic Diagram Showing Completed Solar Cell Structure and Electrical Probes for Current-Voltage Measurements.

4.6 Current-Voltage Measurements

To obtain information on the electric and photovoltaic properties of these devices, current -voltage (I-V) measurements were made. The shape of the I-V characteristic indicates whether a device is ohmic (non-active) or rectifying (active). If a device is rectifying on application of light from the solar simulator, a photocurrent should be observed giving rise to the effects described in section 3.0 (Theory of Solar Cells). All I-V measurements were performed in a box that was sealed to prevent any light reaching the sample to obtain dark I-V characteristics. The box contained a solar simulator to obtain light I-V characteristics. Illumination was from a 250 W tungsten-halogen source adjusted to give 100 $mWcm^{-2}$, using a standard silicon cell as reference. Care was taken to ensure that samples were only illuminated during measurement to prevent sample heating by the lamp.

Sample contacting was performed using micropositioning probes, with spring loaded tips to ensure a good contact was made. The I-V measurement system used in this work was based on a Kiethly 280 Programmable Voltage Source and a Kiethly 619 Electrometer/ Multimeter. The system was under computer control via a standard GPIB interface link that allowed the automated collection and storage of relevant I-V characteristics. The controlling software allowed the user to acquire I-V characteristics in the current range 10^{-2} - 10^{-13} A, and then perform various data interpretation routines which yield the barrier height (ϕ_b) and the diode quality factor (A). I-V data was stored on disk and a spreadsheet was used to determine the values of J_{SC}, V_{OC}, FF and η.

4.7 X-Ray Diffraction

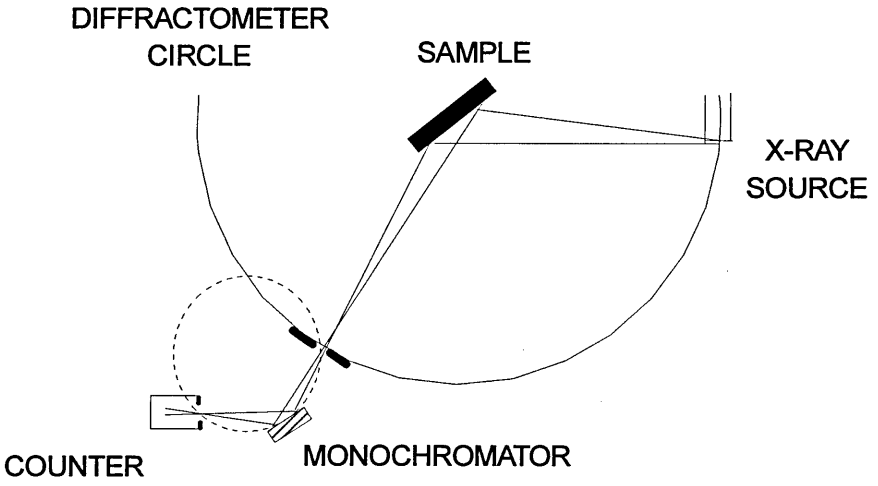

Figure 4.7. Schematic of X-Ray Powder Diffraction Diffractometer

The technique of x-ray powder diffraction gives information on the bulk structure and composition of the thin films [Cullity 1978]. The technique uses the fact that x-rays can be Bragg diffracted from crystal planes in a crystal lattice.

$$2d\sin\theta = n\lambda \qquad (4.1)$$

Figure 4.7 shows how a fixed x-ray source exposes the sample to the x-rays. Both the sample and the detector are then rotated (the counter is rotated about the diffractometer circle). This is known as the Bragg-Bretano geometry. As the x-rays become incident on crystal planes they undergo diffraction (Bragg's Law) and the intensity of x-rays at the counter increases, giving rise to an increased count rate and hence a peak in the spectrum.

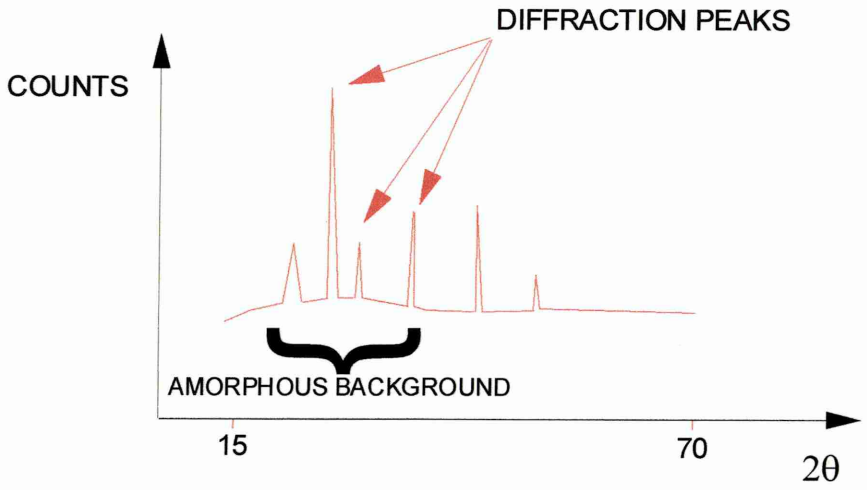

Figure 4.8. Schematic Diagram of XRD Spectrum Showing Diffraction Peaks and Amorphous Background.

The angle (expressed in 2θ) and intensity of these reflections can be compared with data obtained from standards (APD Files) for each element or compound. This comparison gives information on elements and compounds present in the films, their structure/crystal phase and an indication of quantitative composition.

A schematic diagram of an XRD spectrum is shown in Figure 4.8. All XRD spectra in this report are presented in a log linear form with the count axis in log form and the 2θ axis in a linear form. Due to the amorphous nature of glass, the spectrum shows a humped background. Both the TCO and the electrodeposited thin films are polycrystalline and, therefore, several peaks arise from each material, showing preferred directions in the crystallites. Narrow peaks with high intensity indicate good crystal quality of the film.

4.7.1 Experimental Set-up

Spectra were obtained using a Philips PW3710 X-Ray Diffractometer in the Bragg Bretano geometry, using Cu Kα radiation. Spectra were obtained from 15-70° 2θ. The X-Ray generator tension and current were 40 kV and 40 mA, respectively. A step size of 0.020° 2θ and time per step of 1.250 s were used. Sample spinning was used to avoid orientational effects. All quoted values of peak height are the count above background i.e. the total count with the background count subtracted.

4.8 Transmission/Absorption Spectroscopy

Since the generation of both free electrons and free holes is essential to produce a photovoltaic current, intrinsic optical absorption of a single photon across the band gap of the semiconductor is the dominant optical absorption process in a solar cell. The magnitude of absorption is described in terms of an absorption constant $\alpha(\lambda)$, which is a function of the wavelength of the light. If a photon flux $\Gamma_0(\lambda)$ is present at $x = 0$ in the absorbing medium then:

$$\Gamma(\lambda, x) = \Gamma_0(\lambda)\exp[-\alpha(\lambda)] \qquad 4.2$$

The flux Γ may be measured in units of photons $cm^{-2}s^{-1}$ or in $mWcm^{-2}$. The rate of free carrier generation G(x) by intrinsic absorption is:

$$G(\lambda, x)dx = -d\Gamma(\lambda) = \alpha(\lambda)\Gamma(\lambda, x)dx \qquad 4.3$$

For wavelengths of interest, α, is in the range of 10^3 to 10^5 cm^{-1}.

Both CdS and CdTe are direct band gap semiconductors. It is known that semiconductor materials with direct band gaps will absorb photons with an energy, hν, greater than the band gap E_g, since the promotion of an electron from the valence band into the conduction band can occur without any change in momentum of the electron. This process is called "direct absorption". The absorption coefficient in a direct band gap semiconductor is given by:

$$\alpha = C(h\nu - E_g)^{\frac{1}{2}} \qquad (4.5)$$

where C is nearly a constant in the wavelength range of interest in solar cells and depends strongly on the refractive index of the semiconductor. Equation 4.5 shows that α increases sharply as the energy of the photons exceeds E_g, so that a well defined absorption edge is expected in semiconductor materials with a direct band gap. Therefore a plot of α^2 against hν yields a straight line that gives a value of E_g at the intercept of the hν axis as shown in Figure 4.9.

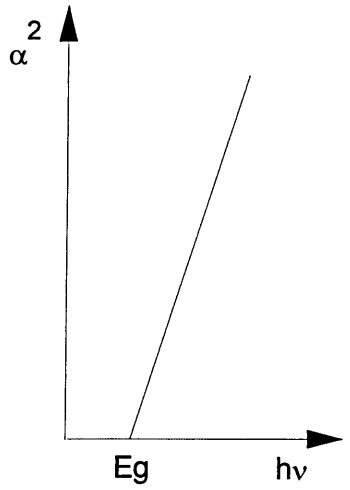

Figure 4.9. Schematic Diagram Showing Variation of Optical Absorption Constant α with photon energy for a direct transition.

This technique was used to determine whether the semiconductor showed any indication of having a defined band gap. A band gap would appear in the absorption/transmission spectrum as a sharp band edge at 510 nm (2.42 eV) for CdS and 850 nm (1.4 eV) for CdTe [Zanio 1978]. The sharpness of this transition gives an indication of the optical absorption of these materials.

4.8.1 Experimental Set-up

To obtain the optical properties of the films, transmission/absorption spectroscopy was performed. The instrument used was a UV-VIS Hitachi U2000 spectrometer. This is a double beam instrument that passed light through both the sample under investigation and also through a reference sample that, in this case, was a TCO coated glass substrate. To calibrate the instrument, a baseline was determined using TCO samples in both the reference and measurement beams. All measurements were then compared against this baseline.

4.9 Scanning Electron Microscopy (SEM)

The SEM has several major advantages over the optical microscope for the study of materials; a high spatial resolution, a large depth of field and the ability to obtain excellent topographic contrast. In obtaining an electron microscopic image, the surface of a solid sample is swept in a raster pattern with a finely focused beam of electrons. Several types of signals are produced from the surface when it is scanned with an energetic beam of electrons. These signals include backscattered, secondary and Auger electrons; x-ray fluorescence and other photons of various energies. All of these signals have been used for surface studies, but the two most common are backscattered and secondary electrons which serve as the basis of scanning electron microscopy.

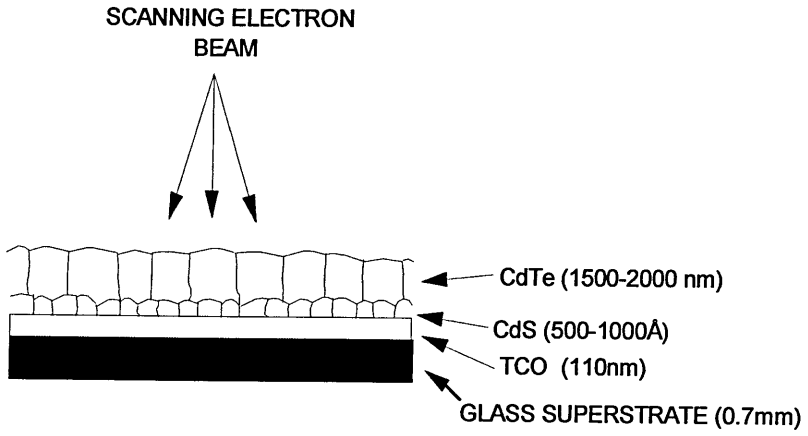

Figure 4.10. Schematic Cross Section of CdS/CdTe Device Showing Columnar Structure of CdTe.

Due to the fact that the CdS layer is of the order of 500 to 1000 Å or less, and the grain size is also of the order of Angstroms, it is very difficult to resolve CdS grains or topographical features in the SEM. The CdTe films are 1.5 to 2.0 μm thick and have grain sizes of the order of μm, and, hence can be readily observed in the SEM. These images are normally taken in plan view, i.e. looking across the surface of the film. Figure 4.10 shows a schematic cross section of the CdS/CdTe device. The TCO is a polycrystalline material with very small grain size (approximately Å) (grains are not shown on diagram). The CdS is also polycrystalline with small grain size (approximately tens of Å) and the CdTe is again polycrystalline, in this case, grows in columns from the substrate, which is an understood growth mechanism for thin films. When observing a CdTe film in plan view, it is the "dome" tops of the columns which is seen, as shown in Figure 4.10.

4.9.1 Experimental Set-up

Micrographs were obtained using a Philips XL40 SEM equipped with an Oxford Instruments Energy Dispersive X-Ray (EDX) Analyser. Accelerating voltages of 15 kV were found not to produce excessive beam damage of the samples. Samples are mounted on metal stubs using silver conducting paint. A conducting path is formed between the semiconducting layers and the metal stub using silver conducting paint to prevent excessive charging of the sample. A spot size of 2 to 5 was found to produce good images.

Chapter 5.0: Development of CdS/CdTe Solar Cells

5.1 Introduction

To obtain working Glass/TCO/CdS/CdTe/Metal solar cells at Sheffield Hallam University, initial work concentrated on the fundamental understanding of the deposition conditions of CdS and CdTe from aqueous solution and subsequent characterisation of the deposited films. A recipe was developed for the production of each layer and subsequent processing for the completion of working devices. In the following results sections excessive repetition of descriptions of deposition conditions have been avoided by reference to previous sections, although key conditions for each experiment are discussed. The understanding of suitable deposition conditions for both CdS and CdTe was achieved using cyclic voltammetry. This investigation was backed up with the x-ray diffraction measurement of samples to confirm the structural properties and crystal qualities of the films produced. The optical properties of the films were investigated using optical absorption, in order to understand the band gap properties of the films. Finally, the electrical performance of completed glass/ITO/CdS/CdTe/Metal devices was evaluated with current-voltage measurements under illumination.

5.2 Cyclic Voltammetry

5.2.1 Deposition of CdS from Aqueous Solution on a Glass/TCO Superstrate

Deposition solutions were prepared, as described in section 4.2.3.1, and an electrochemical cell, as described in section 4.2.3, was used for cyclic voltammetry experiments. Glass/TCO superstrates were prepared as described in section 4.3. Figure 5.1 shows a cyclic voltammagram for CdS on a glass/TCO superstrate. Scans were performed at potentials of 1.0 V to -1.0 V against Ag/AgCl reference electrode. An initial potential of the +1.0 V against Ag/AgCl was applied to the substrate prior to it being placed into the deposition solution, so to prevent any electrochemical reaction at the substrate prior to the commencement of the scan.

On initiation of the scan, at 1.0 V against Ag/AgCl, the current obtained was negative up to a voltage of 0.8 V. As the scan progressed, a plateau region was seen ranging in voltage from 0.6 to -0.3 V, the current began to increase more rapidly at a voltage of -0.4 V, indicating deposition of CdS. The plateau region from -0.4 V to -0.7 V is believed to be the region of CdS deposition. At a voltage of -0.7 V a rapid increase in the current was observed, indicating the deposition of metallic cadmium. This was evident by the growth of small dendrites of metallic cadmium at the edges of the TCO, probably due to high field effects at the edge of the electrodes.

5.2.2 Deposition of CdTe from Aqueous Solution on Glass/TCO/CdS Superstrate

Deposition solutions were prepared, as described in section 4.2.2.1, and an electrochemical cell, as described in section 4.2.2, was used for cyclic voltammetry experiments. Other authors have reported the deposition of CdTe from aqueous solutions directly onto Glass/TCO superstrates [Fulop et al 1982]. Under the conditions used in this investigation it was not possible to produce sustained stable growth of CdTe on Glass/TCO superstrates. Initial deposition progressed normally but as the film became thicker, after circa 25 minutes, the film became unstable and began to detach itself from the substrate. To produce conditions closer to actual deposition conditions for the production of Glass/TCO/CdS/CdTe solar cells, Glass/TCO superstrates covered in CdS deposited by aqueous electrodeposition were used.

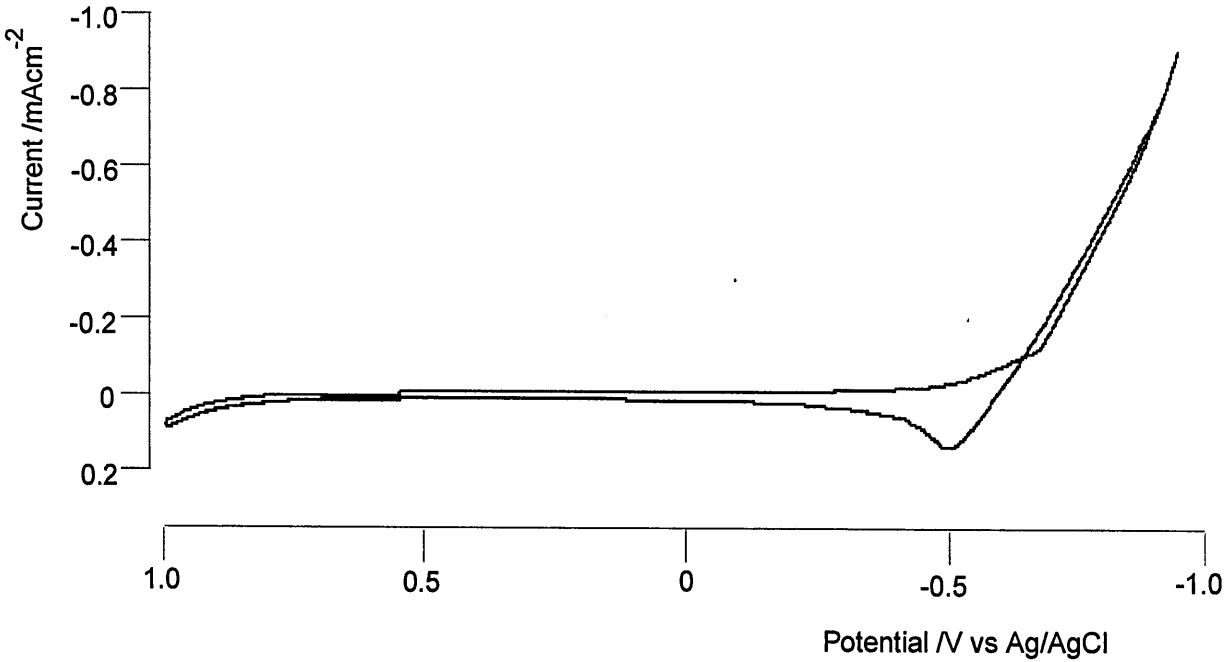

Figure 5.1. Cyclic Voltammogram for CdS Deposition Solution at a 2.3 cm^2 ITO Electrode. Temperature 85 ±2 °C. Scan Rate 20 mVs^{-1}. *pH of solution 3.00 ±0.05.*

Figure 5.2 shows a linear scan voltammogram for CdTe deposition on a glass/TCO/CdS electrode over the voltage range 0.00 to –0.80 V against Ag/AgCl. In this case, positive potentials were not used since this led to stripping of the CdS film on the electrode, giving a superstrate unsuitable for the deposition of CdTe. In this case, a potential of 0.00 V against Ag/AgCl was applied to the superstrate as it was placed in the deposition solution. The scan shows an initial peak centred at -0.10 ± 0.04 V against Ag/AgCl. This is believed to be the onset of elemental tellurium deposition. Following this peak, a steady increase in the current is seen up to a value of voltage of -0.29 ± 0.04 V against Ag/AgCl where a plateau region is observed giving a value of current of 0.35 ± 0.03 $mAcm^{-2}$ in the voltage range –0.29 to –0.68 V against Ag/AgCl. This is the region of CdTe deposition although, as described in section 5.3.1 (XRD determination of composition of CdTe deposited at different potentials), this may not be pure CdTe deposition but a mixture of CdTe with elemental crystalline tellurium. At the potential 0.68 ± 0.04 V against Ag/AgCl a rapid increase in the deposition current was observed. This is the onset of cadmium deposition. Operating in this potential range leads to dentritic growth of cadmium crystals mainly at the edges of the electrode. As with CdS deposition, this is probably due to high field effects at the edge of the electrodes.

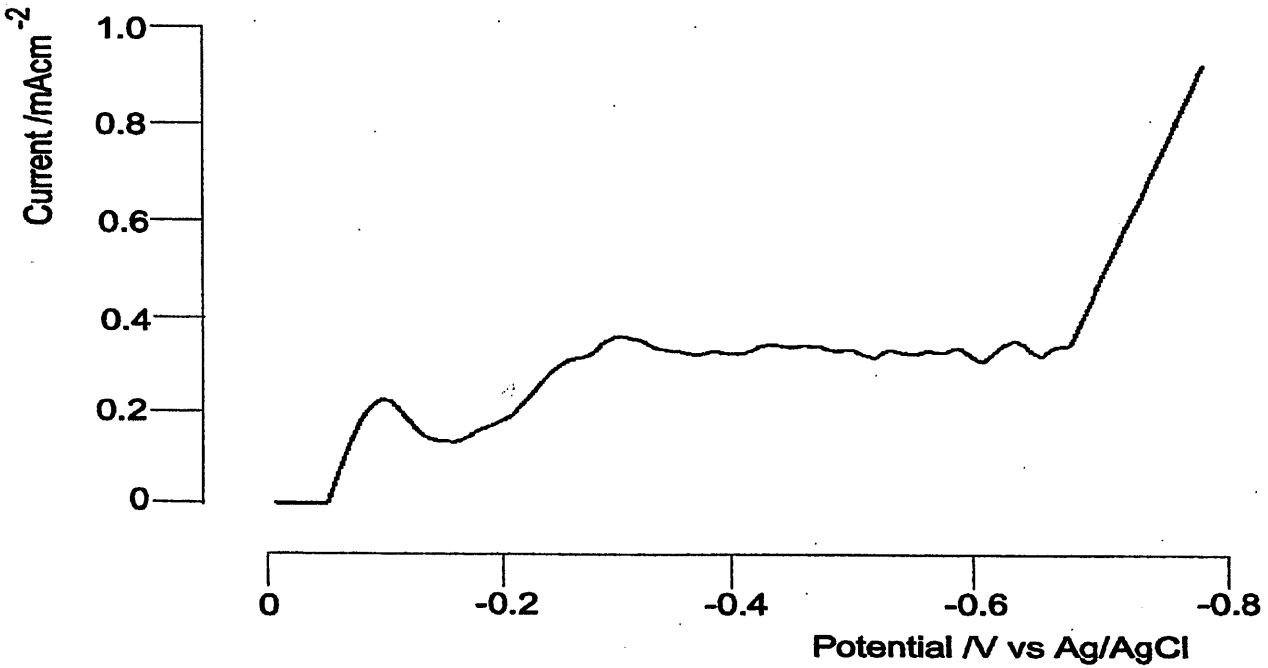

Figure 5.2. Linear Scan Voltammogram for a CdTe Deposition Solution on a 1.8 cm^2 Glass/TCO/CdS Electrode. Temperature 90 ± 2 °C. Scan Rate 5 mVs^{-1}. Value of *pH of solution = 1.76 ± 0.05.*

5.3 X-Ray Diffraction Results

5.3.1 XRD Spectra of CdS Films as Grown and Annealed

The structural properties of as grown and annealed CdS samples were investigated using XRD. The CdS deposition solution was made with $CdCl_2 \cdot H_2O$ (Puratonic Grade) dissolved in Millipore water (18 MΩ Resistance) to make a solution of 0.2 M Cd^{2+}. This solution was then electropurified, as described in section 4.4. $Na_2S_2O_3$ (AR Grade) was added to the purified solution to make it 0.01 M $S_2O_3^{2-}$. The pH value of 2.20 ± 0.05 was achieved with the addition of HCl (AR Grade). Deposition was carried out at a potential of -0.600 ± 0.005 V against Ag/AgCl for a period of two hours. The full deposition period was used to ensure the development of films thick enough to give suitable XRD results.

CdS Plane	Unannealed Peak Height /Counts	Unannealed Peak FWHM /°2θ	Annealed Peak Height /Counts	Annealed Peak FWHM /°2θ	Percentage Increase in Peak Height /%	Percentage Reduction in FWHM /%
(100)	137	0.28	999	0.16	629	-43
(002)	112	0.24	98	0.16	-13	-33
(101)	88	0.48	562	0.16	539	-67
(102)	-	-	49	0.16	-	-
(110)	67	0.40	471	0.16	603	-60
(103)	-	-	37	0.32	-	-
(112)	25	0.80	96	0.20	284	-75
(201)	-	-	71	0.20	-	-

Table 5.1. XRD Results For Unannealed and Annealed CdS Sample on Glass/TCO Superstrate

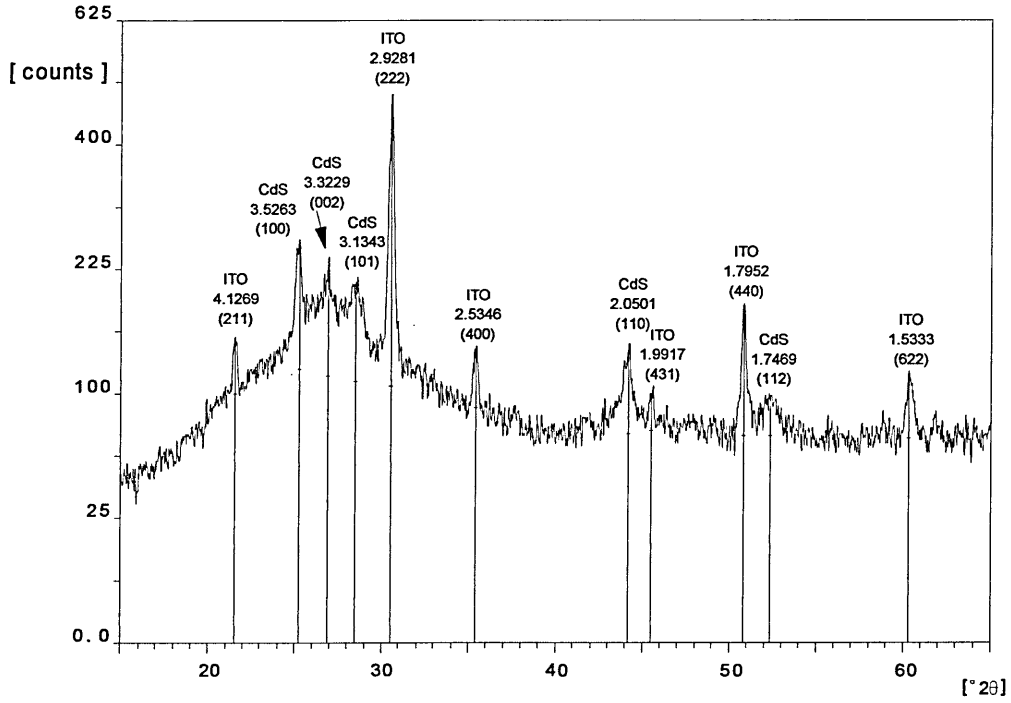

Figure 5.3. Typical XRD Spectrum of CdS sample grown on Glass/ITO superstrate.

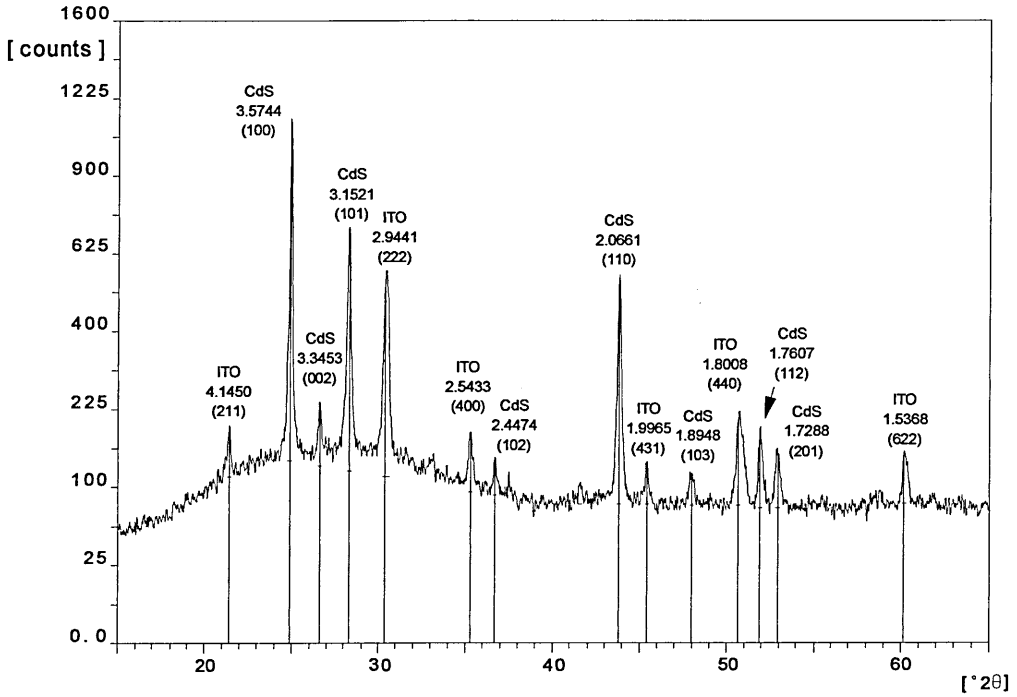

Figure 5.4. XRD Spectrum of CdS sample layer on Glass/ITO Superstrate measured following annealing at 410℃ for 15 minutes in air.

Figure 5.3 shows that this film gives rise to peaks corresponding to CdS. Comparison of the peaks in this spectrum with APD data card 41-1049 confirms that this film consists of CdS in the hexagonal structure. The peaks arise from the (100), (002), (101) and (110) atomic planes and a weaker peak arising from the (112) reflection indicates well formed polycrystalline CdS. It was discovered during initial experiments that using $CdSO_4 \cdot 8\ H_2O$ as the source of cadmium in the CdS deposition solution produces CdS in the cubic structure. The cubic structure of CdS is not considered to be suitable for the window material of the CdS/CdTe solar cell [Farenbruch 1983]. Therefore, $CdCl_2 \cdot H_2O$ was used in all CdS deposition solutions to ensure hexagonal CdS was produced.

Figure 5.4 shows the sample following annealing at 410°C for 15 minutes in air. This anneal simulates the one used in the production of the completed CdS/CdTe cells and hence gives an indication of the crystalline quality of the CdS in the final device. Following the annealing step, the XRD spectrum shows that the CdS peaks have significantly increased in intensity and, in addition to seeing the five peaks seen previously, an additional three peaks corresponding to (102), (103) and (201) reflections are apparent. This data is collated in Table 5.1 and shows the increase in the number of peaks seen in the spectrum following annealing, indicating an increase in crystallinity in the sample. Annealing the CdS produces a large percentage increase in the height of the existing CdS peaks with, for example, the (100) plane showing an increase of 629% and the (110) plane showing an increase of 603%. The only plane to show a decrease in peak height was the (002) plane with a 13% decrease. The values of FWHM for all existing peaks were also significantly reduced with the reductions in the range -33 to -75%, indicating a significant improvement in crystal quality of the CdS.

5.3.2 Effect of Deposition pH on XRD Spectra For CdS Films

This experiment was used to determine the most suitable pH for the deposition of the CdS onto the TCO substrates. During the lifetime of a CdS bath it has been noted that the pH of the deposition solution decreases with use causing the deposition conditions to change. In addition during the deposition of CdS, decomposition of the deposition solution occurs with the formation of a yellow solid in the bulk solution. Due to the fact this yellow solid can be completely digested by the addition of HCl, it is considered that this solid is CdS rather than elemental sulphur [Dennison 1993]. Excessive production of this solid and reduction of pH leads to degradation of the performance of the bath. This degradation limited bath lifetime to two days of normal use. It was possible to filter the solid from the solution but in the long term this would have implications for the concentration of the solution.

On removal of the deposited CdS from the electrodeposition bath, it was necessary to rinse the superstrate in Millipore water to remove any solid material that became attached to the surface of the CdS. If this were not done immediately the CdS would have a dull appearance from attached CdS rather than the bright appearance of the rinsed film having no attached CdS. To understand the effect of different solution pH on the deposition conditions of the CdS, experiments were performed depositing CdS films at different pH values.

To obtain the best performance from the CdS/CdTe solar cell, it is important that the CdS layer is of sufficient thickness to absorb photons having energy greater than 2.4 eV. The CdS should not be so thick as to absorb photons of energy less than 2.4 eV preventing them reaching the CdTe layer and being absorbed there. The CdS must also be of sufficient thickness to form a continuous film without pin holes. It is considered that at lower pH the deposition rate of CdS increases. It is, therefore, important to ensure that the pH of the deposition solution is low enough to produce a suitable film thickness, but not too low so to increase the formation of solid CdS in solution.

The solution preparation conditions for each of the films was as follows; the CdS deposition solution was made with $CdCl_2 \cdot H_2O$ (Puratonic Grade) dissolved in Millipore water (18 MΩ resistance) to make a solution of 0.2 M Cd^{2+}. This solution was then electropurified, as described in section 4.4. $Na_2S_2O_3$ (AR Grade) was added to the purified solution to make it 0.01 M $S_2O_3^{2-}$. The pH of the Cd^{2+} with added $S_2O_3^{2-}$ solution was 4.5 ± 0.2. For reasons of purity, additions to the deposition solution were kept to a minimum so no further chemicals were added to make the solution more alkali and use of the standard pH of the deposition solution as the most alkali. In addition it is known from the process described in Section 3.4 that a decrease in pH is necessary to cause decomposition of $S_2O_3^{2-}$ ions to produce colloidal sulphur. The lower pH values were achieved with the addition of HCl (AR Grade).

All depositions were carried out at a deposition potential of -0.600 ± 0.005 V against Ag/AgCl for a period of two hours. To understand the effect of the pH of the solutions on the deposited films, the films were investigated using the XRD technique. The full deposition period was used to ensure the development of films thick enough to give suitable XRD results.

CdS Plane	Sample	Peak Height /Counts	Peak FWHM /°2θ
(100)	a	137	0.28
	b	52	0.12
	c	26	0.96
(002)	a	112	0.24
	b	50	0.24
	c	34	0.64
(101)	a	88	0.48
	b	52	0.8
	c	31	0.8
(110)	a	67	0.4
	b	31	0.24
	c	-	-
(112)	a	25	0.8
	b	-	-
	c	-	-

Table 5.2. XRD Peak Heights and FWHM of as grown CdS Samples Deposited at a) pH = 2.20 ± 0.05, b) pH = 3.06 ± 0.05, c) pH = 4.23 ± 0.05.

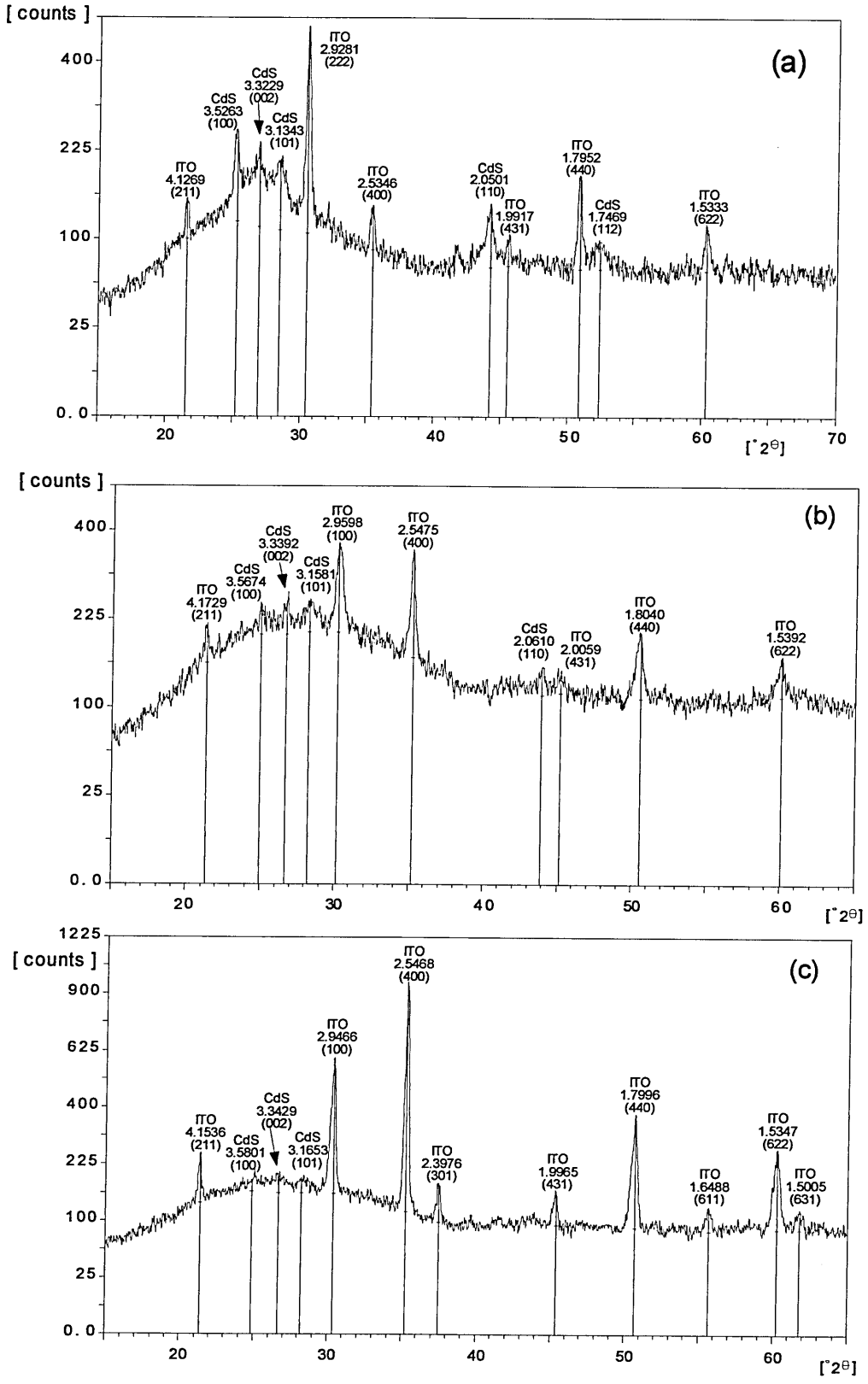

Figure 5.5. XRD Spectra of CdS Samples as Grown Deposited at (a) pH = 2.20 ± 0.05, (b) pH = 3.06 ± 0.05, (c) pH = 4.23 ± 0.05.

Figure 5.5(a) shows an XRD spectrum for a CdS layer grown under the above conditions and a pH value of 2.20 ± 0.05. This sample gave rise to strong peaks in the XRD spectrum arising from the (100), (002), (101) and (110) atomic planes and a weaker peak arising from the (112) reflection indicating well formed polycrystalline CdS.

Figure 5.5(b) shows an XRD spectrum for a CdS sample grown under the conditions described above and a pH value of 3.06 ± 0.05. This sample gave rise to peaks in the XRD spectrum arising from the (100), (002) and (101) reflections and a weaker peak arising from the (111) reflection, again indicating well formed polycrystalline CdS.

Figure 5.5(c) shows an XRD spectrum of a CdS sample grown under the conditions described above and a pH value of 4.23 ± 0.05. This sample gave weak peaks from the (100), (002) and (101) reflection, only indicating that at this pH the CdS is not well formed.

Table 5.2 gives XRD peak heights and FWHM for CdS samples deposited with various pH values of the CdS deposition bath. It is clear that sample (a), which was deposited in a deposition bath at pH 2.2, showed the greatest peak height for all CdS planes observed. Sample (a), grown at the lowest pH, was likely to be the thickest of the CdS samples. The FWHM values do not show a clear trend with sample (a) or sample (b) having the lowest FWHM.

5.3.3 XRD Determination of Composition of CdTe Deposited at Different Potentials

To confirm the results from the cyclic voltammetry, XRD spectra were obtained from films grown at various deposition potentials along the CdTe cyclic voltammetry spectra. Due to the fact that the technique of cyclic voltammetry is a dynamic process, it is not possible to monitor the Quasi Rest Potentials (QRP's) during the scan. To obtain an accurate correlation for the points on Figure 5.2, the deposition potentials used for these experiments were the normal potential against the Ag/AgCl reference electrode and not the QRP. These films were grown under normal experimental conditions, from solutions prepared as described in section 4.2.2.1. Films were grown on glass/ITO/CdS superstrates. Films were grown for a period of three hours to ensure the films were of sufficient thickness to give suitable XRD results.

Figure 5.6(a) shows a film deposited at -0.21 V against Ag/AgCl. Comparison of peaks in this spectrum with the APD data card 36-1452 confirms that films deposited at this potential consist of elemental tellurium in the hexagonal structure. The tellurium formed is polycrystalline, as shown by the large number of tellurium peaks in the XRD spectrum. The XRD spectrum shows no evidence of the formation of CdTe. This film was a well-crystallised continuous film, black in colour, with good adhesion to the superstrate and visually is difficult to distinguish from a well-formed CdTe film.

Figure 5.6(b) shows an XRD spectrum for a CdTe film deposited at -0.32 V against Ag/AgCl. Comparison of peaks in this spectrum with the APD data card 15-770 confirms that this film shows the onset of CdTe deposition. The principal CdTe peak arises from the (111) reflections of CdTe with the cubic structure. Although the XRD spectrum indicates a significant proportion of the film is CdTe, tellurium peaks are also observed arising from the (101) and the (102) reflections. The penetrating nature of the XRD technique is shown by the presence of the CdS peaks in Figure 5.6(b). The film is a nominal thickness of 2 μm and is a continuous film, which adheres well to the superstrate. The presence of the CdS peaks is due to the x-rays penetrating the CdTe film and diffracting from the underlying CdS layer. This is a normal consequence of the XRD technique and is not an indication of a poorly formed CdTe film.

Figure 5.6(c) shows an XRD spectrum for a CdTe film deposited at -0.65 V against Ag/AgCl and shows a well-formed CdTe film. The principal CdTe peak comes from the (111) direction, although this film is still polycrystalline in nature as shown by the presence of several CdTe peaks arising from the (220), (311), (400) and (311) reflections of cubic CdTe. There is no evidence of the formation of elemental tellurium. As in Figure 5.6(b), peaks arising from the underlying CdS can be observed, arising from the (101) and (110) reflections of the CdS. The film was black/dark grey in colour and was a continuous film, which adhered well to the superstrate.

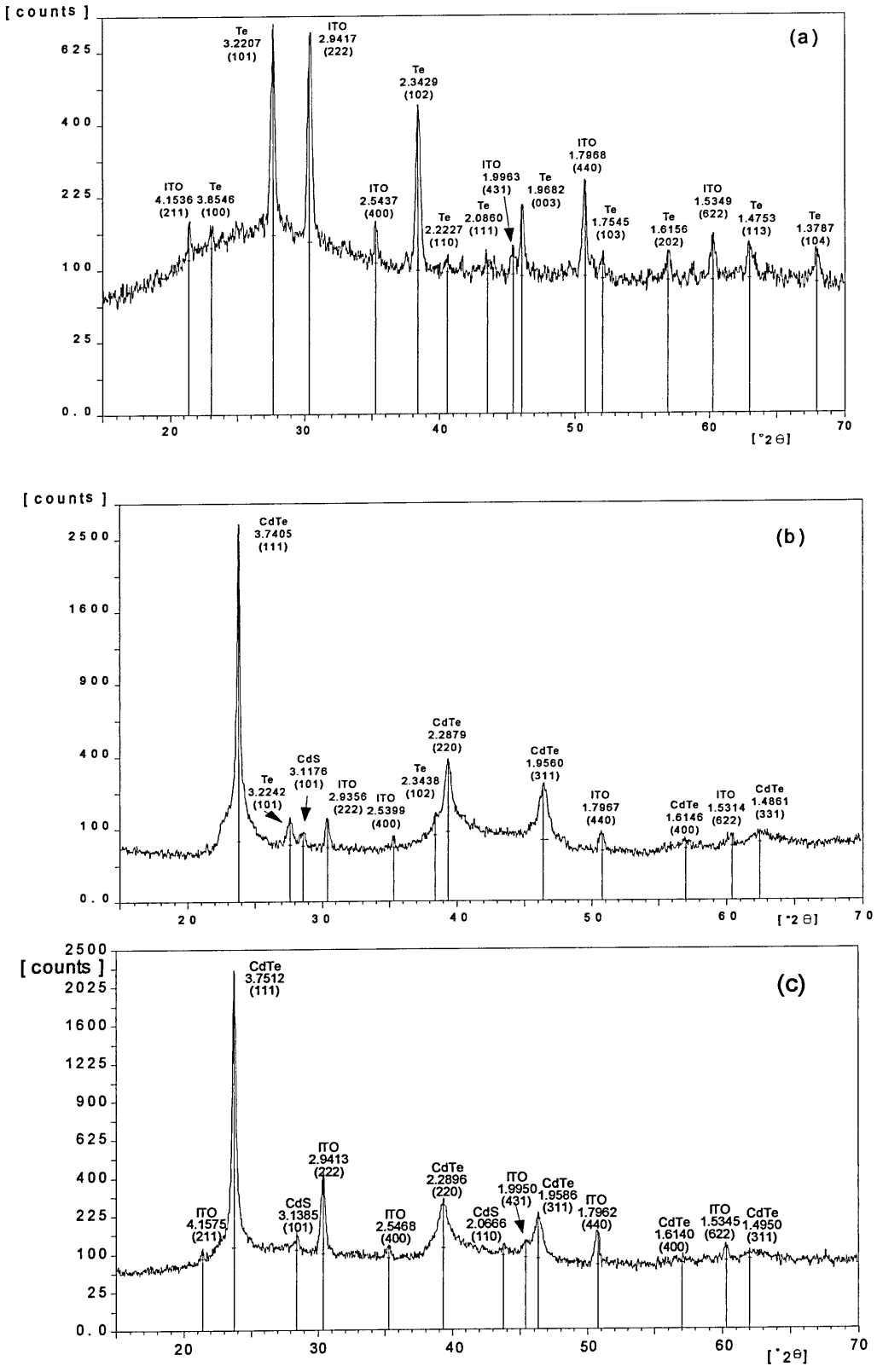

Figure 5.6. XRD Spectra For CdTe Films Deposited on glass/ITO/CdS superstrates at (a) -0.21 V, (b) -0.32 V and (c) - 0.65 V vs. Ag/AgCl

5.3.4 XRD Spectra of CdTe Films as Grown and Annealed

The crystalline properties of as grown and annealed CdTe samples were investigated using XRD. The CdTe deposition solution was prepared as described in section 4.2.2.1. CdTe films were deposited on glass/TCO/CdS superstrates to ensure good adhesion of the CdTe film to the superstrate. Deposition was performed at a QRP of – 0.690 ± 0.005 V against Ag/AgCl with a deposition current of 0.25 $mAcm^{-2}$ for a period of three hours. This value of deposition QRP was chosen as previous experimentation had shown this to be the QRP value that gave the best crystallinity using the maximum over-potential without resulting in metallic cadmium deposition. Films grown at this QRP were continuous dark grey/black films that are well adhered to the superstrate. The full deposition period was used to ensure the development of films thick enough to obtain suitable XRD results.

CdTe Plane	Unannealed Peak Height /counts	Unannealed Peak FWHM /°2θ	Annealed Peak Height /counts	Annealed Peak FWHM /°2θ	Percentage Increase in Peak Height /%	Percentage Reduction in FWHM /%
(111)	25440	0.12	28023	0.12	10.2	0
(220)	132	0.20	190	0.24	43.9	20
(311)	106	0.56	142	0.40	34.0	-28.6
(331)	66	0.40	69	0.40	4.5	0

Table 5.3. XRD Results for Unannealed and Annealed CdTe layers on Glass/TCO/CdS Superstrate

Figure 5.7 shows that the as grown CdTe film gives rise to peaks in the XRD spectrum arising from the (111), (220), (311), and (331) atomic planes, indicating well-formed polycrystalline CdTe. The spectrum is dominated by reflections from the (111) atomic planes, which is the 100% intensity peak for cubic CdTe. Due to the relatively thick film which has been grown (approximately 2 μm) and its good crystallinity, there is no evidence of the amorphous background arising from the underlying glass, although some peaks from the SnO_2:F (FTO, the TCO used for these samples) can be seen.

Figure 5.8 shows the XRD spectrum of the same sample after annealing at 410°C for 12 minutes in air. This anneal is identical to the one used in the production of the completed CdS/CdTe cells and, hence, gives an indication of the crystalline quality of the CdTe in the final device. No new peaks are observed but again the spectrum is dominated by reflections from the (111) plane.

Table 5.3 gives the XRD data for the annealed and unannealed CdTe sample on the glass/FTO/CdS superstrate. The percentage increase in peak height for the CdTe is not as great as the CdS case with the range being 4.5 to 43.9% increase in peak height. The dominant (111) plane showed a 10.2% increase in peak height. In addition percentage reduction in FWHM was not as good as the CdS, case with only the (311) plane showing a reduction in FWHM with a value of -28.6%. The (220) plane showed an increase in FWHM and the other two peaks showed unchanged FWHM.

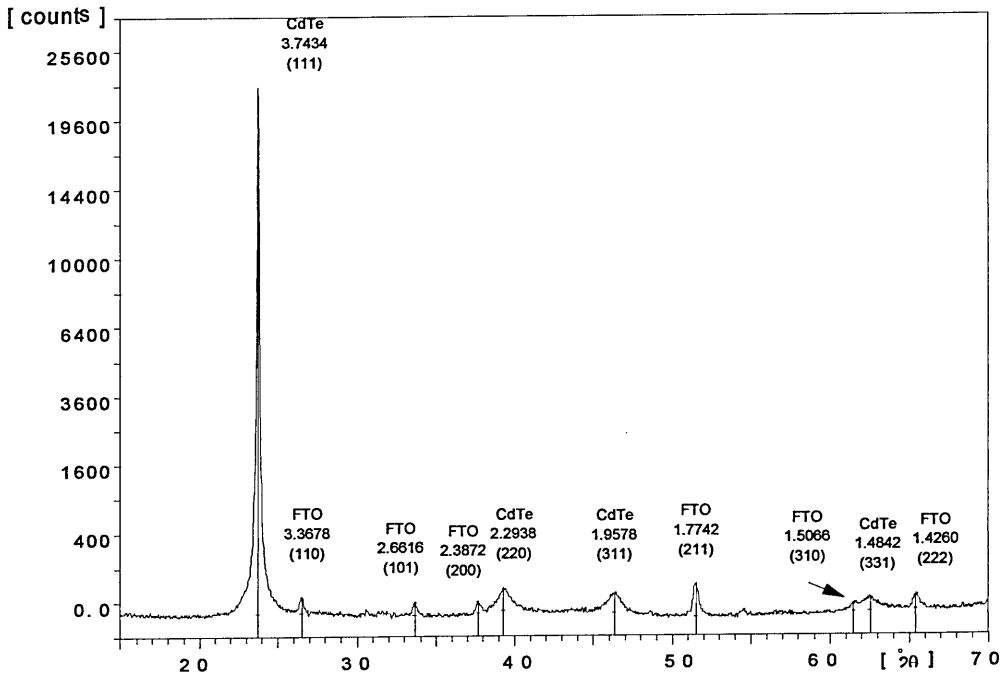

Figure 5.7. XRD Spectrum of CdTe layer grown on a Glass/FTO/CdS superstrate measured as grown.

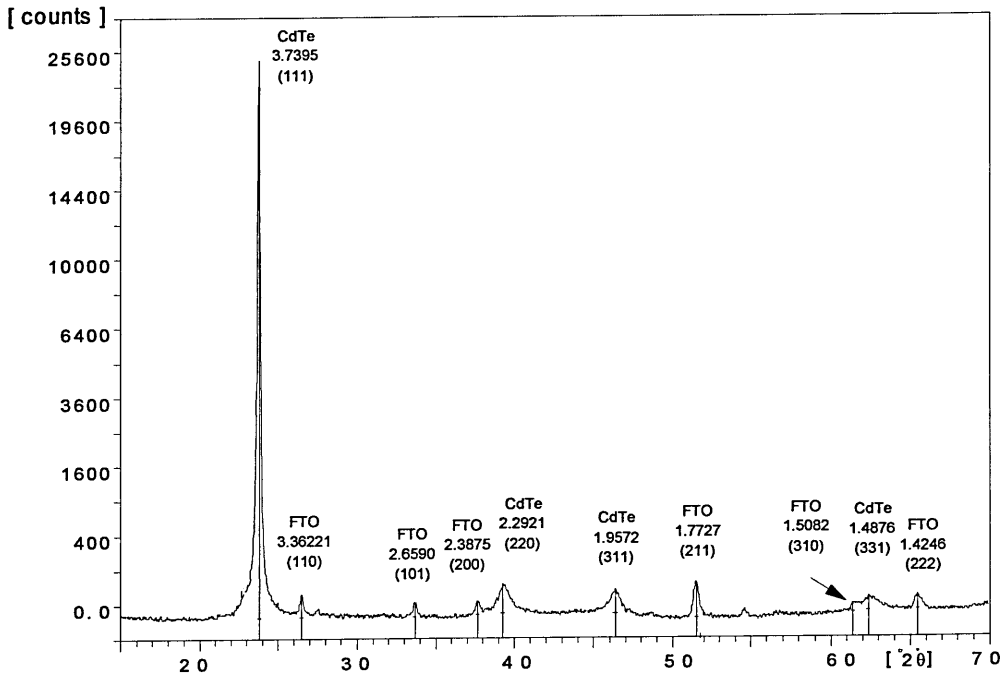

Figure 5.8. XRD Spectrum of CdTe layer Grown on a Glass/FTO/CdS superstrate measured following annealing at 410 °C for 12 minutes in air.

5.4 Optical Absorption Results

5.4.1 Optical Absorption Results for CdS

Optical absorption characteristics were determined for films deposited in a cell, described in section 4.2.3, and under conditions described in section 4.2.3.1. This film was deposited in a solution at pH = 3.06 ± 0.05, a deposition potential of -0.60 ± 0.01 V against Ag/AgCl and a deposition period of 60 minutes. The sample was annealed at 410°C for 15 minutes in air to obtain optical properties of a film under conditions as close as possible to the production conditions of a working device.

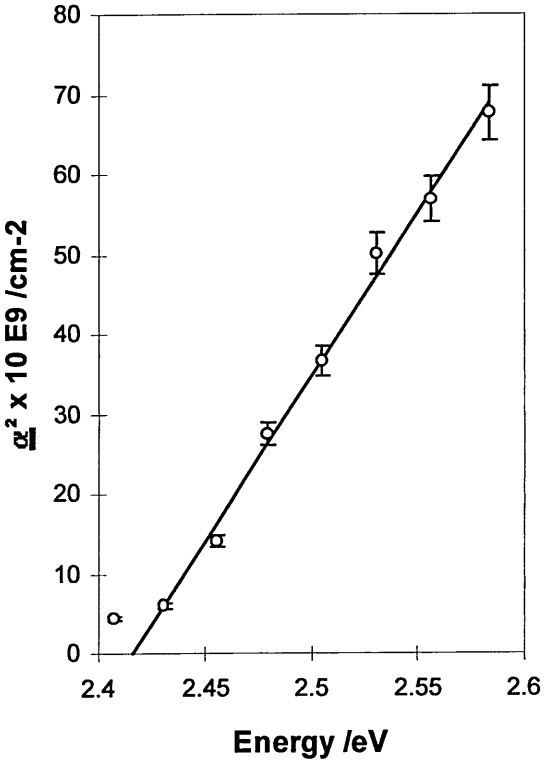

Figure 5.9. Graph Showing Alpha Squared against Energy for Electrodeposited CdS Sample Annealed at 410 °C for 15 minutes in air. Band gap obtained for CdS is 2.42±0.02 eV.

The sample was measured as described in sections 4.8 and 4.8.1. Figure 5.9 shows a graph of alpha squared against energy for this sample. As a double beam spectrometer was used the reference sample was TCO coated glass, which was the same as used for the substrate of the film measured. Regression of the linear section of the graph of alpha squared against energy gives a value of the band gap of the CdS of 2.42 ± 0.02 eV. This is equal to the accepted value of the band gap of CdS of 2.4 eV (Zanio 1978).

5.4.2 Optical Absorption Results for CdTe

The sample for CdTe optical absorption measurements was grown on a glass/FTO/CdS superstrate, the CdS being grown with the same conditions as described in section 5.4.1. The CdTe film was grown at solution temperature 90°C at a QRP of -0.690 ± 0.005 V against Ag/AgCl for a period of 180 minutes. The sample was annealed at 410°C for 12 minutes in air to obtain optical properties of a film under conditions as close to the production conditions of a working device.

The sample was measured as described in section 4.8 and 4.8.1. Figure 5.10 shows a graph of alpha squared against energy for this sample. As a double beam spectrometer was used, the reference sample was FTO coated glass, the same as that used for the substrate of the film measured. Regression of the linear section of the graph of alpha squared against energy gives a value of the CdTe of 1.487 ± 0.020 eV for the band gap almost equal to the accepted value of the band gap of CdTe of 1.45 eV (Zanio 1978).

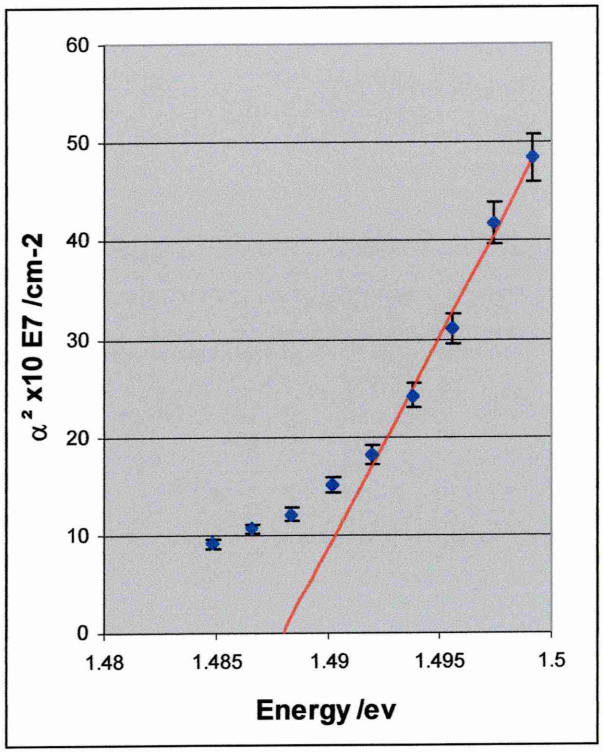

Figure 5.10. Graph Showing Alpha Squared against Energy for Electrodeposited CdTe Sample Annealed at 410℃ for 12 minutes in air. Band gap = 1.49 ± 0.02 eV.

5.5 SEM Analysis of the CdTe Surface

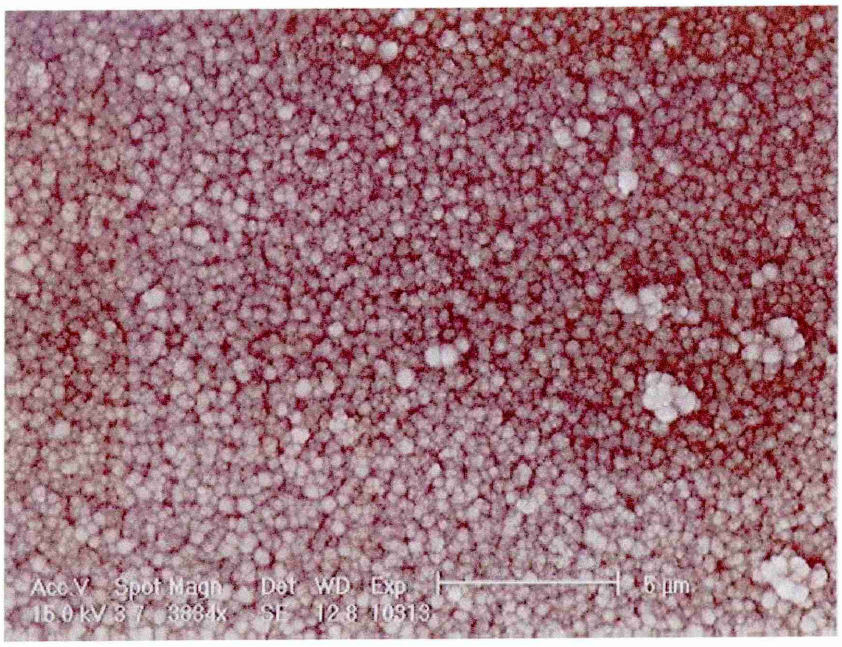

Figure 5.11. Secondary Electron SEM image of the CdTe Surface.

Figure 5.11 shows a secondary electron SEM image of the CdTe surface at a magnification of approximately 3800X and an accelerating voltage of 16 kV. The polycrystalline nature of the sample can be seen from the large number of CdTe grains in the field of view. As discussed in section 4.9, what is seen from the top down SEM image are the tops of the columnar growth of the CdTe grains. These CdTe columns are of the order of 1.5 to 2.0 µm in height. The visual top of the columns ranges in size from 0.1 to 0.5 µm, the grains are compact in nature although to the right of the image clusters of grains, which appear to be on the surface of the film, can be observed. The surface grains range in size from 1 to 3 µm although some larger grains (approximately 5 to 10 µm) were seen out of the field of view of this image and are made from smaller crystallites. General comments about the films are that it appears to be continuous with no pinholes observed in the film, also the film appears well adhered to the superstrate with no peeling of the film observed.

5.6 Current-Voltage (I-V) Results

In order to evaluate how successful the conditions derived above were in the terms of the CdS/CdTe solar cell, devices that were completed as described in section 4.5. All the cells described below were fabricated with gold contacts.

Solar cell I-V characteristics were obtained using the procedure described in section 4.6. The values and associated errors quoted for η, J_{SC}, V_{OC} and FF were calculated from a number of measurements of 5 mm diameter cells on each sample. A minimum of 10 measurements was required from each sample, although generally 20 to 30 cells were measured per sample. Incomplete cells, or cells which had obviously shorted were omitted from the analysis.

5.6.1 Pre-Conditioning of CdTe Deposition Bath

It has been shown that electrodeposited material is of higher purity than the material used to produce the deposition solutions [Lyon et al 1984], i.e. a process of electropurification takes place. To understand the electropurification process, and to investigate whether the bath can be used immediately or requires some pre-conditioning, a series of experiments was undertaken to investigate how efficiency varies with bath life. Deposition solutions were prepared as described in section 4.2.2.1. This process includes an electropurification of the initial 0.5M Cd^{2+} solution as described in section 4.4. Once the solution was prepared depositions were commenced using the deposition conditions of solution temperature 90°C at a potential of -0.690 ± 0.005 V against Ag/AgCl for a period of 180 minutes. The sample was annealed at 410°C for 12 minutes in air. The cells were completed as described in section 4.5 and subsections.

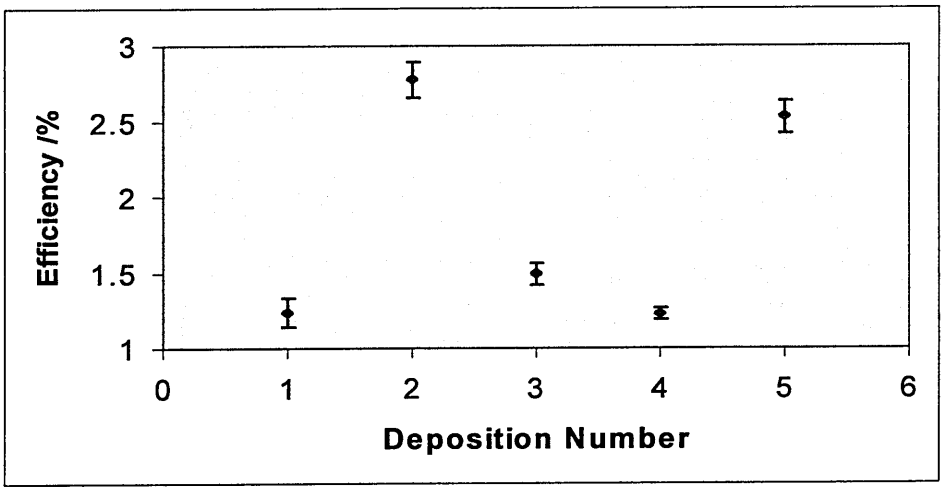

Figure 5.12. Graph Showing Device Efficiency against Deposition Number for a New CdTe Electrodeposition Bath.

To illustrate the variation of device efficiency as the bath is used for deposition, Figure 5.12 shows the variation of device efficiency against deposition number for a new CdTe electrodeposition bath. The graph shows significant variation from deposition to deposition, which is mainly due to significant variations in the J_{SC} value. In order to understand if there are any underlying trends in these overall efficiency trends, graphs of individual parameters J_{SC}, V_{OC} and FF have been plotted.

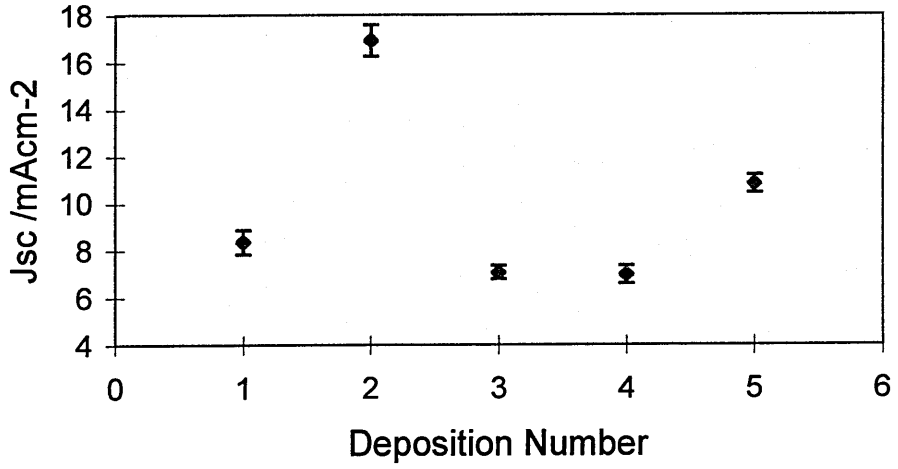

Figure 5.13. Graph Showing J_{SC} against Deposition Number for a New CdTe Electrodeposition Bath.

Figure 5.13 shows a graph of the short circuit current density (J_{SC}) versus the deposition number. This graph shows the large variation in the J_{SC} from deposition to deposition that leads to the large variations in the efficiency of the devices. This graph shows no clear trend of improving J_{SC} with deposition number and so does not demonstrate that the J_{SC} value improves with bath age.

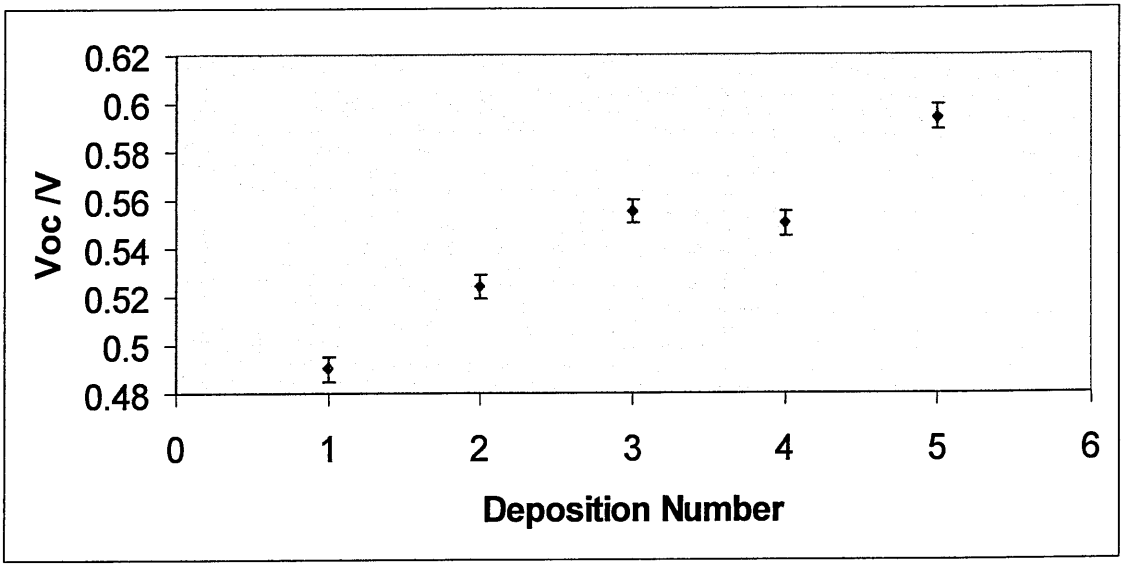

Figure 5.14. Graph Showing Device V_{OC} against Deposition Number for a New CdTe Electrodeposition Bath.

Figure 5.14 shows a graph of device V_{OC} against deposition number for a new CdTe electrodeposition bath. The graph shows a trend of increasing V_{OC} with deposition number. This steady increase in V_{OC} is not of sufficient magnitude to overcome the dominant effect of the J_{SC} on the overall efficiency graph, but it does show how the V_{OC} value is improved by pre-conditioning the bath.

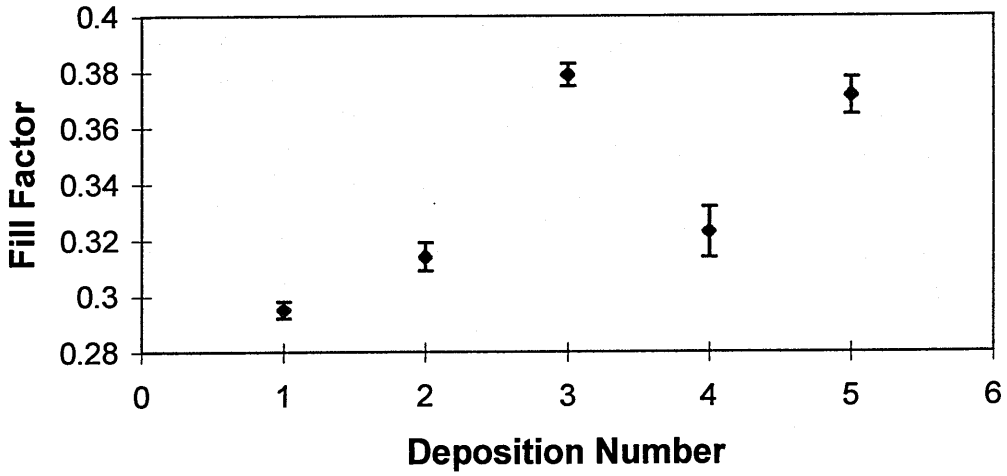

Figure 5.15. Graph showing device Fill Factor against deposition number for a new CdTe electrodeposited bath.

Figure 5.15 shows a graph of device fill factor versus deposition number. The general trend of this graph shows an improvement in fill factor with increasing deposition number. The improvement in the fill factor is not sufficient to overcome the dominant effect of the J_{SC} on the overall efficiency of the devices but, again, this does demonstrate how pre-conditioning the bath improves the fill factor performance of the devices.

5.6.2 I-V Characteristic of Device After Pre-Conditioning of CdTe Deposition Bath

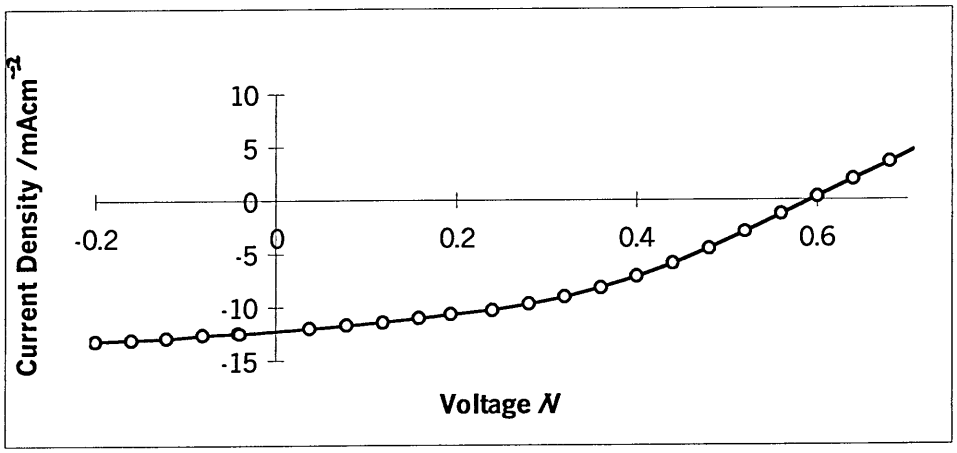

Figure 5.16. Graph showing current against Voltage for a CdS/CdTe electrodeposited solar cell under illumination. No chlorine treatment of CdTe film, Efficiency = 3.0 %, J_{SC} = 12.5 mAcm^{-2}, V_{OC} = 0.60 V, Fill Factor = 0.40.

Figure 5.16 shows an example of a current against voltage characteristic for an electrodeposited CdS/CdTe solar cell under 100 mWcm^{-2} illumination. This characteristic does not show exceptional values for any one parameter but good values for all parameters. Although these device characteristics are not exceptional in comparison to the devices described in Chapter 2 and Chapter 3, this level of efficiency is a suitable starting point for work on investigating the effect of chlorine and indium on the performance of these devices.

Chapter 6: Treatment of CdTe with Chlorine or Indium

As discussed in section 3.7, chlorine treatment of CdTe films, the presence of chlorine in some part of the processing of the CdTe appears to have a beneficial effect on the performance of CdTe/CdS solar cells. The presence of chlorine can be introduced during the deposition of the CdTe as in the case of electrodeposition [Dennison 1994, Das et al 1993]. Alternatively the treatment can be performed by dipping the CdTe in a $CdCl_2$/methanol solution prior to annealing [Birkmire et al 1992, Ringel et al 1991, Sudharsanan et al 1991, Loginov et al 1996, Al-Allak et al 1996]. In order to investigate the effect of chlorine on CdS/CdTe devices, the following section describes a series of experiments involving various chlorine concentrations within the CdTe deposition bath. The aim of these experiments was to investigate changes in the electrical properties of the CdS/CdTe solar cells and the optical and structural properties of the CdTe.

To investigate whether this phenomenon was specific to chlorine or was displayed by other elements, similar experiments were performed with no chlorine inclusion but varying the indium concentration in the deposition bath. Indium was chosen as it is found in Group IIIB of the periodic table and hence is an n-type dopant in CdTe. The choice of indium may seem to go against convention in that the device structure is an n-CdS/p-CdTe heterojunction, but it should be noted that chlorine is found in Group VIIB of the periodic table and is also an n-type dopant in CdTe. In addition previous experiments using p-type dopants, such as copper and silver [Dennison 1994] showed significant degradation of solar cell performance at higher copper and silver concentrations within the deposition bath.

The chlorine and indium were added to the deposition bath during these experiments as this is a relatively simple process which does not require post processing of the samples, as with the $CdCl_2$/methanol dipping procedure. Using this method the chlorine or indium is present throughout the film growth so better film inclusion is likely compared with the more surface orientated technique of dipping. For the large-scale production of these devices inclusion in the deposition bath is better as it reduces the number of process steps required.

To determine the effect of the inclusion of chlorine or indium in the CdTe layer on the performance characteristics of the solar cell device, optimised production conditions as described in Chapter 5 were used to manufacture cells under varying chlorine or indium treatment conditions. To achieve the best results it was necessary to obtain the optimum solar cell performance with no intentional doping of the solution. Prior to commencement of the experiment, several CdTe samples were deposited from the solution, top metal contacts deposited to form the completed solar cells and their characteristics measured. This procedure was repeated until stable cell efficiencies greater than 1.5% were achieved. The value of efficiency of 1.5% was considered to show that the solution had been electropurified to a level where subsequent results were dominated by the added elements and not by any residual impurities within the CdTe deposition bath.

6.1 Treatment of CdTe Bath with $CdCl_2$

The treatment of the CdTe layer with chlorine was achieved by the addition of a stock solution of $CdCl_2$ into the CdTe deposition bath to achieve the required concentrations of Cl^- ions within the bath. The $CdCl_2$ stock solution was made with $CdCl_2 \cdot H_2O$ (Puratonic Grade) dissolved in millipore water (18 MΩ Resistance) to make a solution of 0.2 M Cl^-. To ensure that the addition of this solution did not introduce any further impurities into the deposition solution, the stock solution was electropurified using the same method as used in the production of the CdS deposition solution, as described in section 4.4. The range of chlorine concentrations within the CdTe deposition bath to be used for this experiment was determined by initial experiments on deposition baths used previously.

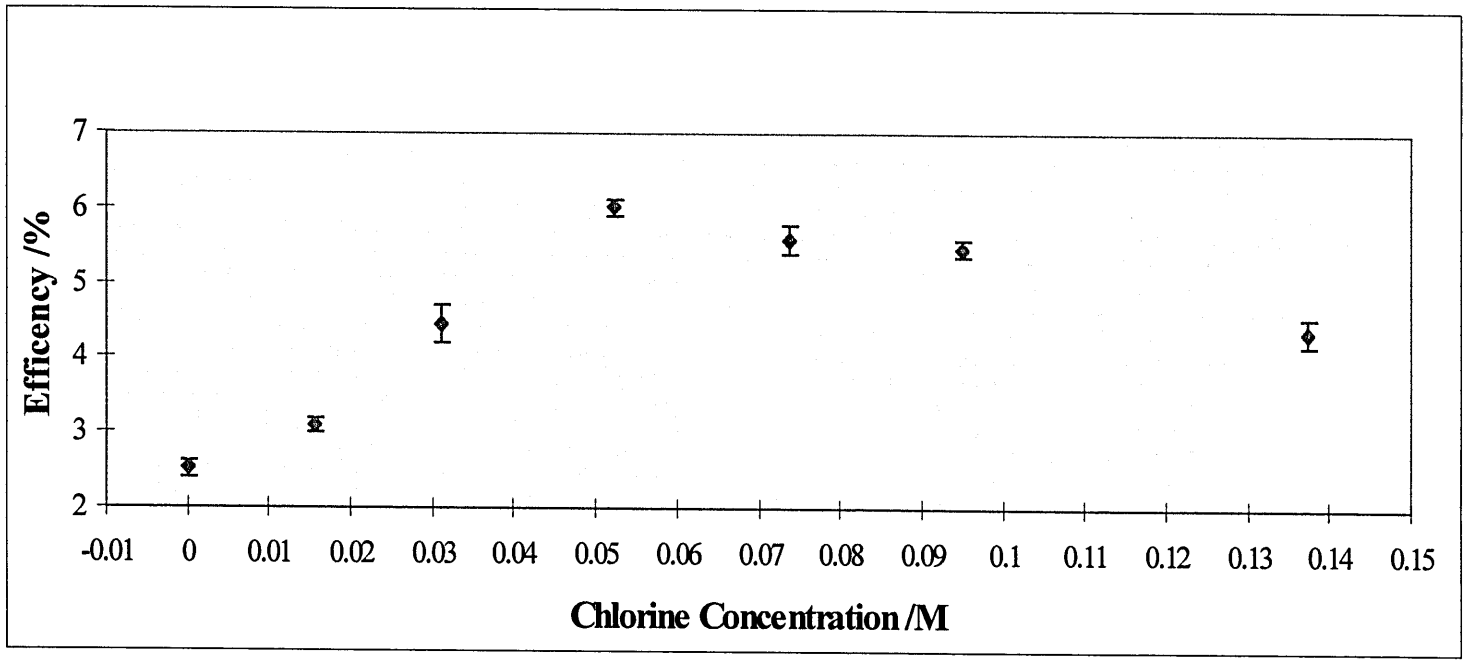

Figure 6.1. Graph Showing Device Efficiency against Chlorine Concentration in the Deposition Bath.

6.1.1 Solar Cell Efficiency Data and I-V Parameters

Solar cell I-V characteristics were obtained using the procedure described in section 4.6. The values and associated errors quoted for η, J_{SC}, V_{OC} and FF are calculated from a number of measurements of 5 mm diameter cells on each sample. A minimum of 10 complete cell measurements was required from each sample, although generally 20 to 30 cells were measured per sample. Incomplete cells or cells which had obviously shorted were ignored from the analysis.

Table 6.1 gives a summary for the solar cell characteristic parameters against chlorine concentration in the CdTe deposition bath. The error values quoted are the standard error of the measurements ($\sigma/\sqrt{n}$, where σ is the standard deviation and n is the number of measurements).

Cl Conc /M	Efficiency /%	Efficiency Error /%	J_{SC} /mAcm^{-2}	J_{SC} Error /mAcm^{-2}	V_{OC} /V	V_{OC} Error /V	FF	FF Error
0.000	2.53	0.11	10.84	0.38	0.594	0.005	0.372	0.007
0.016	3.10	0.10	12.15	0.39	0.603	0.002	0.425	0.008
0.031	4.44	0.25	18.63	0.77	0.607	0.004	0.390	0.007
0.052	6.02	0.11	21.86	0.35	0.625	0.004	0.440	0.003
0.074	5.59	0.18	21.20	0.83	0.605	0.005	0.435	0.005
0.095	5.47	0.10	19.77	0.35	0.642	0.002	0.430	0.004
0.137	4.35	0.19	19.77	0.64	0.640	0.001	0.345	0.004

Table 6.1. Table of Solar Cell Electrical Characteristics against chlorine Concentration in the CdTe Deposition Bath.

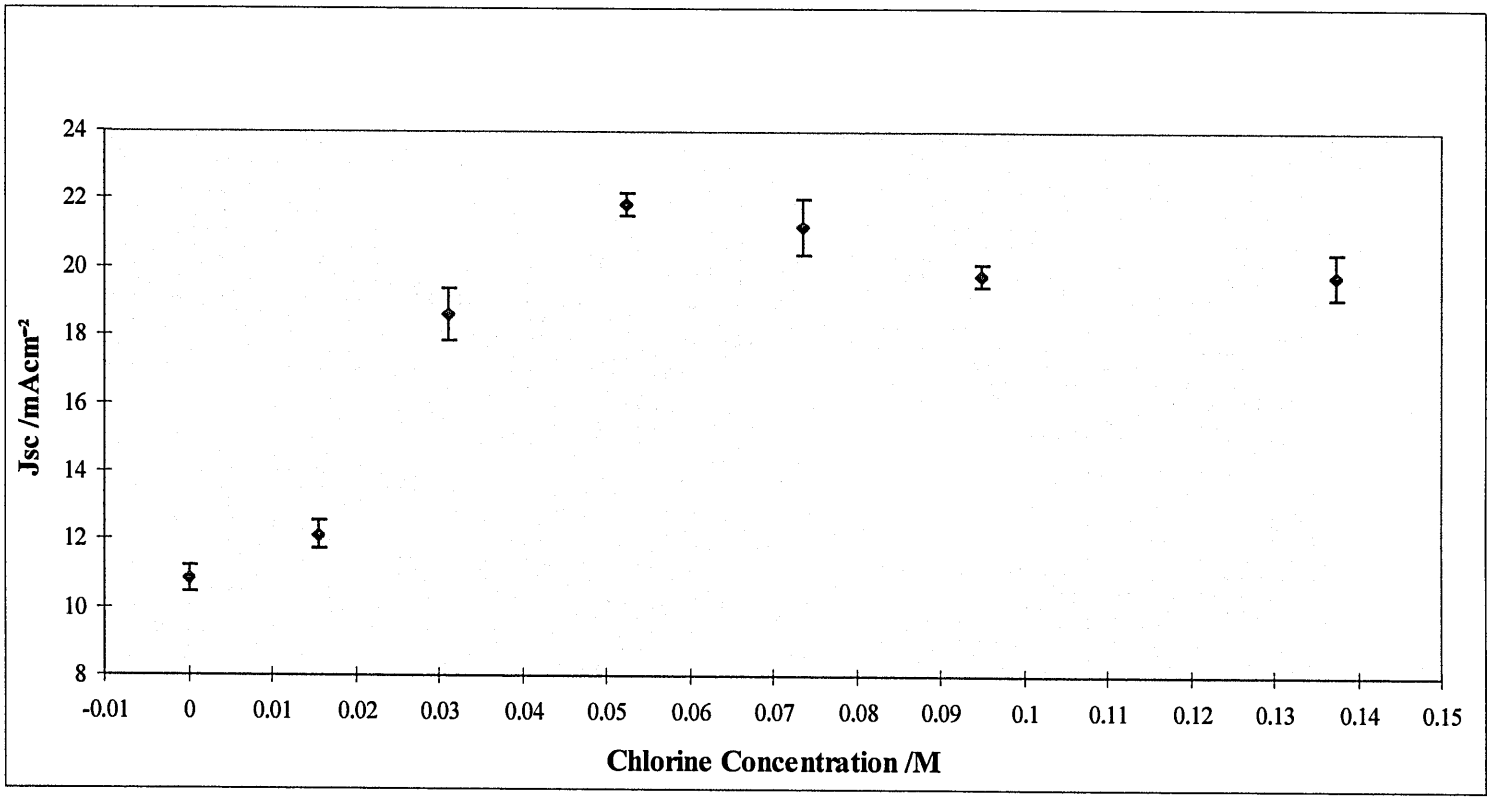

Figure 6.2. Graph Showing Device J_{SC} against Chlorine Concentration in the CdTe Deposition Bath.

Figure 6.1 shows a graph of solar cell efficiency against Cl^- concentration in the CdTe deposition bath. The initial condition of the bath, with no intentional doping with chlorine, gave an efficiency of 2.53 ± 0.11%. On addition of the $CdCl_2$ solution the efficiency increased to a value of 6.02 ± 0.11% with a Cl^- concentration of 0.052 ± 0.005 M. Further addition of $CdCl_2$ solution lead to a tail off in efficiency to the final concentration of 0.137 ± 0.005 M gave an efficiency of 4.35 ± 0.19%. Therefore, the general trend of the graph is a rapid increase in efficiency from the no added chlorine case up to a maximum efficiency for a chlorine concentration of 0.052 ± 0.005 M, with a slight tail off with higher chlorine concentrations. To obtain a better understanding of the effect of the Cl^- ions on the efficiency of the cells, the data is broken down into the individual device components of J_{SC}, V_{OC} and fill factor.

The parameter most obviously driving the overall efficiency of the device is the short circuit current density J_{SC}, as shown in Figure 6.2. This shows J_{SC} against chlorine concentration in the CdTe deposition bath. The lowest value of J_{SC} of 10.84 ± 0.38 $mAcm^{-2}$ was obtained with no Cl^- inclusion. The values of J_{SC} rose to a maximum of 21.86 ± 0.35 $mAcm^{-2}$ with a Cl^- concentration of 0.052 ± 0.005 M. Further addition of $CdCl_2$ solution lead to a tail off in efficiency to the final concentration of 0.137 ± 0.005 M gave a J_{SC} of 19.77 ± 0.64 $mAcm^{-2}$. This graph is identical to the efficiency against chlorine concentration in the CdTe deposition bath (Figure 6.1) showing how the J_{SC} dominates the overall efficiency of these devices.

Figure 6.3 shows a graph of V_{OC} against Cl^- concentration in the CdTe deposition bath. The lowest value of V_{OC} was obtained for the case of no chlorine addition with a V_{OC} value of 0.59 ± 0.01 V. This graph shows a steady increase in the V_{OC} value with increasing Cl^- concentration up to a Cl^- concentration of 0.095 ± 0.005 M giving a maximum V_{OC} value of 0.64 ± 0.01 V. The point where the Cl^- concentration is 0.074 ± 0.005 M gave a V_{OC} of 0.61 ± 0.01 V which does not appear to follow the trend. This graph shows a general increasing trend in V_{OC} with increasing chlorine concentration, up to a chlorine concentration of 0.095 ± 0.005 M. This indicates that the addition of chlorine generally has a positive effect on the V_{OC} value.

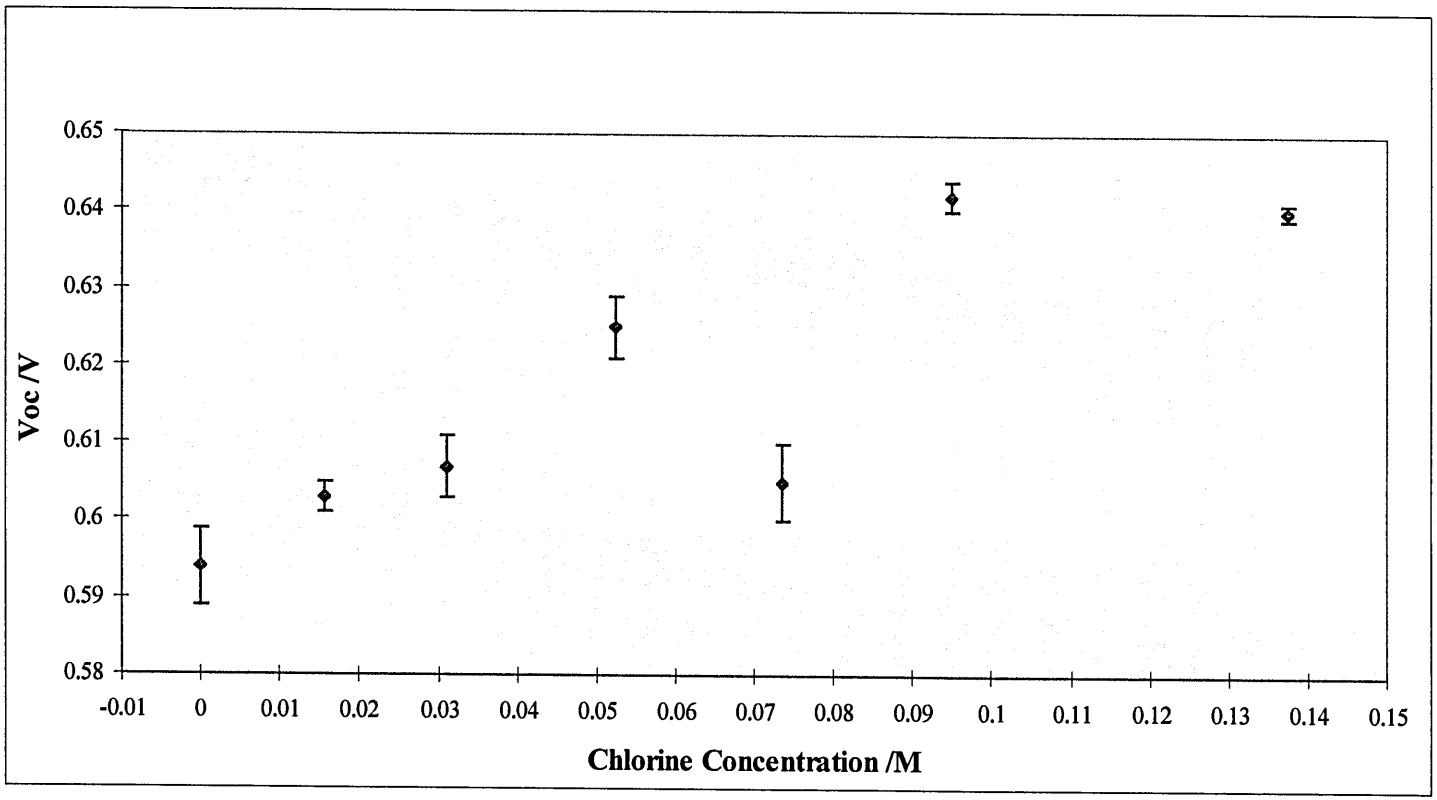

Figure 6.3. Graph Showing Device V_{OC} against Chlorine Concentration in the CdTe Deposition Bath.

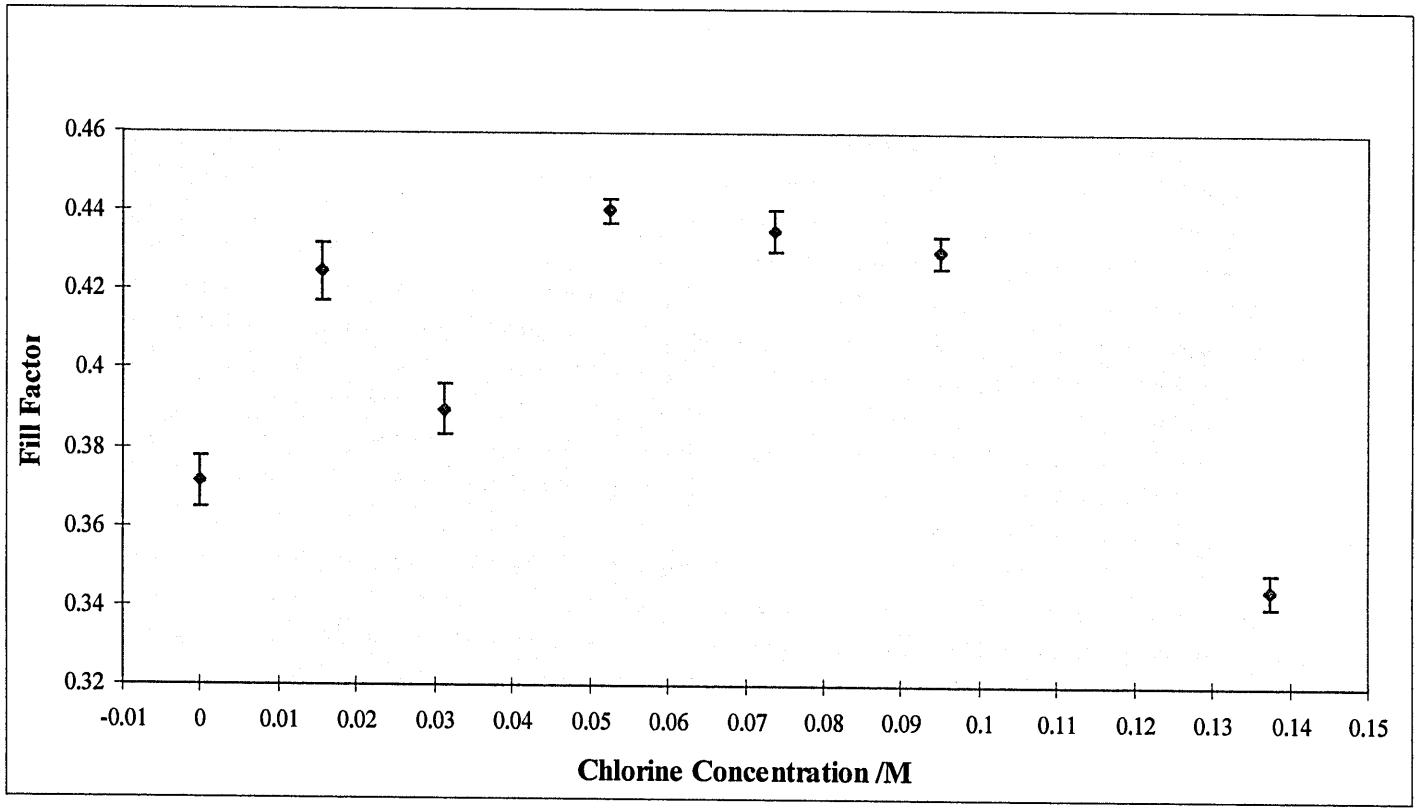

Figure 6.4. Graph Showing Device Fill Factor against Chlorine Concentration in the CdTe Deposition Bath.

Figure 6.4 shows a graph of fill factor against Cl^- concentration in the CdTe deposition bath. Initially, a sharp increase in fill factor with increasing Cl^- concentration was observed, up to a chlorine concentration of 0.052 ± 0.005 M which gave a maximum value of fill factor of 0.44 ± 0.01. Above a chlorine concentration of 0.052 ± 0.005 M the fill factor tails off. The highest concentration of Cl^- within the CdTe deposition bath (0.137 ± 0.005 M) gave the lowest value of fill factor so even though both the J_{SC} and the V_{OC} were good for these devices the low fill factor lead to reduced efficiency. The general shape of the fill factor graph is the same as the efficiency graph, with an increase in fill factor with increasing chlorine concentration up to a maximum value of fill factor at a chlorine concentration of 0.052 ± 0.005 M. A tail off was noted with higher chlorine concentrations.

6.1.1.1 Current-Voltage Characteristic For Optimal Chlorine Treated Cell

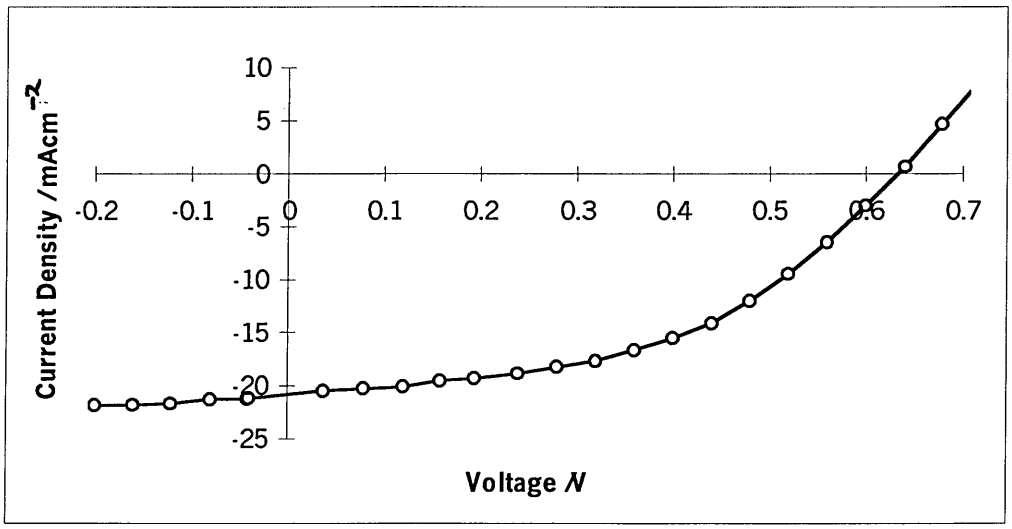

Figure 6.5a. Graph Showing Current against Voltage for a CdS/CdTe Electrodeposited Solar Cell Under Illumination. A Chlorine Concentration of 0.052M in CdTe Deposition Bath, Efficiency = 6.21%, J_{SC} = 21.27 mAcm^{-2}, V_{OC} = 0.64 V, Fill Factor = 0.452

Figure 6.5a shows a current against voltage characteristic under illumination for a cell produced under optimal chlorine treatment. This cell was measured using the procedure described in section 4.6. Illumination was from a 250 W tungsten-halogen source adjusted to give 100 mWcm^{-2}. This cell was treated with a chlorine concentration of 0.052 ± 0.005 M. The device shows a relatively good value of J_{SC} showing the beneficial effect of the chlorine on the J_{SC}, but the V_{OC} and FF would need to be improved significantly to achieve higher efficiencies.

6.1.2 Treatment of CdTe Bath with $CdCl_2$, XRD Results

In order to understand the effect of the chlorine treatment on the crystalline structure of the CdTe Harris analysis was used [Barret 1980]. Harris analysis allows for the determination of the probability (P_{hkl}) of a (hkl) plane lying parallel to the substrate. For this analysis four planes were used those being the (111), (220), (311) and (331) planes as these where the best defined peaks for all samples. As four reflections were considered, a randomly orientated sample would have a P_{hkl} of 25% whereas a completely ordered sample would have a P_{hkl} of 100%. To simplify the analysis the CdTe (111) planes was used to compare the respective samples. The (111) CdTe peak was chosen, as this is the most intense peak in the spectra of the material produced. This is consistent with the APD data for the cubic form of CdTe, the (111) peak that is found at a 2θ value of 23.77° (corresponding to a plane spacing of 3.742Å and is classed as the 100% peak for cubic CdTe (APD card 15-770). All the samples were very highly ordered with respect to the (111) plane i.e. had a P_{111} greater than 90%, all the other P_{hkl} values being less than 3%.

Samples were measured and then re-measured after annealing using the procedure described in section 4.5.1. Samples were annealed in air at 410°C for 12 minutes and allowed to cool slowly. Samples were annealed to replicate the conditions used in the production of the solar cells.

Table 6.2 gives the XRD data for the CdTe P_{111} percentage against chlorine concentration in the CdTe bath. Figure 6.5 shows the XRD count for the CdTe P_{111} percentage against the chlorine concentration in the CdTe deposition bath. Initially, the inclusion of chlorine in the CdTe deposition bath produced a significant increase in the CdTe P_{111} percentage over the P_{111} percentage for a sample with no chlorine treatment. At chlorine concentrations greater than 0.05 M there was a significant reduction in the CdTe P_{111} percentage compared with the P_{111} percentage for a sample with no chlorine treatment.

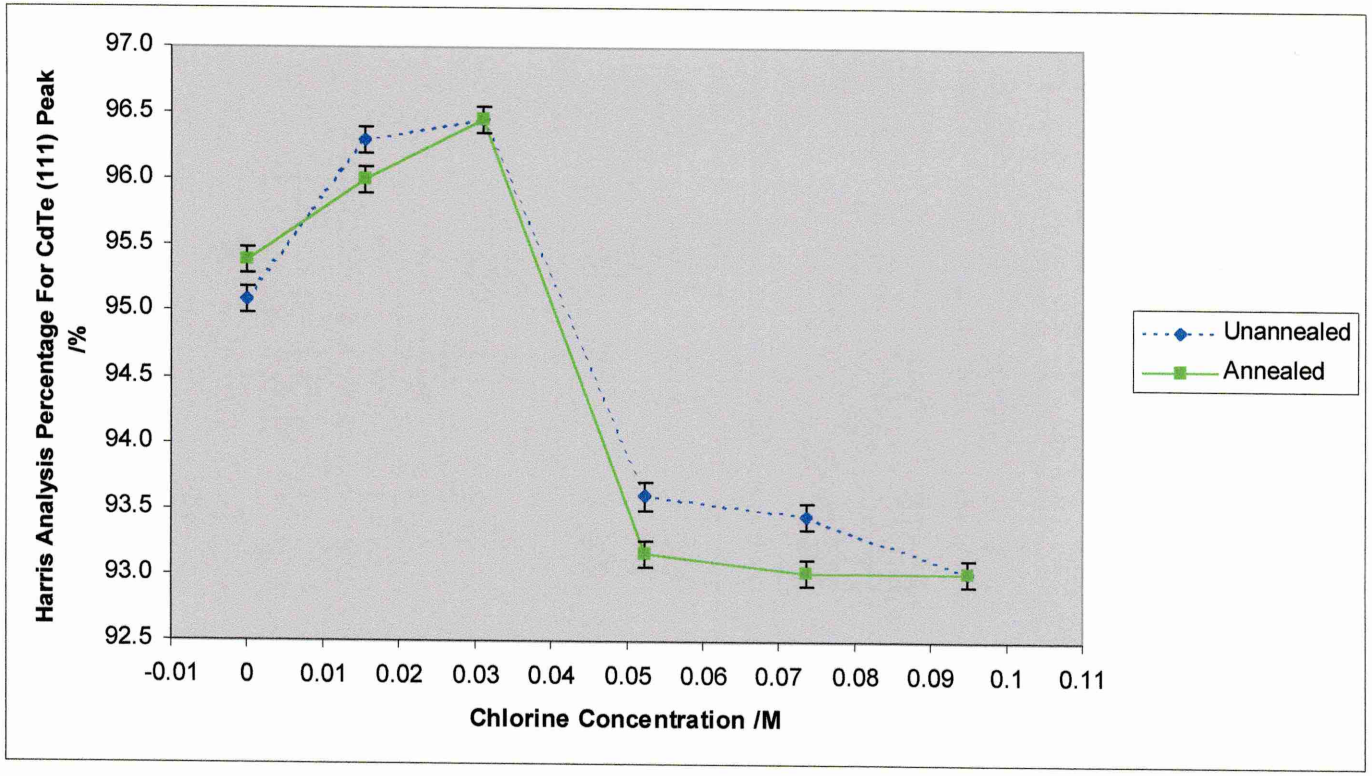

Figure 6.5b. Graph Showing CdTe P_{111} Percentage against Chlorine Concentration in the CdTe Deposition Bath.

Chlorine Concentration /M	Unannealed CdTe P_{111} Percentage /% (±0.1 %)	Annealed CdTe P_{111} Percentage /% (±0.1%)
0.000	95.1	95.4
0.016	96.3	96.0
0.031	96.5	96.5
0.052	93.6	93.2
0.074	93.5	93.0
0.095	93.0	93.0

Table 6.2. Table Showing CdTe P_{111} Percentage against Chlorine Concentration in the CdTe Deposition Bath for Both Annealed and Unannealed Samples.

6.1.3 Treatment of CdTe Bath with $CdCl_2$, Optical Absorption Results

The optical properties of the chlorine treated samples were investigated using the technique of Optical Absorption as described in section 4.8 using experimental conditions as described in section 4.8.1. Figures 6.6 and 6.7 show values of alpha squared against energy for the chlorine treated samples both unannealed and annealed respectively. These graphs show how the various chlorine treatments induce varying values of band gap in the CdTe. The value of band gap is determined from a regression of the linear section of the graph of alpha squared against energy. The values of the band gap determined from the regression are given in Table 6.3 for both the annealed and unannealed samples. The estimated error associated with these measurements of ± 0.02 eV arises from measurement error and error arising in the determination of the linear regression.

To see more clearly the effect of the chlorine treatment on the CdTe, graphs of CdTe band gap against chlorine concentration in the CdTe bath were plotted, these are shown in Figures 6.8 and 6.9 for unannealed and annealed samples, respectively. Figure 6.8 shows that the sample with no chlorine treatment had a band gap of 1.49 ± 0.02 eV. Initially samples with higher concentrations of chlorine in the deposition bath showed reduced band gap up to the sample treated with a chlorine concentration of 0.031 M, which gave a band gap of 1.42 ± 0.02 eV. Subsequently, higher concentrations of chlorine in the CdTe deposition bath gave higher band gaps, although not as high as the non chlorine treated sample, and the sample with a chlorine concentration of 0.095 M had a band gap of 1.47 ± 0.02 eV.

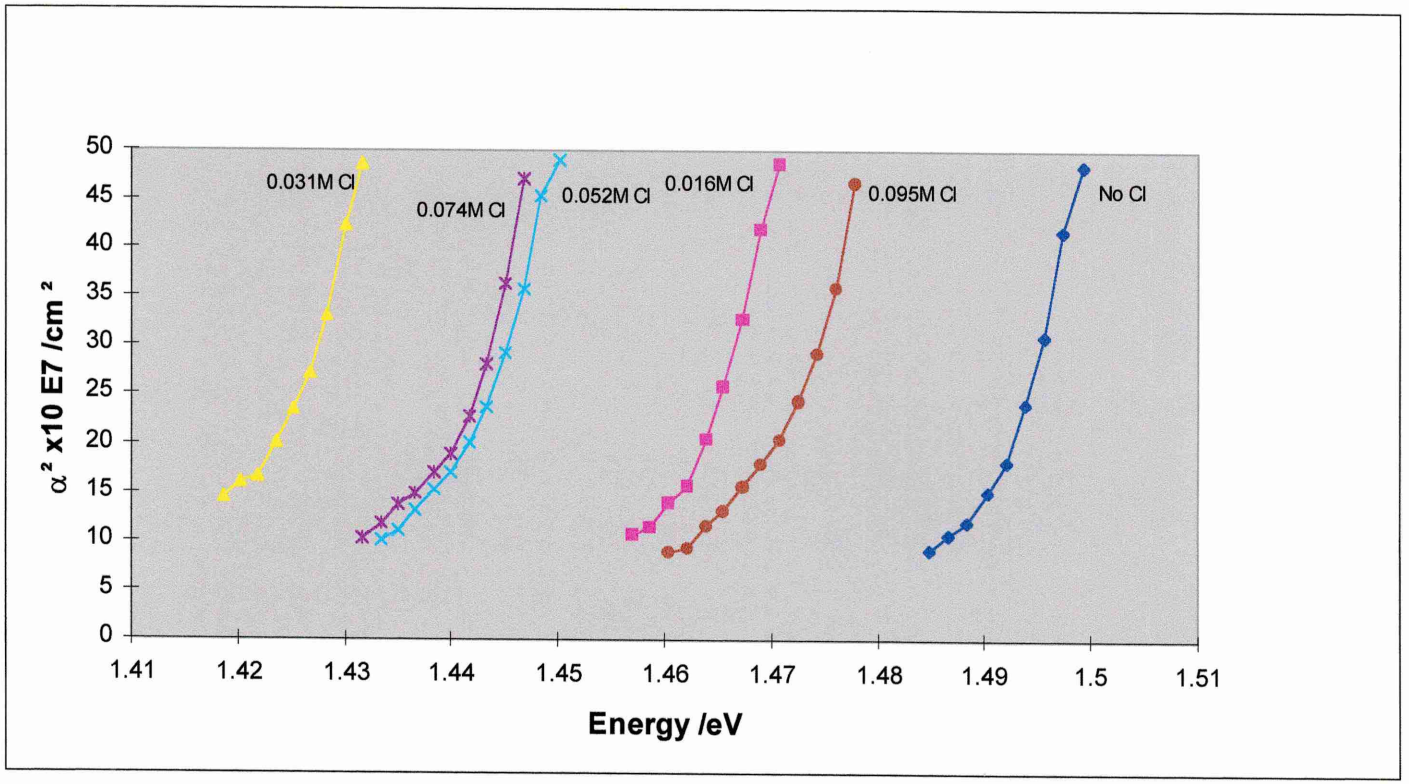

Figure 6.6. Graph Showing Alpha Squared against Energy for Unannealed Samples

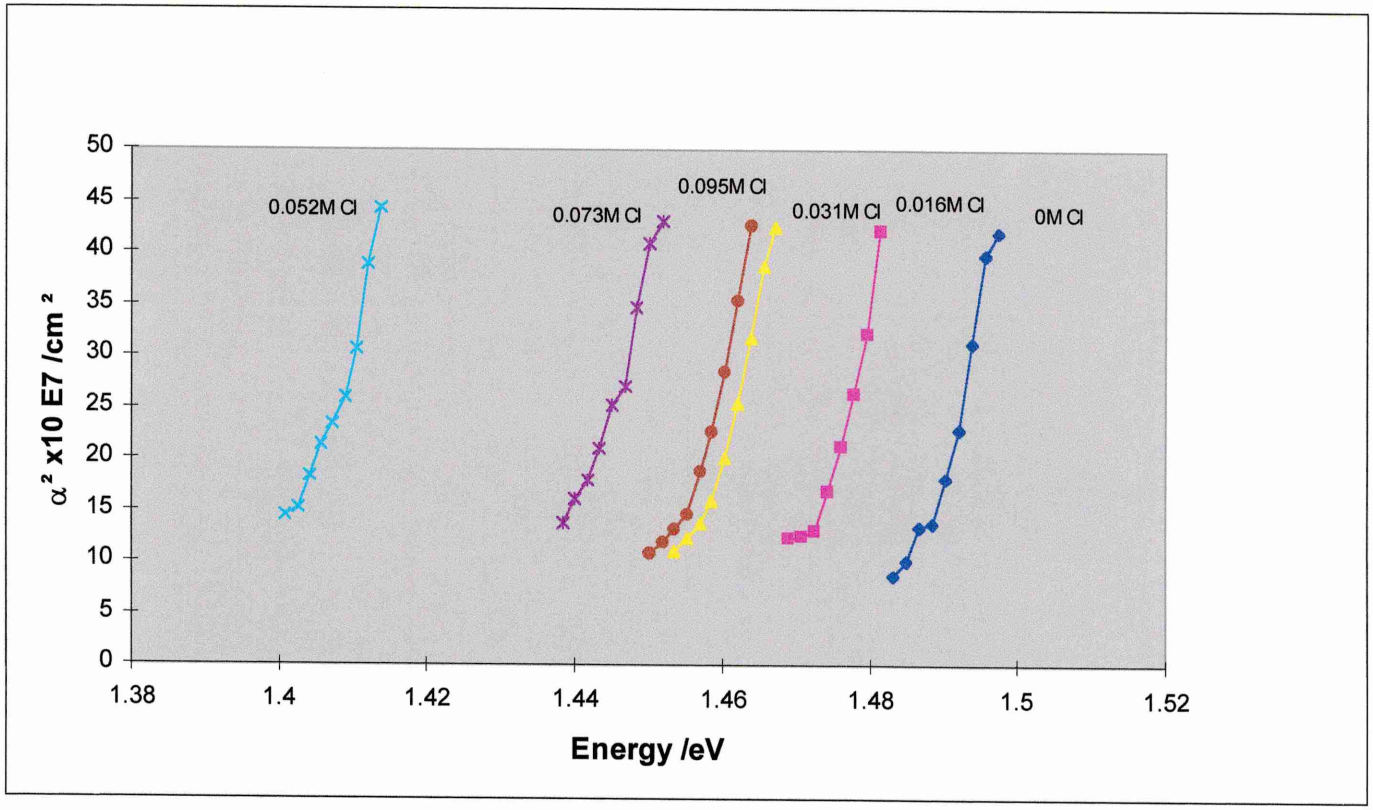

Figure 6.7. Graph Showing Alpha Squared against Energy for Annealed Samples

Figure 6.9 shows the CdTe band gap against chlorine concentration in the CdTe deposition bath for the annealed samples. The sample with no chlorine treatment following annealing had a band gap of 1.49 ± 0.02 eV. As with the unannealed samples, increasing the chlorine concentration in the CdTe deposition bath initially reduced the band gap, although in this instance the minimum band gap occurred at a chlorine concentration of 0.052 M and gave a band gap of 1.40 ± 0.02 eV. Again, with the unannealed samples subsequently higher concentrations of chlorine in the CdTe deposition bath gave higher band gaps. These values were not as high as the no chlorine treatment sample, and the sample with a chlorine concentration of 0.095 M had a band gap of 1.45 ± 0.02 eV.

Chlorine Concentration /M	Unannealed Band Gap /eV (±0.02 eV)	Annealed Band Gap /eV (±0.02 eV)
0.000	1.49	1.49
0.016	1.46	1.47
0.031	1.42	1.45
0.052	1.44	1.40
0.074	1.44	1.44
0.095	1.47	1.45

Table 6.3. Table showing CdTe Band Gap against Chlorine Concentration in the CdTe Deposition Bath for Unannealed and Annealed Samples.

It should be noted that the graph showing CdTe band gap against chlorine concentration in the CdTe deposition bath for the annealed samples (Figure 6.9) shows a good correlation to both the efficiency (Figure 6.1) and J_{SC} graphs (Figure 6.2) for the chlorine treated samples. The correlation shows the minima in the annealed samples band gap graph coincides with the maxima in the efficiency and J_{SC} graphs. This correlation will be discussed further in Chapter 7, in the discussion of results.

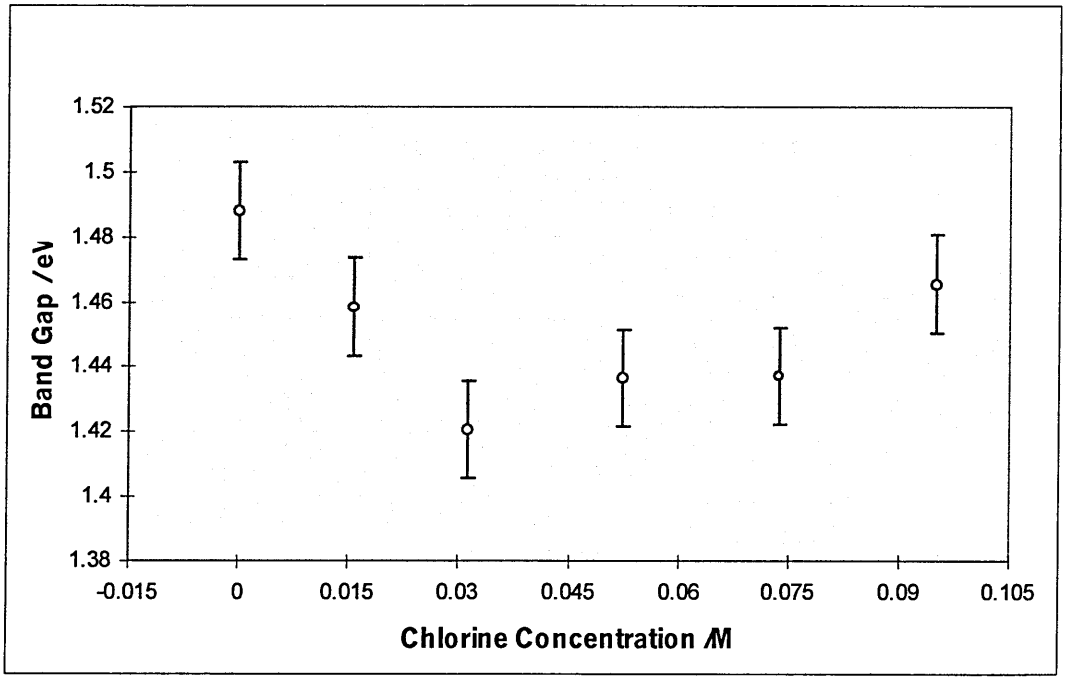

Figure 6.8. Graph Showing CdTe Band Gap against Chlorine Concentration in the CdTe Deposition Bath for Unannealed Samples.

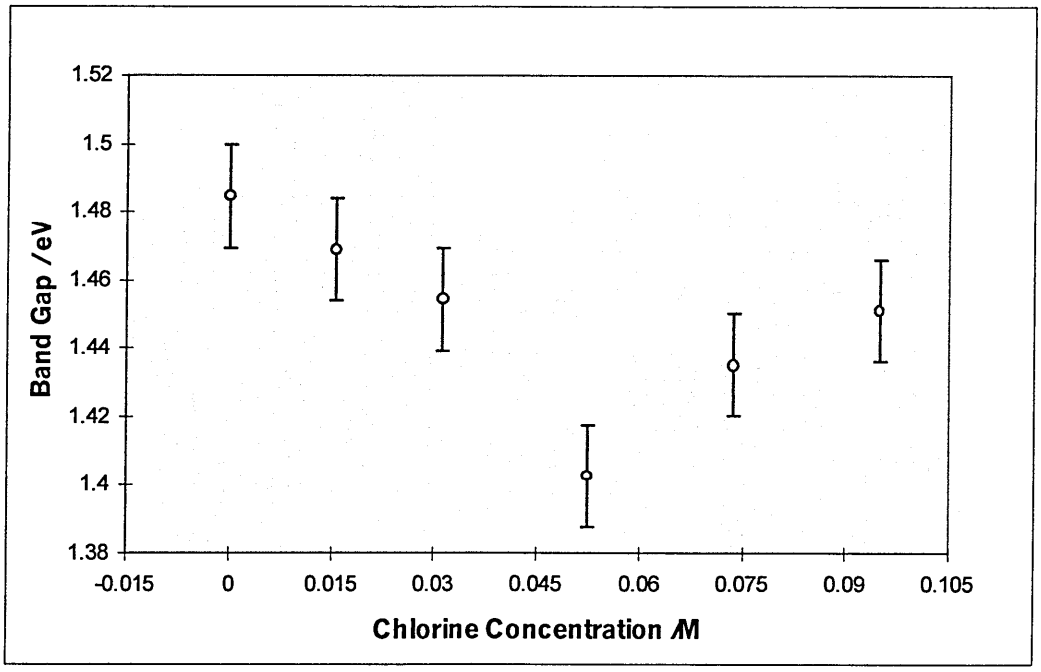

Figure 6.9. Graph Showing CdTe Band Gap against Chlorine Concentration in the CdTe Deposition Bath for Annealed Samples

6.1.4 SEM Images of CdTe Surface

Figures 6.10 and 6.11 show a secondary electron SEM image of the CdTe surfaces under various chlorine treatments at a magnification of ~3800x, an accelerating voltage of 15 kV and a spot size of four. Samples were prepared as described in section 4.6. Figure 6.10 shows unnannealed samples and Figure 6.11 shows annealed samples. The samples were chosen for analysis to show the extremes of chlorine treatment. Sample (a) had no intentionally added chlorine, sample (b) had 0.052 M chlorine in the CdTe deposition bath which gave rise to the highest efficiency devices and sample (c) had 0.137 M chlorine in the CdTe deposition bath. Sample (c) showed a tail off in efficiency compared to sample (b) and was the highest chlorine concentration used in these experiments.

Figure 6.10 shows the as-grown samples, which do not show any significant difference in the grain size between the three samples. All three samples show the surface grains of size 0.25 - 1.00 μm although the sample with no chlorine (sample a) and the 0.137 M chlorine treatment (sample c) do appear to show more, larger surface clusters in the area shown. These grains were 1.5 -3.0 μm in size and appeared to be polycrystalline in nature. Figure 6.11 shows the same samples as Figure 6.10 but following annealing. The annealing treatment did not appear to produce any significant increase in grain size in any of the samples and the surface of the CdTe appears similar in both the annealed and unannealed cases. The samples (a) and (c) do not appear to have as many of the large surface clusters of polycrystalline CdTe as in the annealed case as for the unannealed case.

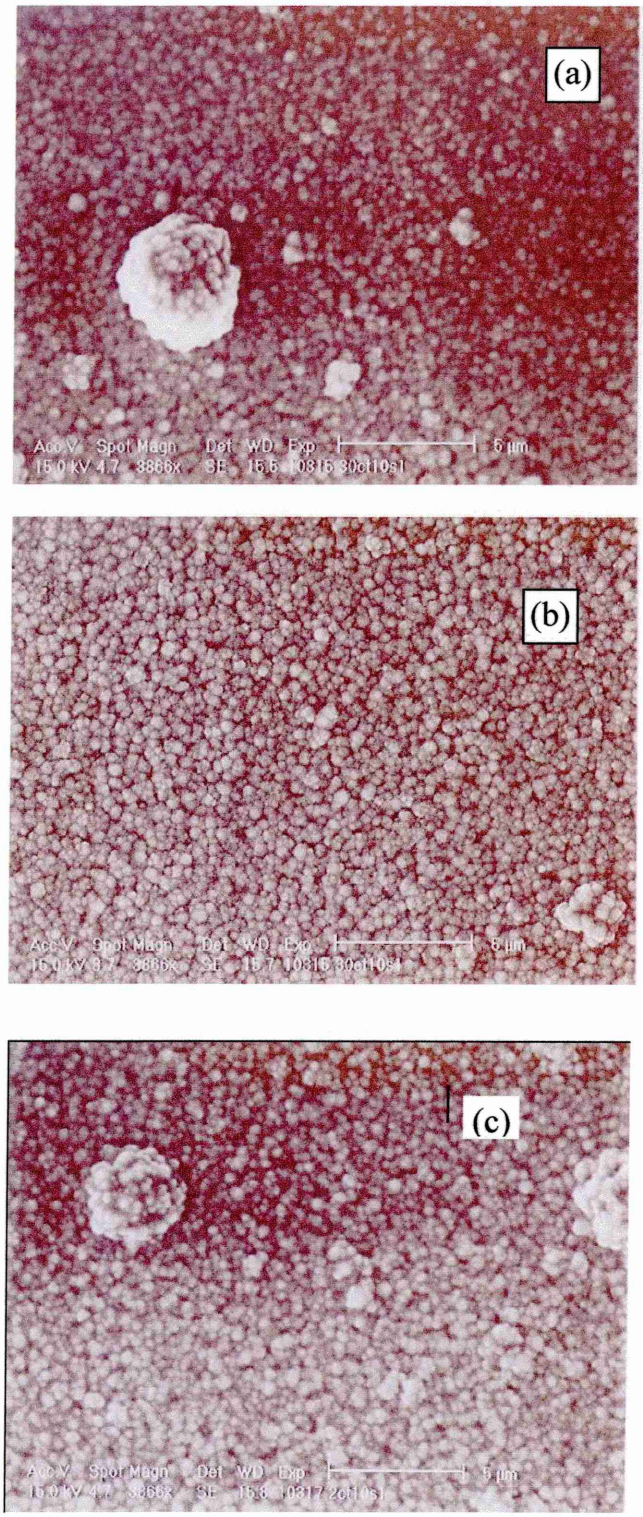

Figure 6.10. CdTe Surface Secondary Electron SEM Image of As-Grown Samples with Chlorine Concentrations of (a) 0.000 M, (b) 0.052 M, and (c) 0.137 M

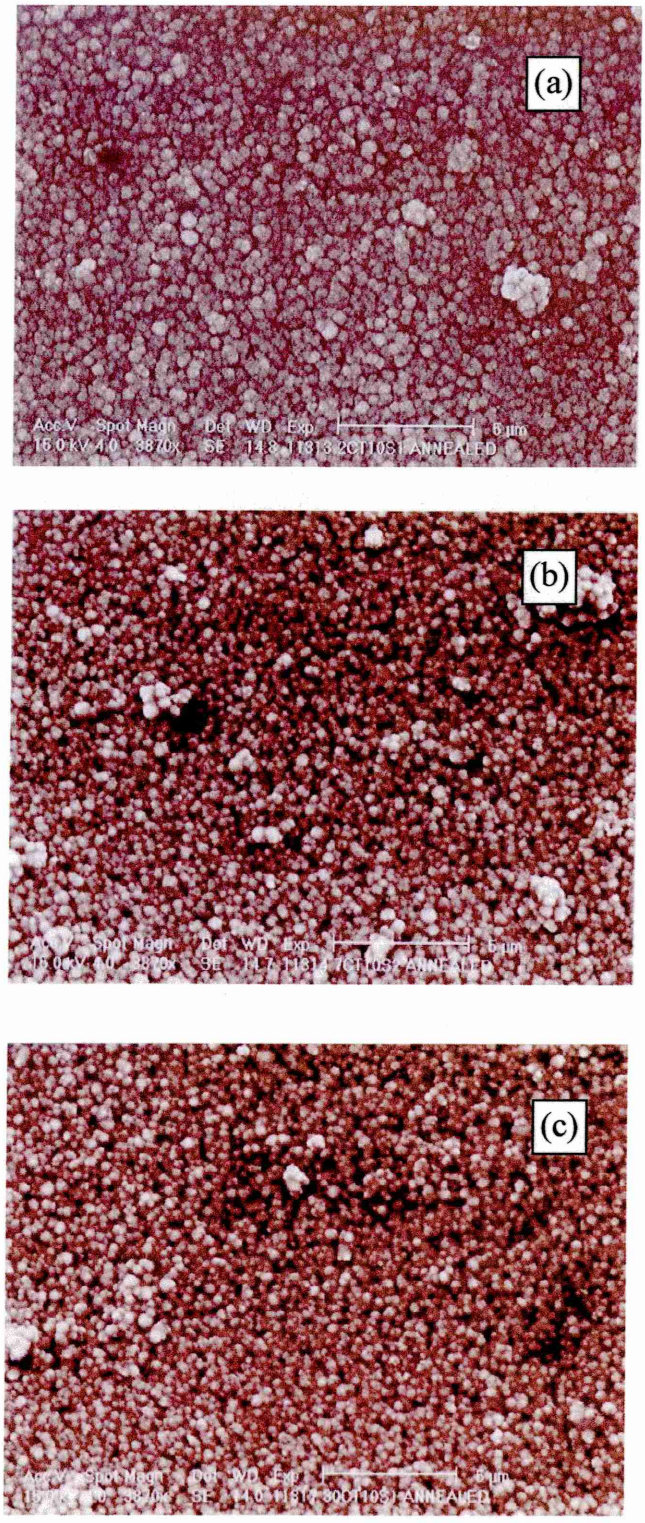

Figure 6.11. CdTe Surface Secondary Electron SEM Image of Annealed Samples with Chlorine Concentrations of (a) 0.000 M, (b) 0.052 M, and (c) 0.137 M

6.2 Treatment of CdTe Bath with $In_2(SO_4)_3$

The treatment of the CdTe layer with indium was achieved by the addition of a stock solution of $In_2(SO_4)_3$ into the CdTe deposition bath to achieve the required In^{3+} concentrations within the bath. $In_2(SO_4)_3$ was chosen as the source of In^{3+} ions as the counter ion of SO_4^{2-} is the same as that for the source of Cd^{2+} ions i.e. $CdSO_4$, which is used for the CdTe deposition itself. To ensure that the addition of the indium stock solution did not introduce any further impurities into the deposition solution the stock solution was electropurified using a method similar to that described in section 4.4. Initial experiments involving the addition of the indium stock solution showed that indium concentrations similar to those in the chlorine addition experiments were used then the devices immediately showed very low efficiencies (<0.1 %). It was, therefore, decided to use much smaller indium concentrations in the ppb range.

6.2.1 Solar Cell Efficiency Data and I-V Parameters

Solar cell I-V characteristics were obtained using the procedure described in section 4.6. As with the chlorine treated samples, the electrical parameters quoted below are calculated from a number of measurements of 5 mm diameter cells on each sample. A minimum of 10 measurements was required from each sample, although generally 20 to 30 cells were measured per sample.

In Conc. /ppb	Efficiency /%	Efficiency Error /%	J_{SC} /mAcm^{-2}	J_{SC} Error /mAcm^{-2}	V_{OC} /V	V_{OC} Error /V	FF	FF Error
0	1.78	0.05	12.90	0.28	0.61	0.01	0.23	0.01
10	1.52	0.11	10.70	0.51	0.59	0.01	0.24	0.01
20	0.96	0.03	7.76	0.26	0.55	0.01	0.24	0.02
30	0.92	0.03	9.43	0.31	0.60	0.01	0.16	0.01
40	0.01	>0.01	0.06	0.01	0.63	0.01	0.20	0.01
50	0.01	>0.01	0.04	0.01	0.63	0.01	0.21	0.01

Table 6.4. Table of Solar Cell Electrical Characteristics against Indium *Concentration in the CdTe Deposition Bath.*

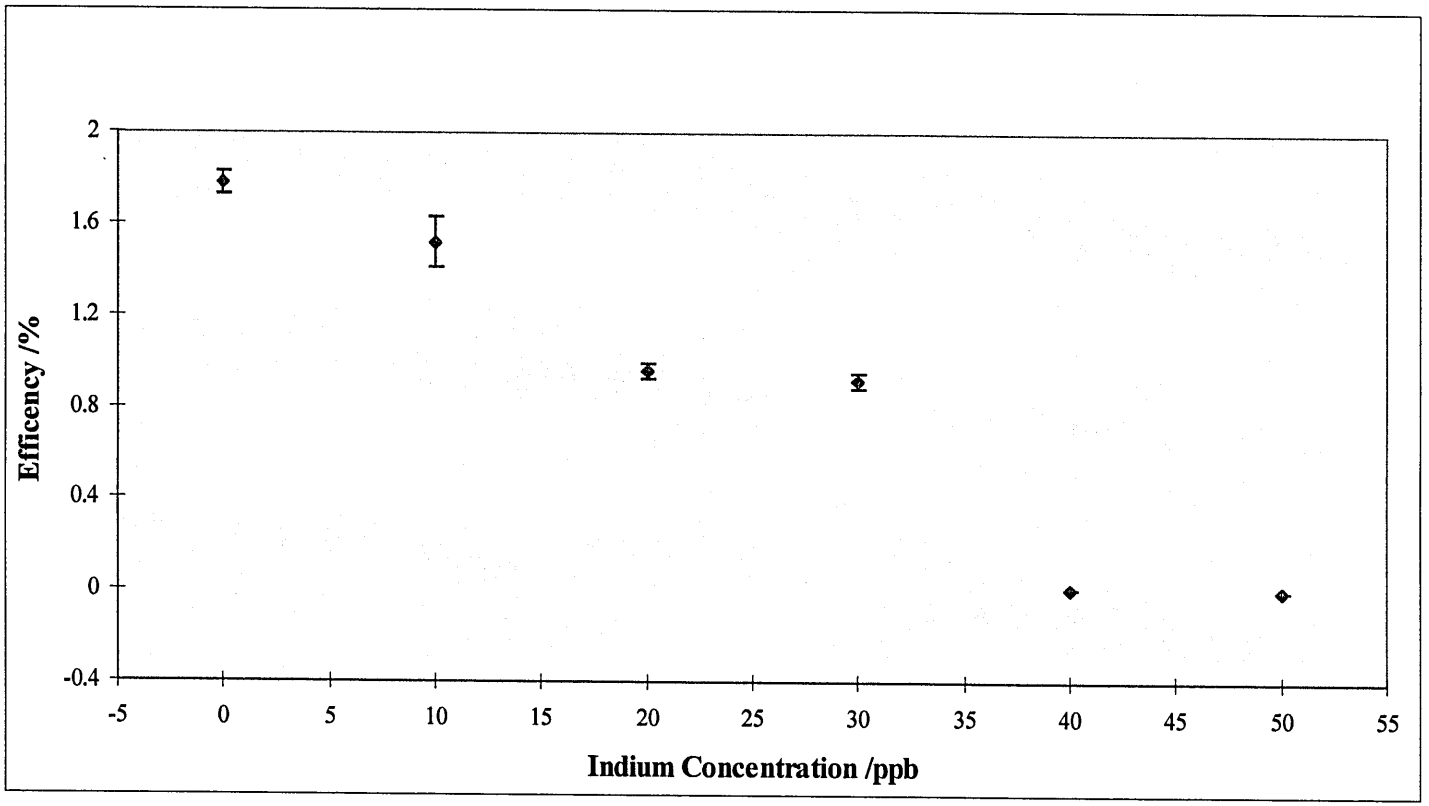

Figure 6.12. Graph Showing Device Efficiency against Indium Concentration in the CdTe Deposition Bath.

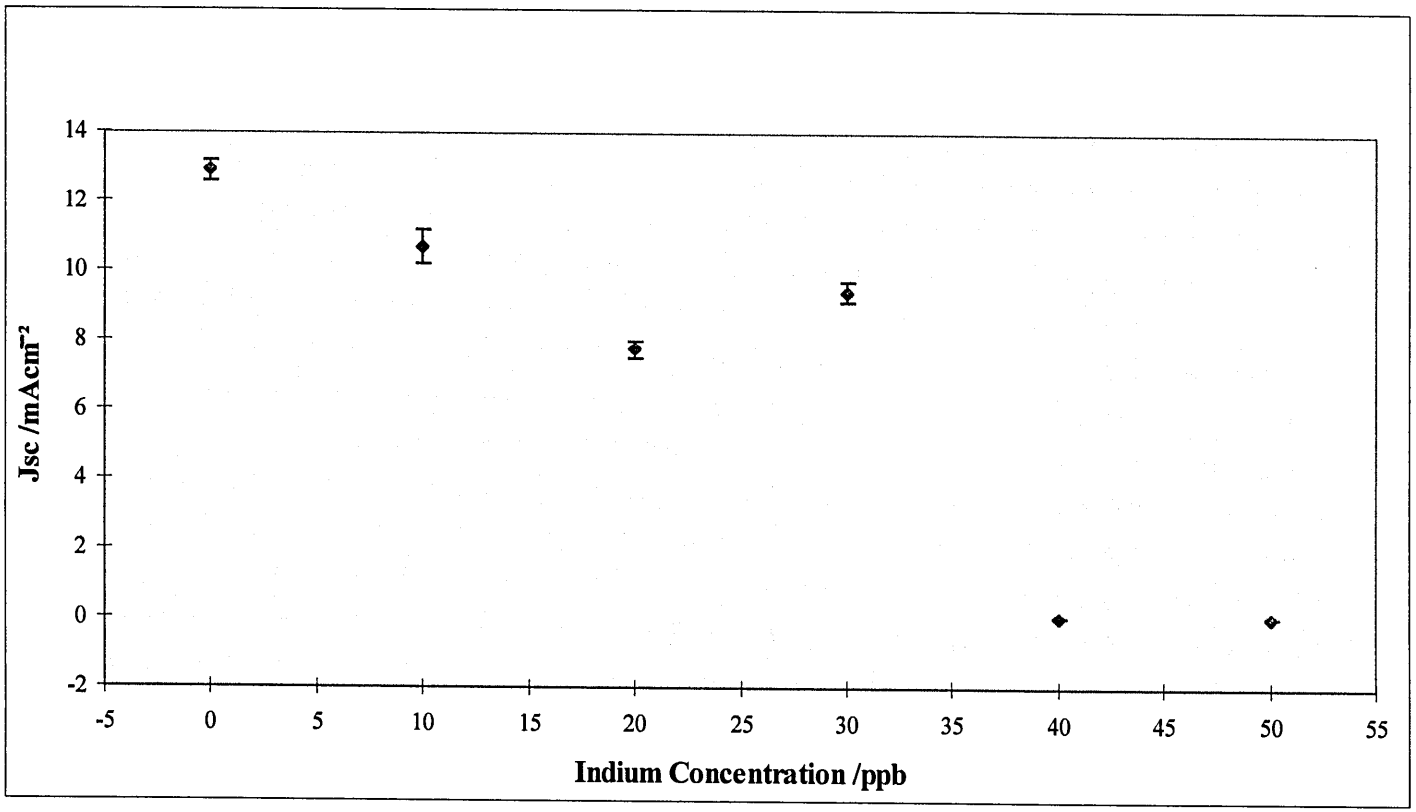

Figure 6.13. Graph Showing Device J_{SC} against Indium Concentration in the CdTe Deposition Bath.

Table 6.4 gives a summary of the solar cell characteristic parameters against indium concentration in the CdTe deposition bath. The error values quoted are the standard errors of the measurements. Figure 6.12 shows a graph of solar cell efficiency against In^{3+} concentration in the CdTe deposition bath. The initial condition of the bath with no intentional doping with indium gave an efficiency of 1.78 ± 0.05 %. The graph shows how the addition of indium produces a rapid decrease in efficiency. The efficiency of devices is below 0.1 % for an addition of 20 ppb indium and below 0.01 % for an addition of 40 ppb indium. It was decided to stop the experiment at an indium concentration of 50 ppb as the cells had such low efficiencies they were barely measurable.

As with the Cl^- treatment of the CdTe films, the parameter most significantly affected by the treatment is the J_{SC}. The untreated film showed a good value of J_{SC} of 12.9 ± 0.3 $mAcm^{-2}$ considering it had not been subjected to Cl^- treatment. Figure 6.13 shows how the J_{SC} rapidly declines with the addition of indium, to the point of 40 ppb indium concentration when the J_{SC} was barely measurable with a value of 0.064 ± 0.008 $mAcm^{-2}$. This trend continued to decrease until at a concentration of 50 ppb a value of 0.036 ± 0.002 $mAcm^{-2}$ for J_{SC} was measured. At these very low efficiency and J_{SC} values it was decided to stop the experiment.

Figure 6.14 shows the device V_{OC} against indium concentration in the CdTe deposition bath. In contrast to the efficiency and J_{SC} results, the V_{OC} data does not show the same downward relationship on increasing the indium concentration in the CdTe deposition bath. The initial condition of no indium treatment gives a value of V_{OC} of 0.61 ± 0.01 V with the next two points of indium concentration, 10 and 20 ppb, being lower than the initial condition with values of 0.59 ± 0.01 V and 0.55 ± 0.01 V, respectively. The point with an indium concentration of 30 ppb is not significantly different from the initial condition with a value of 0.60 ± 0.01 V. The two points of highest indium concentration of 40 and 50 ppb are higher than the initial position with values of 0.63 ± 0.01 V and 0.63 ± 0.01 V, respectively.

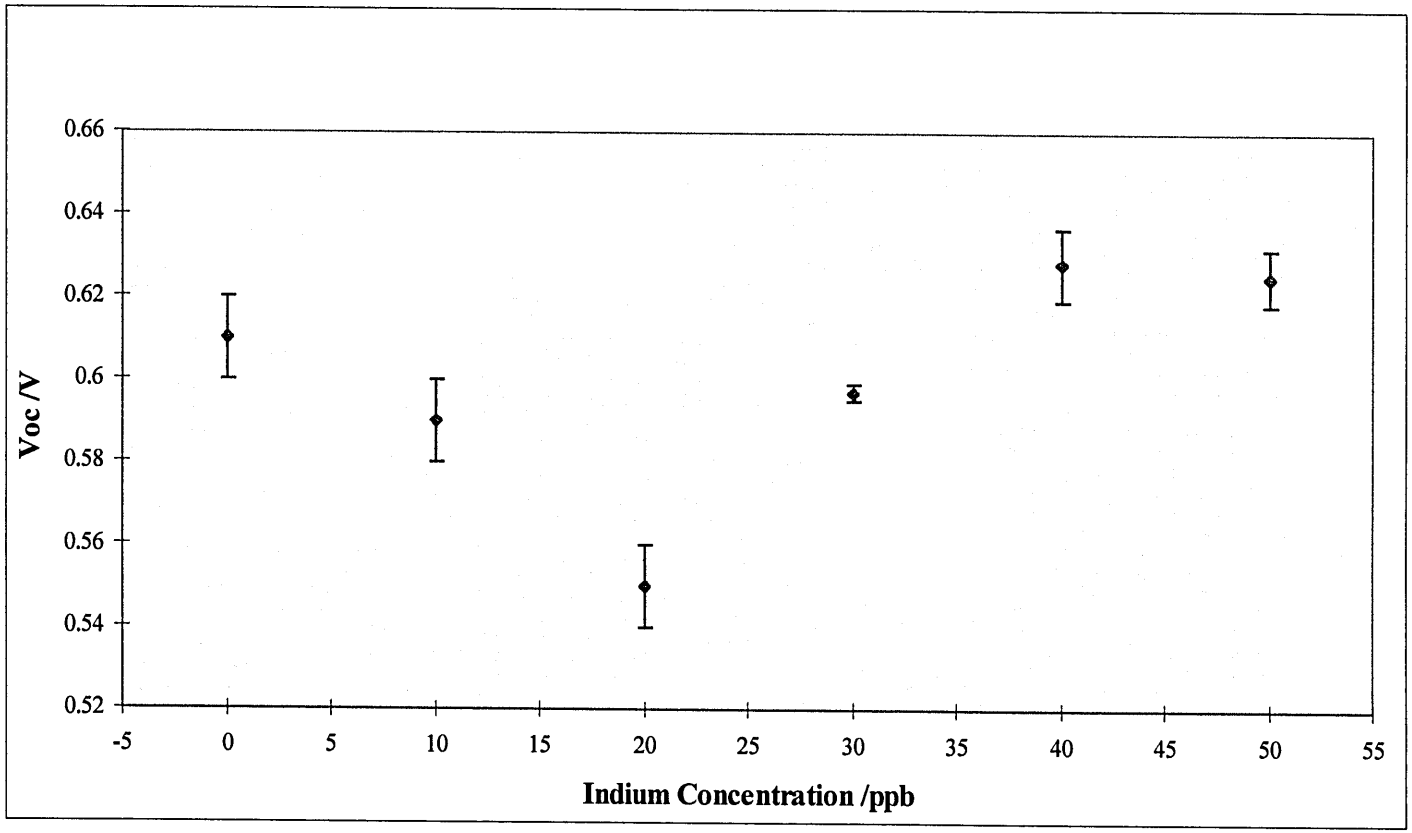

Figure 6.14. Graph Showing Device V_{OC} against Indium Concentration in the CdTe Deposition Bath.

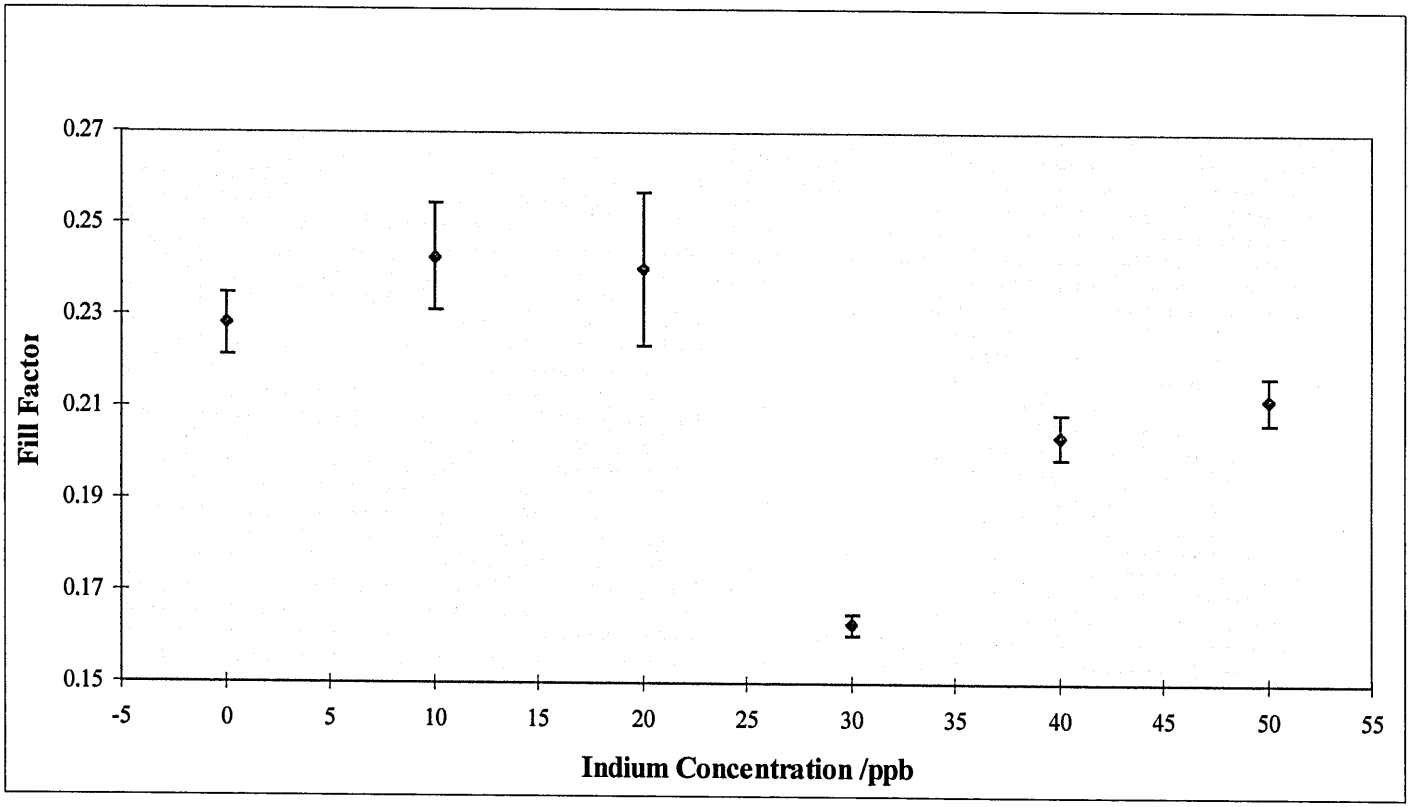

Figure 6.15. Graph Showing Device Fill Factor against Indium Concentration in the CdTe Deposition Bath

Figure 6.15 shows the device fill factor against indium concentration in the CdTe deposition bath. There is no clear trend for this graph, with the first two points of indium addition with concentrations of 10 and 20 ppb giving values of fill factor of 0.24 ± 0.01 and 0.24 ± 0.02 respectively. These initial values are not significantly different to the condition of no indium treatment with a value of 0.23 ± 0.01. The higher values of indium concentration are significantly lower than the initial no indium treatment condition. In particular, the point with an indium concentration 30 ppb has a low fill factor value of 0.16 ± 0.01. This indicates that the addition of indium into the CdTe deposition bath does have an affect on the fill factor at higher concentrations in the range used.

6.2.2 Treatment of CdTe Bath with $In_2(SO_4)_3$ XRD Results

Figure 6.16 shows the CdTe P_{111} Percentage against the indium concentration in the CdTe deposition bath. Samples were measured and then re-measured after annealing using the procedure described in section 4.5.1. Samples were annealed in air at 410°C for 12 minutes and allowed to cool slowly. Samples were annealed to replicate the conditions used in the production of the solar cells. Table 6.5 shows the data for the CdTe P_{111} Percentage against the indium concentration in the CdTe bath. The estimate in the error in the CdTe P_{111} Percentage of ± 0.1 % is obtained from estimates of measurement repeatability.

Indium Concentration /ppb	Unannealed CdTe P_{111} Percentage /% (±0.1 %)	Annealed CdTe P_{111} Percentage /% (±0.1 %)
0	95.8	95.4
10	88.6	87.8
20	78.7	77.2
30	74.7	74.6
40	72.7	72.7
50	70.9	70.9

Table 6.5. Table Showing CdTe P_{111} Percentage against Indium Concentration in the CdTe Deposition Bath.

The condition of no indium addition shows the highest CdTe P_{111} Percentage peak for both the unannealed and annealed sample. On addition of the indium stock solution, the CdTe P_{111} Percentage decreases significantly. Further increase of indium concentration produced further reduction of the CdTe P_{111} Percentage. The samples with added indium did not show significantly different CdTe P_{111} Percentage between the unannealed and annealed samples.

6.2.3 Treatment of CdTe Bath with $In_2(SO_4)_3$, Optical Absorption and SEM Results

Indium treated samples were measured by optical absorption as described in section 4.8, using experimental conditions, as described in section 4.8.1. Indium treated CdTe samples were measured both under unannealed and annealed conditions. There was no significant difference in the measured band gap of any of the samples, which had undergone different indium treatments, and also no significant difference in band gap between samples unannealed or annealed.

Several indium treated samples were inspected using SEM as described in section 4.6. Samples were inspected both in the as grown and annealed state. Again, no significant difference in grain structure or size was observed when comparing samples under different indium treatment conditions or when comparing unannealed to annealed samples.

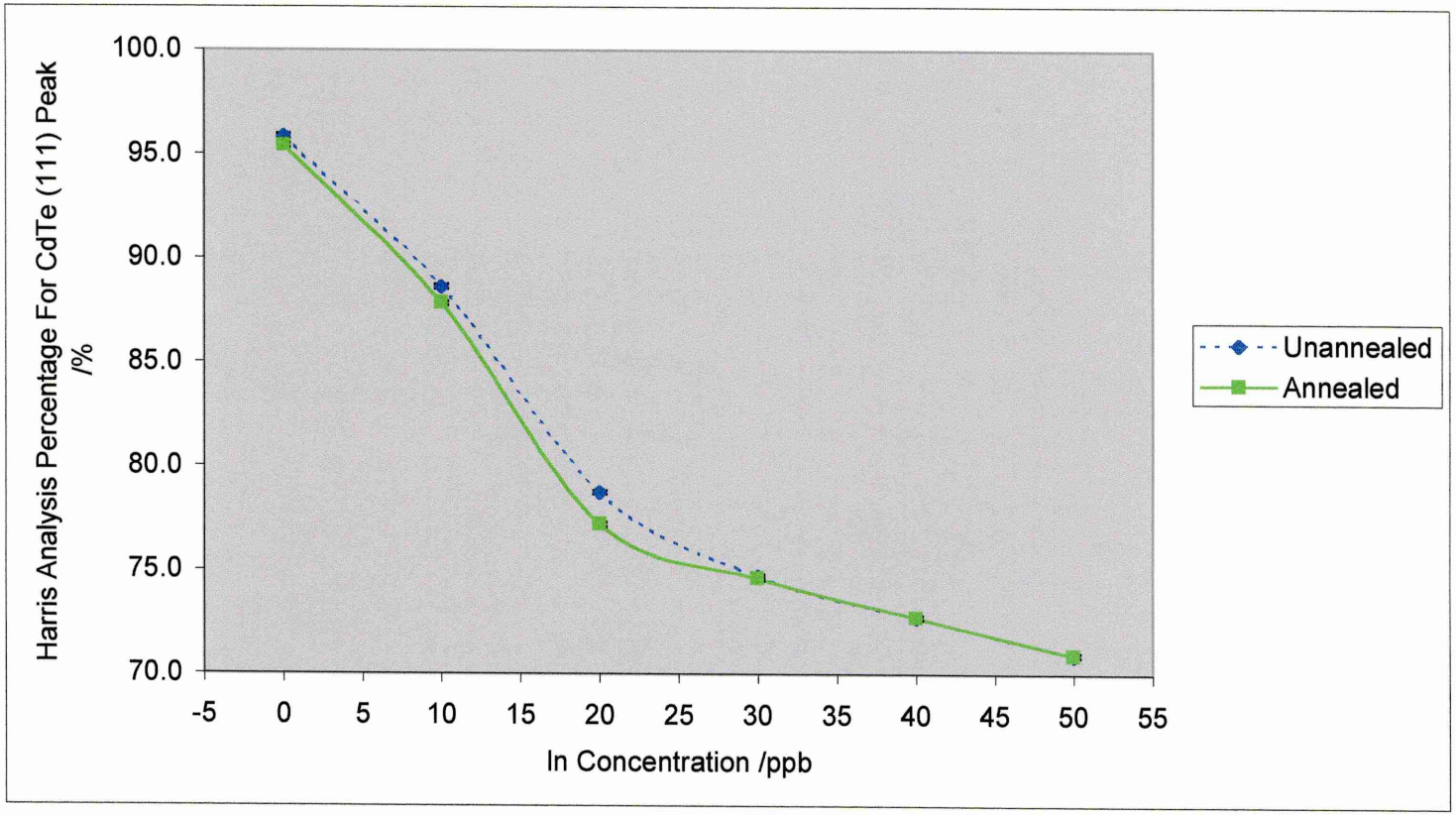

Figure 6.16. Graph Showing CdTe P_{111} Percentage against Indium Concentration in the CdTe Deposition Bath.

Chapter 7.0: Discussion of Results

7.1 Introduction

The previous two chapters showed results on the development at Sheffield Hallam University of the deposition of CdS and CdTe by electrodeposition and the formation of glass/CTO/CdS/CdTe/metal solar cells (Chapter 5). Chapter 6 gave results following treatment of the CdTe layer in these devices with either chlorine or indium. This chapter discusses the individual films produced, followed by the overall performance of the device with respect to the chlorine or indium treatment of the CdTe layer.

7.2 Deposition of CdS

7.2.1 Cyclic Voltammetry of CdS

Cyclic voltammetry on a standard CdS solution (section 5.2.1) showed a large plateau region (-0.4 V to -0.7 V against Ag/AgCl) over which CdS could be grown. Generally films are grown at the more negative end of the plateau to ensure high deposition rates. Deposition potential is chosen to be close to, but not at, the point where cadmium metal deposition begins i.e. at the point where the sharp increase in current is observed. For the deposition solution used, a potential of -0.60 ± 0.01 V against Ag/AgCl was found to produce an acceptable rate of growth without the formation of dentritic cadmium. The fact that the cyclic voltammetry graph showed a large plateau region over which CdS can be grown indicated that growth potential is not as critical a parameter as for the growth of CdTe (section 7.3).

7.2.2 XRD of CdS

XRD measurements of the CdS showed that films deposited at -0.60 ± 0.01 V against Ag/AgCl produced well formed hexagonal CdS (section 5.3.1). Figure 5.3 shows the XRD spectrum of an unannealed CdS sample grown on a glass/ITO superstrate. Comparison of this spectrum with APD data confirms that the CdS is polycrystalline and in the hexagonal structure. The CdS film is relatively thin (approximately 200 to 400 nm) when compared with the CdTe layer (1.5 to 2.0 μm) but still produces well-defined peaks in the XRD spectrum. Although a good correlation is found between the CdS XRD data and the APD data for hexagonal CdS (APD card 41-1049) recent work has brought this type of analysis under scrutiny. Gibson et al 1998 used the technique of Glancing Angle XRD (GAXRD) to investigate CdS grown by CBD and electrodeposition. The use of GAXRD allows the investigation of very thin films with the removal of substrate effects. This work found the films to be composed of a mixture of cubic and hexagonal CdS. Rietveld analysis was used to determine if the CdS showed the Polytype structure. Polytype material can be described as an intermediate between face-centred cubic and hexagonal structures. The stacking sequence of a hexagonal structure is ab-ab-ab-...while that of fcc is abc-abc-abc... In a polytype material neither stacking sequence dominates, and either a random sequence or a more complicated sequence is found. Gibson et al concluded that their CdS films both as deposited and annealed have a polytype structure. The Sheffield Hallam University CdS films could also be of this structure although they are provisionally assigned to be hexagonal. Further analysis of the films using GAXRD would be required to confirm this.

Upon annealing the sample, the CdS peaks significantly increased in intensity and, in addition to seeing the same five peaks, as previously, an additional three peaks corresponding to (102), (103) and (201) reflections are apparent. Table 5.1 shows the percentage increase in peak height and the percentage reduction in FWHM. The increase in peak heights indicated the significant increase in crystallinity of the CdS upon annealing. In addition, the reductions in peak FWHM show the significant improvement in crystal quality brought about by annealing.

Section 5.3.2 shows results for an experiment on the effect of deposition pH on the XRD spectra of CdS films. Figure 5.5 shows the XRD spectra grown with different pH values. Table 5.2 gives the XRD peak heights and FWHM of the CdS samples. It is clear that the lowest pH value of 2.20 ± 0.05 gives rise to the largest peak count. The highest pH value of 4.23 ± 0.05 gives rise to the smallest peak count. In this case, as no annealing has been performed on these samples, the increase in peak height is indicating an increase in thickness of the CdS. This increase in CdS thickness with reduction in deposition bath pH value is a result of the reaction given in equation 3.15, which shows how the thiosulphate ions disproportionate, is pH dependent [Power et al 1981]. The lower the pH the more the reaction progresses to the right and, as the solubility product of CdS is very small [Kröger 1978], an extremely low concentration of sulphur would lead to CdS formation given the high concentration of cadmium ions.

The ability to control the deposition rate of the CdS by varying the pH of the deposition bath would be useful as it appears that the mechanism of growth does not allow for significant variation in deposition characteristics with variation in the deposition potential as is the case for CdTe. Problems occur, as it was observed that the deposition bath pH value reduces spontaneously with time, even when the bath is not being used. This means that growth rates will increase with bath lifetime and, in addition, the formation of CdS within the deposition bath increases. Dennison 1993 saw a similar phenomenon in his aqueous CdS deposition bath. Dennison monitored the pH of the bath over a period of 75 hours as he deposited films. He found that the decrease in pH and, hence, the production of CdS in solution, was accelerated when the bath was used for electrodeposition.

Using a deposition bath pH of 3.06 ± 0.05, a compromise value of pH which while maintaining a reasonable growth rate does not result in excessive CdS formation in the deposition bath, would not solve this problem as the pH would change with time. It would not be acceptable to add alkali to increase the pH as this would introduce impurities into the deposition bath. This is a serious problem for the implementation of aqueous electrodeposition of CdS for the large-scale production of CdS/CdTe solar cells. Bath lifetime will have to be extended beyond the current two-day limit if electrodeposition is to become a viable method of producing CdS.

7.2.3 Optical Absorption of CdS

Section 5.4.1 gives optical absorption results for a CdS film grown at pH = 3.06 ± 0.05, a deposition potential of -0.60 ± 0.01 V against Ag/AgCl and a deposition period of 60 minutes. The sample was annealed in air to obtain optical properties of a film under conditions as close as possible to the production conditions of a working device. Figure 5.9, a graph of alpha squared against energy, gives a value of the band gap of the CdS of 2.42 ± 0.02 eV. This is equal to the accepted value of the band gap of CdS of 2.4 eV (Zanio 1978).

7.3 Deposition of CdTe

7.3.1 Cyclic Voltammetry of CdTe

Linear scan voltammetry on standard CdTe solution (Section 5.2.2) was undertaken the result of which is shown on Figure 5.2. The scan shows an initial peak centred at -0.10 ± 0.04 V against Ag/AgCl, which is considered to be the onset of elemental tellurium deposition. Following this peak, a steady increase in the current is seen up to a value of voltage of -0.29 ± 0.04 V where a plateau region is observed in the voltage range –0.29 to –0.68 V. This is considered to be the region of CdTe deposition. This plateau region indicates that over this range the process is diffusion controlled. At the potential 0.68 ± 0.04 V, a rapid increase in the deposition current was observed. This is considered to be the onset of cadmium deposition.

Although the plateau region from –0.29 to –0.68 V against Ag/AgCl is believed to be the region of CdTe deposition, several authors have suggested this may not be pure CdTe but may be a mixture of CdTe and elemental tellurium. Danaher et al 1984 suggested that from the kinetics of the CdTe deposition process it would be likely that free elemental tellurium would be formed in films grown within this potential range. Bhattacharya et al 1984 showed, using EDAX semiquantitative estimates, that the relative Cd:Te ratio in the film yielded an average of approximately 45:55. To confirm the results from the cyclic voltammetry, XRD spectra were obtained from films grown at various deposition potentials along the CdTe cyclic voltammetry spectra.

7.3.2 XRD of CdTe

Figure 5.6(a) shows a film deposited at -0.21 V against Ag/AgCl. This XRD spectrum confirms the film consists of elemental tellurium in the cubic structure. The tellurium formed is polycrystalline, as shown by the large number of tellurium peaks in the XRD spectrum. This film was a well-crystallised continuous film, black in colour, with good adhesion to the superstrate and was visually difficult to distinguish from a well-formed CdTe film. Hence, this result confirms the cyclic voltammetry result that the initial peak in the voltammagram centred at -0.10 ± 0.04 V against Ag/AgCl is the onset of tellurium deposition.

Figure 5.3 (b) shows a film grown at -0.32 V against Ag/AgCl showing reflections arising from both CdTe and tellurium. This value of deposition potential was chosen to show the composition of the CdTe at the lower end of the plateau region. Although the XRD spectrum indicates a significant proportion of the film is CdTe, tellurium peaks are also observed arising from the (101) and the (102) reflections. The multiple peaks from both the CdTe and tellurium show the material is polycrystalline. The principal CdTe peak arises from the (111) plane of CdTe with the cubic structure. The CdTe (111) plane is classed as the 100% intensity direction for cubic CdTe (data from APD data card 15-770). The CdTe (111) plane is generally found to be the principal peak in electrodeposited CdTe [Shkedi et al 1980, Morris et al 1992].

Figure 5.3 (c) shows a film grown at -0.65 V against Ag/AgCl, which shows reflections arising from well-formed cubic CdTe. This value of deposition potential was chosen to be at the more negative end of the plateau region, although not in the deposition of dentritic cadmium region. The principal peak, again, arises from the CdTe (111) plane although other peaks are observed showing the polycrystalline nature of the CdTe. This film shows no evidence of the formation of elemental tellurium.

The formation of free tellurium in the films is detrimental to the semiconducting properties of the film, as elemental tellurium is metallic in nature. In the worst case, the presence of elemental tellurium could lead to short-circuiting in the device. This shows that, unlike the case of CdS where it is possible to grow well formed CdS over a large potential range with only a small change in deposition current, the deposition potential of CdTe is limited by the formation of elemental tellurium. This work shows the importance of good potential control during the growth of CdTe.

Section 5.3.4 gives results for the XRD spectra of unannealed and annealed CdTe. The CdTe sample used in this experiment was grown at a QRP of -0.69 ± 0.01 V against Ag/AgCl, with a deposition current of 0.25 $mAcm^{-2}$ for a period of three hours. Figure 5.7 shows the XRD spectrum of the as grown CdTe film. The film is polycrystalline with the principal peak arising from the (111) plane of cubic CdTe.

Figure 5.8 shows the XRD spectrum of the same sample after annealing at 410°C for 12 minutes in air. No new peaks are observed in the spectra upon annealing, although Table 5.3 shows that all the peaks showed a significant increase in peak height. This change in peak height ranges from an increase of 4.5% for the (331) plane to an increase of 43.9% for the (220) plane. The principal peak arising from the (111) plane gave an increase in peak height of 10.2%. Overall, there is no significant change in the FWHM of these peaks, with the (311) plane reducing its FWHM, the (220) increasing its FWHM and the other two peaks remaining unchanged. This indicates that annealing improves the crystallinity of the sample but does not significantly improve the crystal quality of the CdTe.

7.3.3 Optical Absorption of CdTe

Section 5.4.2 gives optical absorption results for a CdTe film grown at solution temperature of 90°C at a QRP of -0.69 ± 0.01 V against Ag/AgCl for a period of 180 minutes. The sample was annealed in air to obtain optical properties of a film under conditions as close as possible to the production conditions of a working device. Figure 5.10 shows a graph of alpha squared against energy that gives a value of the CdTe band gap of 1.49 ± 0.02 eV. This value is almost equal to the accepted value of the band gap of CdTe of 1.45 eV (Zanio 1978). This value, even taking into consideration experimental error, is higher than the accepted value. The band gap value obtained in this Sheffield Hallam University study agrees with the results obtained by Dutta et al 1995. Their values of band gap varied from 1.485 – 1.494 eV for an electrodeposited film of CdTe on a SnO_2 coated glass substrate.

7.3.4 SEM of the CdTe Surface

Figure 5.11 shows a secondary electron SEM image of the CdTe surface. The polycrystalline nature of the sample can be seen from the large number of CdTe grains in the field of view. This as-grown film shows relatively good crystal size for an electrodeposited film of CdTe in the range from 0.1 to 0.5 μm. Dutta et al 1995 estimated the grain size of their films deposited at various potentials SnO_2 coated glass substrates to be in the range 0.19 – 0.31 μm. Dennison 1995 quoted the mean diameter of the nodules on his films as being approximately 0.3 μm. Therefore, the Sheffield Hallam University produced films show grain diameters at least as good as those quoted by other groups.

7.4 Formation of Glass/TCO/CdS/CdTe/Metal Solar Cells

Once initial deposition conditions for the preparation of both the CdS and CdTe layers were defined as described previously, samples were made into solar cell devices to investigate their performance. Section 5.6.1 describes experimental results investigating the effect of pre-conditioning the CdTe deposition bath on the solar cell performance of the devices.

Figure 5.12 shows the variation of efficiency against deposition number for a newly prepared CdTe deposition bath. A large variation in efficiency is observed from deposition to deposition. Comparison of Figure 5.12 with Figure 5.13, which is a graph showing variation of the J_{SC} against deposition number, shows that the large variation in efficiency is due to large variations in the J_{SC} value. As yet the reasons for such large variations in J_{SC} are not known although it may be due to impurity related issues which are discussed later.

It was clear that the parameter showing significant improvement with the pre-conditioning of the CdTe bath was the V_{OC} value. Figure 5.14 shows a graph of device V_{OC} against deposition number for a newly prepared CdTe deposition bath. The improvement observed varied from the initial film with a V_{OC} value of 0.49 ± 0.01 V to a value of 0.59 ± 0.01 V for the fifth deposition. This steady increase in V_{OC} was not of sufficient magnitude to over come the dominant effect of the J_{SC} on the overall efficiency graph, but it does show how the V_{OC} value was improved by pre-conditioning the bath.

Improvements in the V_{OC} value are normally associated with improvements in the CdS/CdTe interface properties. In this case, it appeared that an electropurification process was taking place with each subsequent deposition, giving rise to higher V_{OC} values. It is unlikely that this improvement is solely related to improvements in the CdS/CdTe interface quality but is related to improvement in the electronic property of the CdTe leading to an improvement in the overall device characteristic.

Figure 5.15 shows a graph of device fill factor against deposition number from the newly prepared CdTe bath. Significant improvement in the fill factor value was seen upon pre-conditioning the bath. The improvement varied from the initial film with a fill factor value of 0.30 ± 0.01 to a value of 0.37 ± 0.01 for the fifth deposition. As with the V_{OC} value, the increase in fill factor is not of sufficient magnitude to over come the dominant effect of the J_{SC} on the overall efficiency graph, but it does show how the fill factor value is improved by pre-conditioning the bath.

It has been shown that electrodeposited CdTe films contain fewer impurities than CdTe single crystals, supplied as 5N pure as measured by SIMS [Lyons et al 1984]. Further work [Lyons et al 1989] investigated the source of impurities found in the CdTe deposition solution and also using SIMS in the CdTe films. Both of these investigations made extensive use of pre-electrolysis of the $CdSO_4$ solution prior to addition of the sulphuric acid to adjust the pH of the deposition solution or the addition of the tellurium ions. No comment was made as to whether further improvements in impurity reduction were made upon deposition of CdTe films from the bath. The Sheffield Hallam University results show that some electropurification process is taking place, which can be observed in the device performance. This is observed as a significant increase in the V_{OC} and fill factor values by pre-conditioning the electrodeposition bath.

7.5 Treatment of CdTe with Chlorine

The treatment of CdTe with chlorine in glass/TCO/CdS/CdTe/metal solar cells has been widely used [Abou-Elfotouh et al 1993], although the improvement mechanism is not well understood. The aim of these experiments was to treat the CdTe film with chlorine in a controlled manner to further understand this mechanism. In the electrodeposition technique the CdTe film is produced from an electrochemical bath so it is relatively easy to include the chlorine in the deposition bath [Basol et al 1986, Das et al 1993, Dennison 1994]. Basol et al 1986 varied the Cl^- concentration from 0 to 0.015 M using HCl as the source of Cl^- ions. Cells were made with Cl^- concentrations up to 0.03 M, though those began to show poor adhesion to the superstrate after heat treatment.

The University of Queensland group prepared the CdTe deposition both using $3CdSO_4 \cdot 8H_2O$ (A.R. grade) and $CdCl_2 \cdot H_2O$ (A.R. grade) [Morris et al 1990] as the sources of Cd^{2+} and Cl^- ions. The ratio of Cl^- to SO_4^{2-} ions was 1:33 in a 2.5 M Cd^{2+} solution. No reference was given as to whether this was an optimised value of Cl^- ion inclusion.

Dennison 1994 used a Cl^- concentration of 0 to 300 ppm, using $CdCl_2$ as the source of Cl^- ions. This work highlighted the importance of Cl^- treatment for improving J_{SC} values. This study used a chlorine concentration range of 0 to 0.137 M, which from calculation is believed to encompass all the above Cl^- concentrations. This range is considered to go beyond the values used in previous studies in order to understand limitations of the chlorine treatment.

7.5.1 Discussion of I-V Results

Section 6.1 gave results for the treatment of CdTe with $CdCl_2$, with Section 6.1.1 covered specifically the solar cell efficiency data and I-V parameters. It is clear from figure 6.1 that the addition of $CdCl_2$ to the CdTe deposition bath significantly improved the efficiency values for the glass/TCO/CdS/CdTe/metal devices. Comparison of Figure 6.1 with Figure 6.2 shows that this significant improvement is mainly due to improvements in the J_{SC} values for the devices. Figure 6.2 shows a rapid increase in J_{SC} value up to a chlorine concentration of 0.052 M followed by a slight tail of at higher chlorine concentrations.

This study verifies the work of the authors mentioned in section 7.5, in that the addition of chlorine does bring about significant improvements in the J_{SC} value. This work shows that the amount of chlorine added could be larger than previous studies have suggested, for example 0.052 M is almost 3.5 times greater than the 0.015 M chlorine ion concentration used by Basol et al 1986. In addition, chlorine concentrations above 0.052 M produced lower efficiency devices than the optimum value showing that the treatment does have some limiting factors on efficiency improvement.

In terms of the V_{OC} performance of the device, this investigation showed that there was a trend of improving V_{OC} with increasing chlorine concentration (Figure 6.3). The V_{OC} value increased from 0.59 ± 0.01 V with no chlorine treatment to a value of 0.64 ± 0.01 V with a chlorine treatment of 0.095 M. Dennison 1994 did not see a corresponding improvement in V_{OC} with increasing chlorine concentration, although his devices did show higher V_{OC} values (of approximately 0.72 V) than those observed in this study. One possibility is that the chlorine was overcoming limiting effects in the Sheffield Hallam University devices that were not affecting Dennison's devices.

CdTe films grown by methods other than electrodeposition also show significant improvement in V_{OC} values with $CdCl_2$ treatment. Ringel et al 1991 showed a device with CdTe grown by MBE showed an improvement in the V_{OC} value from 385 mV with no chlorine treatment to 720 mV with chlorine treatment. Loginov et al 1996 showed a device with CdTe grown by CSS showed an improvement in the V_{OC} value from 0.55 V with no chlorine treatment to 0.68 V with chlorine treatment. In general, devices with V_{OC} values below 0.7 V appear to show improved V_{OC} performance with chlorine treatment. The Sheffield Hallam University devices did not show any limitations in improvement in V_{OC} with increasing chlorine concentration i.e. the V_{OC} value increased with chlorine concentration across the whole range of chlorine concentrations used in this experiment.

Figure 6.4 shows the variation of device fill factor against chlorine concentration. The general shape of the fill factor graph was the same as the efficiency graph. An increase in fill factor with increasing chlorine concentration was observed up to a maximum value of fill factor of 0.44 ± 0.01 at a chlorine concentration of 0.052 ± 0.005 M, with a tail off at higher chlorine concentrations. The highest concentration of chlorine of 0.137 ± 0.005 M gave a value of fill factor of 0.35 ± 0.01 which was lower than the condition of no chlorine addition (fill factor of 037 ± 0.01), showing excessive addition of chlorine had a detrimental effect on the fill factor. This shows that up to a value of 0.052 ± 0.005 M the addition of chlorine had a beneficial effect on the fill factor performance of these devices. Above this value additional chlorine lead to a tail off in fill factor values.

Basol and Dennison do not comment on improvements to the fill factor of their devices with the addition of chlorine. Groups who used the $CdCl_2$/methonal surface treatment reported significant improvements in the fill factor. Ringel et al 1991 reported an improvement in fill factor from 0.32 to 0.51 with chlorine treatment. Loginov et al 1996 reported an improvement in fill factor from 0.39 to 0.57 with chlorine treatment.

7.5.2 Discussion of XRD Results

Section 6.1.2 gave XRD results for the $CdCl_2$ treated CdTe samples both unannealed and annealed. Figure 6.5b shows an initial increase in the CdTe P_{111} Percentage upon addition of chlorine. The CdTe P_{111} Percentage remains higher than the no added chlorine case, up to a chlorine concentration of 0.031 ± 0.005 M. Samples having chlorine concentrations in the deposition bath greater than 0.031 ± 0.005 M showed lower CdTe P_{111} Percentage compared with the sample with no chlorine treatment.

$CdCl_2$ is a well-established fluxing agent for both CdS and CdTe when they are formed by the screen printing/sintering technique [Ikegami 1988], and therefore some improvement would be expected with the addition of $CdCl_2$/annealing. Abou-Elfotouh et al 1993 reported an increase in the preferred CdTe (111) orientation upon $CdCl_2$ treatment and annealing of samples with CdTe grown by various techniques, although this increase was not quantified. It is believed that these Sheffield Hallam University XRD results are the first to relate the degree of chlorine treatment to the structural properties of the CdTe film.

Lee et al 1998 showed that the preferred orientation of the CdTe (111) plane reduced with increasing annealing temperature during $CdCl_2$ treatment. The reduction in preferred orientation was accompanied by an increase in grain size. Qi et al 1996 investigated the normalised XRD intensity ratio as a function of annealing temperature and annealing time. This work found nonmonotomic behaviour of the intensity ratio as a function of annealing time suggesting this is not a single activated process. This group showed the recrystallisation rate of CdTe when annealed without $CdCl_2$ treatment is much lower than that with the $CdCl_2$ treatment, indicating that the presence of $CdCl_2$ reduces the recrystallisation energy. This indicates the importance of optimisation of the degree of chlorine treatment, annealing temperature and annealing time in the production of high efficiency CdS/CdTe solar cells.

Moutinho et al 1997,1998 used XRD to show structural changes in CdTe thin films are enhanced when $CdCl_2$ is present. Moutinho et al demonstrated that these changes occur due to recrystallisation and subsequent grain growth. Recrystallisation is a function of lattice strain energy, time of heat treatment and temperature of heat treatment. As in this experiment time and temperature were constant for the $CdCl_2$ treated and non $CdCl_2$ treated samples they concluded that the effect of the $CdCl_2$ is to increase the initial strain energy of the material so that recrystallisation can occur. They proposed the mechanism was via diffusion of Cl atoms into the film, mainly through grain boundaries, and the consequent increase in defect concentration.

Comparing the XRD results with the I-V results discussed earlier, the XRD graph (Figure 6.5b) and the chlorine treatment efficiency and J_{SC} graphs (Figures 6.1 and 6.2) show a trend increasing to a maximum and then tailing of to higher values of chlorine concentration in the deposition bath.. The maximum values in the XRD and electrical results are not at the same value of chlorine concentration; the maximum value of XRD count being at a chlorine concentration of 0.031 ± 0.005 M and the maximum value of efficiency and J_{SC} being at a chlorine concentration of 0.052 ± 0.005 M. This indicates a close relationship between chlorine-induced improvements in CdTe structural properties and electrical properties, although the relationship may not be absolute.

7.5.3 Discussion of Optical Absorption Results

Section 6.1.3 gave optical absorption results for the $CdCl_2$ treated CdTe samples both unannealed and annealed. Figures 6.6 and 6.7 show values of alpha squared against energy for the chlorine treated samples both unannealed and annealed, respectively. To see more clearly the effect of the chlorine treatment on the CdTe, graphs of CdTe band gap against chlorine concentration in the CdTe bath were plotted. These are shown in Figures 6.8 and 6.9 for unannealed and annealed samples, respectively. Figure 6.8 shows how the unannealed samples showed an initial decrease in band gap value compared with the untreated sample. This decrease continues up to a chlorine concentration 0.031 ± 0.005 M giving a CdTe band gap value of 1.42 ± 0.02 eV. Values of chlorine treatment higher than 0.031 ± 0.005 M gave higher values of band gap but did not achieve values as high as the non-chlorine treated sample.

Figure 6.9 shows the variation of CdTe band gap against chlorine treatment for the annealed samples. The annealed samples also showed a decrease in band gap following chlorine treatment. In this case the minimum value of band gap of 1.40 ± 0.02 eV was achieved with a chlorine concentration of 0.052 ± 0.005 M. Values of chlorine treatment higher than 0.052 ± 0.005 M gave higher values of band gap, although not as high as the non-chlorine treated case. As stated in Section 6.1.3, it should be noted that the graph showing CdTe band gap against chlorine concentration in the CdTe deposition bath for the annealed samples (Figure 6.9) shows a good correlation with both the efficiency (Figure 6.1) and J_{SC} graphs (Figure 6.2) for the chlorine treated samples. The correlation shows that the minimum for annealed samples on the band gap graph matches up with the maximum in the efficiency and J_{SC} graphs. This is believed to be the first report showing the direct relationship of chlorine treatment inducing a reduction in CdTe band gap and correlating this with device efficiency and J_{SC} values. The annealing of the samples at 410°C obviously has an important part to play in this process as although the unannealed samples do show a minimum in band gap across the range of chlorine treatment, it is not until the samples are annealed that the direct relationship is obtained.

The changes in band gap observed in this study were relatively small with a maximum band gap change of 0.08 eV between the non-chlorine treated sample and the sample having 0.052 M chlorine treatment (both samples were annealed). Considering this small change in terms of a theoretical understanding of solar cells, the maxima of theoretical efficiency against band gap graphs lies in the range 1.4 to 1.5 eV [Farenbruch et al 1983]. This range encompasses all the values measured in this study. This range is around the maxima of the graph, hence, changes in band gap of approximately 0.1 eV would only bring about changes in maximum efficiency of approximately one percent [Loferski 1956].

The changes in efficiency observed during this investigation ranged from 2.53 ± 0.11 % with no chlorine treatment to 6.02 ± 0.11 % with 0.052 M chlorine treatment. Other groups have observed even more dramatic increases in efficiency on chlorine treatment Loginov et al 1996 showed an increase from 3.6 % with no chlorine treatment to 10% with $CdCl_2$/methanol treatment. These large changes in efficiency, with small changes in band gap brought about by chlorine treatment, can not be explained by conventional theoretical considerations. The theoretical conditions are based on ideal devices, when obviously the real devices are not ideal. In addition, theses devices did not have efficiencies approaching the maximum theoretical efficiency so were obviously limited by some mechanism, which the chlorine treatment may be helping to overcome.

It should be noted that theoretical curves of band gap against efficiency represent a compromise between the number of solar photons usefully absorbed by the cell (which increases as the band gap decreases) and the thermally activated forward-bias diode current (which increases as the band gap decreases, thereby decreasing V_{OC}). It is considered that the change in band gap in this study was too small to observe this effect on the chlorine treated CdTe I-V results.

Birkmire et al 1992 reported a decrease in band gap upon $CdCl_2$ of the CdTe film. Although spectra were presented, the change in band gap was not quantified. This group attributed the change in band gap to the formation of a $CdTe_{1-x}S_x$ layer where the CdTe band gap decreases with the addition of sulphur for x less than 0.1. Birkmire et al quoted supporting evidence for this was a reduction in lattice constant for CdTe layer on $CdCl_2$ treatment measured by XRD. This investigation observed no significant difference in lattice constant (as measured by XRD) with chlorine treatment of the samples. The work of Birkmire was further developed by Dhere et al 1997a whose work showed diffusion of sulphur to the CdS/CdTe interface using SIMS measurements. PL measurements gave evidence of a reduced band gap in the interface region arising from alloyed material (the peak shift to lower energies is expected for Te-rich $CdTe_{1-x}S_x$). Toyama et al 1997 used electroreflectance spectroscopy to probe the CdS/CdTe interface. An electroreflectance feature at 1.46 eV was ascribed as being due to a mixed crystal $CdTe_{0.95}S_{0.05}$ layer formed at the CdS/CdTe interface. Previous work on Te-rich $CdTe_{1-x}S_x$ alloys [Ohata et al 1973] indicates that the band gap decreases as x increases from 0 to 0.25.

Ohata expresed the band gap as a quadratic equation of the composition of x as given in equation 7.1,

$$E_g(x) = 1.74x^2 - 1.01x + 1.51 \qquad (7.1)$$

This equation is displayed in graphical form in Figure 7.1.

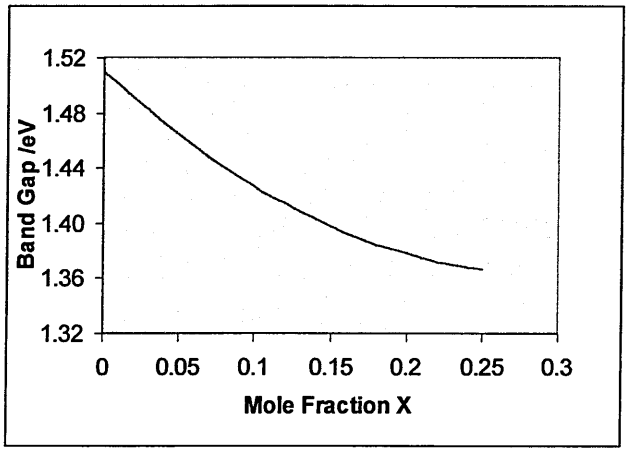

Figure 7.1. Graph Showing Variation of Mole fraction x against Band Gap for $CdTe1_{-x}S_x$

The implication of this for the results in this thesis is that the minimum value of band gap of 1.40 ± 0.02 eV relates to a mole fraction value of 0.145. This suggests that under the optimal conditions of chlorine treatment an interfacial layer of $CdTe_{0.855}S_{0.145}$ is formed. These results are based solely on the optical absorption results and further investigation would be required to confirm the presence of the interfacial layer, for example SIMS or TEM could be used to probe the interface.

7.5.4 Discussion of SEM Results

Section 6.1.4 described the SEM results for three films both unannealed and annealed. The samples were chosen for analysis to show the extremes of chlorine treatment i.e. sample (a) had no intentionally added chlorine. Sample (b) had 0.052 M chlorine in the CdTe deposition bath which gave rise to the highest efficiency devices and sample (c) had 0.137 M chlorine in the CdTe deposition bath. Sample (c) showed a tail off in efficiency compared to sample (b) and was the highest chlorine concentration used in these experiments. Although the samples were chosen to show the extremes of chlorine treatment, using plan view SEM it was not possible to distinguish any significant difference in the three samples either unannealed or annealed. A general comment is that the annealed samples did not seem to show the same number of the large surface particles that are polycrystalline in nature. It is possible the annealing in some way removes the large surface particles or that they are in some way incorporated into the bulk film.

Ringel et al 1991 reported an increase in average grain size for MBE grown films, from approximately 0.25 μm for the as grown and air annealed films without a $CdCl_2$ dip to approximately 1 μm for the $CdCl_2$/annealed films. They attribute this increase to the presence of $CdCl_2$ during the anneal, inducing a sintering mechanism within the CdTe film that acts to decrease inter-grain pore size and increase average grain size. The Sheffield Hallam University films, with a grain size ranging from 0.25 to 1 μm had a larger starting grain size so this may be a reason why the change was not so marked as that noted by Ringel at al.

7.6 Treatment of CdTe with Indium

Valvoda et al 1986 tried to introduce indium and copper as dopants into cathodically deposited CdTe on nickel substrates from an aqueous solution of $CdSO_4$ and TeO_2. Indium doped CdTe produced rectifying gold contacts, indicating n-type conductivity. This work was to investigate the fundamentals of doping the films, both p and n type, rather than an investigation of an optimisation of a specific device.

No reports of the treatment of the CdTe layer in a CdS/CdTe solar cell with indium have been identified. Most reports have concentrated on attempts to enhance the p-type behaviour of the CdTe [Bhattacharya et al 1985, Ondris 1989, and Dennison 1994]. It is considered this is the first investigation to deliberately add indium to the CdTe deposition bath to investigate the affect of the indium on the structural, optical and electrical properties of a CdS/CdTe solar cell.

7.6.1 Discussion of I-V Results

Section 6.2 discussed the treatment of CdTe with $In_2(SO_4)_3$ and Section 6.2.1 covered specifically the solar cell efficiency data and I-V parameters. It is clear from Figure 6.12 that the addition of $In_2(SO_4)_3$ to the CdTe deposition bath significantly degraded the efficiency values for the glass/TCO/CdS/CdTe/metal devices. Comparison of Figure 6.12 with Figure 6.13 shows that this significant degradation was mainly due to decrease in the J_{SC} values for the devices. Table 6.4 shows that the untreated film demonstrated a good value of J_{SC} of 12.9 $\pm$ 0.3 $mAcm^{-2}$, indicating the bath was capable of producing relatively well performing devices. Upon addition of 40 ppb of indium the J_{SC} value fell to 0.06 $\pm$ 0.01 $mAcm^{-2}$. This dramatic reduction in the J_{SC} value with the introduction of small amounts of indium shows the importance of impurity control in the production of these devices.

Figure 6.14 shows the device V_{OC} against indium concentration in the CdTe deposition bath. In contrast to the efficiency and J_{SC} results, the V_{OC} data does not show the same downward relationship on increasing the indium concentration in the CdTe deposition bath. The graph does not show any clear trend, in particular at the point with an indium concentration of 20 ppb and a V_{OC} value of 0.55 ± 0.01 V, which is unexplainably low. The two highest values of indium concentration, 40 and 50 ppb, used in these experiments gave the highest V_{OC} values of 0.63 ± 0.01 V and 0.63 ± 0.01 V, respectively. These values are higher than the initial film with no indium treatment. Therefore, the indium treatment does not have any detrimental affect on the V_{OC} performance of these devices.

Figure 6.15 shows the device fill factor against indium concentration in the CdTe deposition bath. The graph does not show any clear trend, although the three points of highest indium concentration, 30, 40 and 50 ppb, did show significantly lower values of fill factor than the device having no indium treatment. Therefore, the indium treatment could have a detrimental affect of the fill factor performance of the device.

This work showing the overall reduction in efficiency upon the addition of indium, in particular the significant reduction in the J_{SC} value clearly shows indium does not have any beneficial effect on the device performance. The most obvious conclusion to be drawn from these results is that the inclusion of indium introduces n-type behaviour in the CdTe. This behaviour is in conflict with the understood structure of the device, which is n-CdS/p-CdTe.

The consequence of the indium results in terms of the chlorine results is that chlorine appears to be unique in it's ability to produce significant improvement in CdS/CdTe solar cells when introduced into the CdTe. Dennison 1994 showed that the addition of the p-type dopants silver and copper did not improve the device performance and this work shows that the n-type dopant indium does not improve the device performance. Chlorine is an n-type dopant in CdTe and hence in theory induce behaviour similar to that seen with the indium treatment in this work. This indicates that the chlorine may not act as a simple n-type dopant in this case. Ringel et al 1991 performed DLTS on $CdCl_2$ treated CdS/CdTe solar cells which showed a hole trap at $E_V + 0.64$ eV. This defect was tentatively attributed to a $(V_{Cd}Cl)^-$ defect complex resulting from the interaction between cadmium vacancies introduced by the heat treatment and chlorine from the $CdCl_2$. A $(V_{Cd}Cl)^-$ defect complex was also eluded to by Chung et al 1995 where the CdTe film was formed by CSS in an O_2 environment. Further work is required to understand the defect behaviour of chlorine treated CdTe.

7.6.2 Discussion of XRD Results

Figure 6.16 shows the XRD count for the CdTe P_{111} Percentage against the indium concentration in the CdTe deposition bath. It is clear from Figure 6.16 that the addition of indium to the CdTe deposition bath has a detrimental affect on the CdTe P_{111} Percentage. Hence, the addition of indium has a detrimental effect on the improvements in preferred orientation of the CdTe. In addition, it is clear from Figure 6.16 that in general samples with indium addition did not show significantly different CdTe P_{111} Percentage following annealing. This indicates that the indium is inhibiting improvements in preferred orientation upon annealing the sample.

7.6.3 Discussion of Optical Absorption and SEM Results

As described in Section 6.2.3, no significant difference was observed in the band gap of the indium treated samples in both the unannealed and annealed states. This result may have been anticipated when considering the relatively small amounts of indium added to the bath. However the fact that the low concentrations had a significant detrimental effect on the CdTe (111) peak height may have suggested some change would be observed.

In addition Section 6.2.3, described that no significant difference in the grain structure or size was observed in the top down SEM images of CdTe with differing indium treatments. This result is understandable considering that much larger concentrations of chlorine were used in the chlorine treatment experiment than in the indium treatment experiment. The chlorine treatment experiment SEM investigation showed no significant difference in grain structure or size so it is understandable that the small amounts of indium added did not make a discernible difference.

Chapter 8.0: Conclusions and Recommendations For Further Work

8.1 Conclusions

The aim of this study was to understand the properties of glass/TCO/CdS/CdTe/metal solar cells, the CdS and CdTe being grown by aqueous electrodeposition. Deposited films and completed cells were characterised using electrical, structural and optical techniques.

8.1.1 Deposition of CdS

Cyclic voltammetry measurements showed that it was possible to deposit CdS from an aqueous solution over a potential range of -0.4 V to -0.7 V against Ag/AgCl. For the deposition solution used, a potential of -0.60 ± 0.01 V against Ag/AgCl was found to produce an acceptable rate of growth without the formation of dentritic cadmium. XRD measurements of the CdS showed that films deposited at -0.60 ± 0.01 V against Ag/AgCl produced well-formed polycrystalline CdS, with a hexagonal structure. In the light of recent research [Gibson et al 1998] the possibility of the film being of the polytype structure (not purely hexagonal but a mixture of hexagonal and cubic) is discussed.

An experiment was performed to investigate the effect of pH on the deposition CdS. The changes in the CdS were monitored using XRD. It was found that lowering the pH increased the intensity of the CdS peaks indicating that thicker films were being deposited. This can be explained by the increased dispropitiation of thiosulphate ions at reduced pH leading to the formation of CdS. This is due to the small solubility product of CdS and the high cadmium concentration. The ability to control the deposition rate of the CdS by varying the pH of the deposition bath would be useful. Problems occurred as it was observed that the deposition bath pH value reduces spontaneously with time, even when the bath is not being used. This means that growth rates will increase with bath lifetime and the formation of CdS within the deposition bath increases. This is an area for future work as discussed in section 8.3.

8.1.2 Deposition of CdTe

Linear scan voltammetry showed an initial peak centred at -0.10 ± 0.04 V against Ag/AgCl, which is considered to be the onset of elemental tellurium deposition. A plateau region was observed in the voltage range –0.29 to –0.68 V against Ag/AgCl. This is the region of CdTe deposition, although subsequent XRD analysis of films grown at various points along this plateau region showed the films were not necessarily pure CdTe.

XRD analysis showed that a film deposited at -0.21 V against Ag/AgCl consisted of polycrystalline elemental tellurium in the cubic structure, confirming the initial peak at -0.10 ± 0.04 V against Ag/AgCl in the linear voltammetry scan is the onset of tellurium deposition. A film grown at -0.32 V against Ag/AgCl showed reflections arising from both CdTe and tellurium. A film grown at -0.65 V against Ag/AgCl showed reflections arising from well-formed polycrystalline cubic CdTe. This shows that unlike the case of CdS where it is possible to grow well formed CdS over a large potential range with only a small change in deposition current, the deposition potential of CdTe is limited by the formation of elemental tellurium. This work shows the importance of good potential control during the growth of CdTe.

It was determined that the optimum deposition potential for CdTe was at a QRP of –0.690 ± 0.005 V against Ag/AgCl with a deposition current of 0.25 $mAcm^{-2}$ for a period of three hours. The XRD spectrum of a film deposited at this potential showed well-formed polycrystalline CdTe in the cubic structure. Annealing this sample at 410°C for 12 minutes in air brought about significant increases in peak height but did not significantly reduce the FWHM of the peaks.

8.1.3 Formation of Glass/TCO/CdS/CdTe/Metal Solar Cells

Initial results showed that the efficiency of the produced devices improved as films were deposited from the CdTe deposition bath. An experiment was then performed to investigate the effect of pre-conditioning of the CdTe bath on the efficiency of devices. A fresh CdTe bath was prepared from which five CdTe films were deposited and their I-V solar cell performance was measured.

The five films deposited from the new bath showed variation in efficiency, which could be attributed to variations in J_{SC}. The reasons for such large variations in J_{SC} are not completely understood although it may be due to impurity related issues. It was clear that the parameter showing significant improvement with the pre-conditioning of the CdTe bath was the V_{OC} value. This steady increase in V_{OC} was not of sufficient magnitude to over come the dominant effect of the J_{SC} on the overall efficiency graph, but it does show how the V_{OC} value was improved by pre-conditioning the bath. In addition, significant improvement in the fill factor value was observed upon pre-conditioning the bath. It appears that an electropurification process was taking place with each subsequent deposition, giving rise to higher V_{OC} and fill factor values.

8.1.4 Treatment of CdTe with Chlorine

It has been known for some time that treating the CdTe layer of a CdS/CdTe solar cell with chlorine brings about significant improvements in the efficiency of these devices. One advantage of the electrodeposition technique is that the chlorine can be added directly to the deposition bath rather than using the $CdCl_2$/methanol surface treatment employed by groups growing CdTe by other techniques. This report presents results on a systematic variation of the chlorine concentration within a CdTe deposition bath giving results on the electrical, structural and optical characteristics of these films.

Solar simulated I-V measurements of completed devices clearly show that the addition of $CdCl_2$ to the CdTe deposition bath significantly improved the efficiency values for the glass/TCO/CdS/CdTe/metal devices. The electrical parameter most significantly affected by the addition of chlorine is the J_{SC} value. A rapid increase in J_{SC} value up to a chlorine concentration of 0.052 M gave a J_{SC} value of 21.86 $\pm$ 0.35 $mAcm^{-2}$, followed by a slight tail off at higher chlorine concentrations.

In terms of the V_{OC} performance of the device, this investigation showed that there was a trend of improving V_{OC} with increasing chlorine concentration. The Sheffield Hallam University devices did not show any limitations in improvement in V_{OC} with increasing chlorine concentration i.e. the V_{OC} value increased with chlorine concentration across the whole range of chlorine concentrations used in this experiment.

Chlorine appears to be unique in its ability to produce significant improvement in CdS/CdTe solar cells when introduced into the CdTe. Chlorine is an n-type dopant in CdTe and hence in theory induces behaviour similar to that seen with the indium treatment in this work. This indicates that the chlorine may not act as a simple n-type dopant in this case. Further work is required to understand the defect behaviour of chlorine treated CdTe.

XRD results for the $CdCl_2$ treated CdTe samples showed at lower concentrations the chlorine had a beneficial effect on the preferred orientation CdTe samples both in terms of as-grown preferred orientation and also giving an improvement in the annealed sample preferred orientation. At higher concentrations, the chlorine had a detrimental effect on the as-grown preferred orientation compared to the sample with no chlorine treatment. The chlorine also appeared to limit improvements in preferred orientation upon annealing, with samples showing lower values of preferred orientation than unannealed samples. Comparing the XRD results with the I-V results, the general trend is similar indicating a close relationship between chlorine induced improvements in CdTe structural properties and electrical properties.

Optical absorption results for the $CdCl_2$ treated CdTe samples showed a minimum in the band gap vs. chlorine concentration graph. The graph showing CdTe band gap against chlorine concentration in the CdTe deposition bath for the annealed samples showed a good correlation with both the efficiency and J_{SC} graphs for the chlorine treated samples. The correlation showed that the minimum for annealed samples on the band gap graph matches up with the maximum in the efficiency and J_{SC} graphs. The annealing of the samples at 410°C obviously has an important part to play in this process. The unannealed samples do show a minimum value of band gap across the range of chlorine treatment, it is not until the samples are annealed that the direct relationship is obtained.

This relationship was discussed in terms of a theoretical understanding of the effect of varying the band gap of the CdTe on the theoretical efficiency of the cell. It was concluded that these large changes in efficiency, with small changes in band gap brought about by chlorine treatment, could not be explained by conventional theoretical considerations. The theoretical conditions are based on ideal devices, when obviously the real devices are not ideal. In addition, these devices did not have efficiencies approaching the maximum theoretical efficiency so were obviously limited by some mechanism, which the chlorine treatment may be helping to overcome. Considering the formation of an interfacial layer of $CdTe_{1-x}S_x$ at the CdS/CdTe interface the optical absorption results suggest a layer of $CdTe_{0.855}S_{0.145}$ is formed. This conclusion is based solely on optical results and further conformation would be required for example with SIMS or TEM analysis.

8.1.5 Treatment of CdTe with Indium

No reports of the treatment of the CdTe layer in a CdS/CdTe solar cell with indium have been identified. It is considered this is the first investigation to deliberately add indium to the CdTe deposition bath to investigate the effect of the indium on the structural, optical and electrical properties of a CdS/CdTe solar cell.

Solar simulated I-V measurements of completed devices clearly show that the addition of $In_2(SO_4)_3$ to the CdTe deposition bath significantly reduced the efficiency values for the glass/TCO/CdS/CdTe/metal devices. The electrical parameter most significantly affected by the addition of indium is the J_{SC} value. The most obvious conclusion to be drawn from these results is that the inclusion of indium introduces n-type behaviour in the CdTe. The reduction in the J_{SC} value with the introduction of small amounts of indium shows the importance of impurity control in the production of these devices.

In contrast to the efficiency and J_{SC} results, the V_{OC} data does not show the same downward relationship on increasing the indium concentration in the CdTe deposition bath. The graph of V_{OC} against indium concentration does not show any clear trend, with some V_{OC} values being higher and some lower than the film with no indium treatment. Therefore, the indium treatment does not appear to have any significant detrimental affect on the V_{OC} performance of these devices.

The addition of indium to the CdTe deposition bath has a detrimental affect on the CdTe P_{111} Percentage. Hence, the addition of indium also has a detrimental effect on the preffered orientation of the CdTe. In general, samples with indium addition did not show significantly different CdTe P_{111} Percentage following annealing. This indicates that the indium is inhibiting improvements in preffered orientation upon annealing the sample.

8.2 Recommendations for Further Work

An investigation is required into the changing pH of the CdS deposition bath with time. Although the reducing pH acts to increase the deposition rate of the CdS, it also increases the rate of formation of CdS in the CdS deposition bath. This problem limits the practical lifetime of the bath to approximately two days. Bath lifetime will have to be extended beyond the current two-day limit if electrodeposition is to become a viable method of producing CdS for large-scale production of CdS/CdTe solar cell modules.

It is clear that there is some electropurification process taking place when a freshly prepared bath is being used to deposit the initial films. It is important to further understand this process as it could prove useful for the production of high efficiency devices with very low impurity levels. It would be useful to investigate the films, possibly using SIMS, to determine what impurities are being removed in the initial films. This investigation may lead to a better understanding of the impurity effects on these devices and the source of impurities in the deposition baths so these can be reduced if possible prior to any depositions performed. This would enable the bath to be prepared with a minimum of pre-conditioning.

Further investigation of the relationship between the structural, optical and electrical results should be undertaken to further understand the mechanism by which significant improvements in efficiency are obtained by small changes in the CdTe band gap. Current theory is not able to explain this satisfactorily. This discrepancy most likely arises from the non-ideal performance of these devices. It is clear that the addition of chlorine can bring about significant improvements in device efficiency but this study has shown that this improvement is limited at higher chlorine concentrations. The understanding of these limitations could provide useful information to achieve optimal chlorine treatment for these devices.

It was also noted that the direct correlation between the maximum value of efficiency and minimum value of CdTe band gap was obtained following annealing. It would be useful to perform a matrix experiment to determine the best value of chlorine treatment with annealing temperature to obtain the optimum conditions of both chlorine treatment and annealing temperature. This optimisation could lead to further increases in efficiency of the Sheffield Hallam University Devices.

Chlorine in an n-type dopant in CdTe and further understanding is required of how addition of an n-type dopant to the theoretically p-type CdTe layer can bring about such significant improvements in efficiency. The mechanism of the incorporation of the chlorine in the defect structure of the CdTe needs to be fully understood to explain these effects.

Although the treatment of the CdTe layer with indium experiment was repeated several times in each case a significant a reduction in the device efficiency was observed due to significant reductions in the J_{SC} value. It is interesting to note that an improvement in the V_{OC} value was observed. It would be interesting to repeat this experiment using smaller increments of indium addition to observe more accurately any increase in V_{OC} as the J_{SC} decreases. This experiment could provide further understanding of the efficiency loss mechanisms in CdS/ CdTe Solar cells.

Acknowledgements

I wish to thank Sheffield Hallam University for funding this project. I wish to thank the academic and technical staff within the departments of physics and chemistry and the MRI. I wish to acknowledge the director of studies for this project Dr I M Dharmadasa and the additional supervision of Professor C Care and Dr I Wadsworth. In particular I would like to express my appreciation to Mr Kevin Blake for his assistance and technical support with XRD and SEM investigations. Also to Mr Mark Jarrat for assistance with SEM investigation.

I acknowledge Dr Stephen Dennison and Professor Greame Morris for useful discussions concerning this project. Their wealth of experience was invaluable during this project bringing light to where there was sometimes darkness.

I am most grateful for financial assistance during this PhD from the Castle Bolton and Redmire Educational Foundation. Their additional funds were very much appreciated during my studies.

I wish to thank my parents for supporting me financially and for being there for me throughout my studies. Finally I wish to thank Lisa, her love and support has kept me going to the end. She has never faltered in her persuasion and encouragement and for that I can never thank her enough.

References

Abou-Elfotouh F A, Moutinho H R, Hasson F S, Ahrenkiel R K, Levi D, Kazmerski L L, 1993 Proc. 23rd IEEE Photovoltaics Specialits Conference Louisville Kentucky, pp 491-494

Adams W G, Day R E, 1877 Proc. R. Soc. London Ser. A Vol 25, pp 113

Adirovich E I, Yuabov Y M, Yagudaev G R, 1969 Sov. Phys. Semicond. Vol 3 pp 61 or 1971 Phys. Stat. Sol. (A) Vol 6 pp 311

Al-Allak H M, Brinkman A W, Richter H, Bonnet D, 1996 J. Crystal Growth Vol 159, pp 910-915

Albright S P, Ackerman B, Jordan J F, 1990 IEEE Trans. Electron Dev. Vol 37 No 2, pp 434-437

Albright S P, Chamberlin R C, Ackerman B, Jordan J F, 1992 Int. J. Solar Energy Vol 12, pp 109-120

Anthony T C, Fahrenbruch A L, Bube R H, 1992 J. Electronic Mat. Vol 11 No 1, pp 89

Balakrishnan K S, Rastogi A C, 1991 Solar Energy Materials, Vol 23, pp 61-73

Baranski A S, Fawcett W R, McDonald A C, de Nobriga R M, MacDonald J R, 1981 J. Electrochem. Soc.Vol 128 No 5, pp 963-968

Baranski A S, Fawcett W R, 1984 J. Electrochem. Soc.Vol 131 No 11, pp 2509-2514

Barker J, Binns S P, Johnson D R, Marshall R J, Oktik S, Özsan E, Patterson H, Ransome S J, Roberts S, Sadeghi M, Sherbourne, Turner A K, Woodcock J M 1992 Int. J. Solar Energy Vol 12, pp 79-94

Barnett A M, Bragagnolo J A, Hall R B, Phillips J E, Meakin J D, 1978 Proc 13th IEEE Photovoltaic Specialists Conf, pp 419-420

Barret C S, Massalski T B 1980 Structure of Metals, Pergamon, Oxford

Basol B M, Tseng E S, Rod R L, Ou S S, Stafsudd O M, 1982 4th European Solar Energy Conference, pp 719-726

Basol B M, Tseng E S, Rod R L, 1982a 16th IEEE Photovoltaic Specialits Conference,IEEE New York pp 805-808

Basol B M, Tseng E S, Rod R L, 1983 US Patent 4 388 483

Basol B M, 1984 J. Appl. Phys. Vol 55 No 2, pp 601-603

Basol B M, Ou S S, Stafsudd O M, 1985 J. Appl. Phys. Vol 58 No 10, pp 3809-3813

Basol B M, Tseng E S, Lo D S, 1986 US Patent 4 629 820

Basol B M, 1988 Solar Cells Vol 23, pp 69-88

Becquerel E, 1839, C. R.Hebd. Seances Acad. Sci. Vol 9, pp 561

Bhattacharya R N, Rajeshwar K, 1984 J. Electrochem. Soc.Vol 131 No 9, pp 2032-2037

Bhattacharya R N, Rajeshwar K, 1985 J. Appl. Phys. Vol 58 No 9, pp 3590-3593

Bhattacharya R N, Rajeshwar K, Noufi R N,1985a J. Electrochem. Soc.Vol 132, No 3, pp 732-734

Birkmire R W, McCandless B E, Hegedus S S, 1992 Int. J. Solar Energy Vol 12 pp 145-154

Blomfield C J, 1995 PhD Thesis, Sheffield Hallam University

Bonnet D, Rabenhorst H, 1972 Proc. IEEE Photovoltaic Specialists Conf. pp 129-132

Bonnet D, Henrichs B, Richter H, 1992 Int. J. Solar Energy Vol 12, pp 133-136

D. Bonnet, H. Richter and K. Jäger, 1995 Conf. Record, 13th European Photovoltaic Solar Energy Conference, Nice, pp. 1456-1461.

Britt J, Ferekides C, 1993 Appl. Phys. Lett. Vol 62 No 22, pp 2851-2852

Chadi D J, Walter J P, Cohen M L, Petroff Y, Balkanski M, 1972 Phy. Rev. B Vol 5, No 8, pp 3058-3064

Chamberlin R R, Skarman J S, 1966 J. Electrochem. Soc.Vol 113 No 1, pp 86-89

Chapin D M, Fuller C S, Pearson G L 1954, J. Appl. Phys. Vol 25, pp 676

Chu T L, 1988 Solar Cells Vol 23, pp 31-38

Chu T L, Chu S S, Han K D, Mantravadi M, 1988 Proc. 20th IEEE Photovoltaic Specialists Conf. pp 1422-1424

Chu T L, Chu S S, Ang S T, 1988a J. Appl. Phys. Vol 64 No 3, pp 1233-1237

Chu T L, Chu S S, Ferekides C, Britt J, Wu C W, 1990 Proc. 21st IEEE Photovoltaic Specialists Conf. Vol 1, pp 777-781

Chu T L, Chu S S, Ferekides C, Britt J, Wu C Q, 1991 J. Appl. Phys. Vol 69 No 11, pp 7651-7655

Chu T L, Chu S S, 1992 Int. J. Solar Energy Vol 12, pp 121-132

Chu T L, Chu S S, Britt J, Ferekides C, Wang C, Wa C Q, Ullal H S, 1992a IEEE Electron Device Letters Vol 13 No 5, pp 303-304

Chu T L, Chu S S, Ferekides C, Britt J, Wu C Q, 1992b J. Appl. Phys. Vol 71 No 8, pp 3870-3876

Chu T L, Chu S S, 1995 Solid State Electronics Vol 38 No 3, pp 533-549

Chung G Y, Park S C, Cho K, Ahn B T, 1995 J. Appl. Phys. Vol 78, No 9, pp 5493-5498

Cotal H L, Lewandowski A C, Markey B G, McKeever S W S, Cantwell E, Aldridge J, 1990 J. Appl. Phys. Vol 67 No 2, pp 975-982

Cullity B D, 1978 "Elements of X-Ray Diffraction", Addison-Wesley Publishing Company Inc London

Cunningham D W, Skinner D E, NREL Subcontractor Report October 1999, Phase 1 Technical Report, NREL/SR-520-26948

Cuomo J J, Gambino R J, 1968 J. Electrochem. Soc.Vol 115 No 7, pp 755-759

Cusano D A 1963 Solid-State Electron, Vol 6, pp 217-232

Danaher W J, Lyons L E, 1978 Nature Vol 271 pp 139

Danaher W J, Lyons L E, 1984 Aust. J. Chem. Vol 37, pp 689-701

Danaher W J, Lyons L E, Morris G C, 1985 Applications of Surface Science Vol 22/23, pp 1083-1090

Danaher W J, Lyons L E, Marychurch M, Morris G C, 1986 Applied Surface Science Vol 27, pp 338-354

Darjowski A, Cocivera M, 1985 J. Electrochem. Soc.Vol 132 No 11, pp 2768-2771

Darjowski A, Cocivera M, 1987 J. Electrochem. Soc.Vol 134 No1, pp 226-229

Das S R, Cook J G, Rowell N L, Aouadi M S, 1990 J. Appl. Phys. Vol 68 No 11, pp 5796-5803

Das S K, Morris G C, 1992 J. Appl. Phys. Vol 72 No 10, pp 4940-4945

Das S K, Morris G C 1993 Solar Energy Materials and Solar Cells Vol 28, pp 305-316

Das S K, 1993a Thin Solid Films Vol 229, pp 259-264

Dean J A (Ed.), 1973 Handbook of Chemistry, 11th Ed. McGraw-Hill, New York, Section 6, pp 14

DeMattei R C, Elwell D, Feigelson R S, 1978 J. Crystal Growth Vol 43, pp 643

Dennison S, 1993 Electrochimica Acta, Vol 38 No 16, pp 2395-2403

Dennison S, 1994 J. Mater. Chem. Vol 4 No 1, pp 41-46

Dennison S, 1995 J. Mater. Chem. Vol 5 No 11, pp 1885-1892

Dennison S, 1996 Private Communication

De Nobel D, 1959 Philips Res. Rep. Vol 15, pp 361

Dharamadasa I M, Thornton J M, Williams R H, 1989 Appl. Phys. Lett. Vol 54 No 2, pp137-139

Dhere R G, Ramanathan K, Keyes B M, Moutinho H R, 1993 12th NREL Photovoltaic Program Review, Denver Colarado, Eds R Noufi, H S Ullal, AIP New York, pp 335-344

Dhere R G, Rose D, Albin D, Asher M, Al-Jassim M M, Cheong H, Swartzlander A, Moutinho H R, Coutts T, Sheldon P, 1997 Proc. 26th IEEE Photovoltaic Specialists Conf. Anahiem California.

Dodero M, 1934 Compt. Rend. Acad. Sci. Paris Vol 109, pp 556

Dodero M, 1939 Bull. Soc. Chim. France Vol 6, pp 209

Dutta J, Bhattacharya D, Maiti A B, Chaudhuri, Pal A K, 1995 Vacuum Vol 46 No 1, pp 17-21

Eisgruber I L, Sites J R, 1993 12th NREL Photovoltaic Program Review, Denver Colarado, Eds R Noufi, H S Ullal, AIP New York, pp 407-413

Engelken R D, Van Doren T P, 1985 J. Electrochem. Soc.Vol 132 No 12, pp 2904-2909

Engelken R D, Van Doren T P, 1985 J. Electrochem. Soc.Vol 132 No 12, pp 2910-2919

Engelken R D, 1987 J. Electrochem. Soc.Vol 134 No 4, pp 832-836

Engelken R D, 1988 J. Electrochem. Soc.Vol 135 No 4, pp 834-839

Fabre M, 1888 Ann. Chim. Phys. Vol 14, pp110

Farenbruch A L, Vasilchenko V, Buch F, Mitchell K, Bube R H 1974 Appl. Phys. Lett., Vol 25, No 10, pp 605-608

Farenbruch A L, Buch F, Mitchell K, Bube R H 1975 11th IEEE Photovoltaics Specialists Conf. Scots Dale Arizona, pp 490-496

Farenbruch A L, Bube R H, 1983 Fundamentals of Solar Cells, Academic Press, London

Fatas E, Duo R, Herrasti P, Arjona F, Garcia-Camarero E, 1984 J. Electrochem. Soc.Vol 131 No 10, pp 2243-2246

Figueroa J M, Sánchez-Sinencio F, Mendoza-Alvarez J G, Zeleya O, Vázquez-López C, Helman J S, 1986 J. Appl. Phys. Vol 60 No 1, pp 452-454

Foerster F, Umbach H, 1934 Z. Anorg. Allg. Chem. Vol 217, pp 175

Frerichs R, 1947 Phys. Rev. Vol 72, pp 594

Fulop G F, Betz J F, Meyers P V, Doty M E, 1981 US Patent 4 260 427

Fulop G, Doty M E, Meyers P, Betz J F, Liu C H 1982 Appl. Phys. Lett. Vol 40, No 4, pp 327- 328

Fulop G F, Taylor R M, 1985 Ann. Rev. Mater. Sci. Vol 15, pp197-210

Gessert T A, Coutts T J, 1993 12th NREL Photovoltaic Program Review, Denver Colarado, Eds R Noufi, H S Ullal, AIP New York, pp 345-353

Gibson P N, Őzsan M E, Sherbourne J M, Lincot D, Cowache P, 1998 Proc. 2nd World Conference on Photovoltaic Energy Conversion pp1089-1092

Grovener C R M, 1989, "Microelectronic Materials", Adam Hilger, Bristol and Philadelphia, p436

Hodes G, Manassen J, Cahen C, 1976 Nature Vol 261, pp 403-404

Hodes G,1995 in Physical Electrochemistry : Principles, Methods and Applications Ed by Rubenstien I, Marcel Dekker Inc. New York, pp 515-555

Ikegami S, 1988 Solar Cells Vol 23, pp 89-105

Ives D J G,Janz G J, 1961 "Reference Electrodes, Theory and Practice" Academic Press New York and London

Jackowska K, Skompska M, 1986 Polish J. Chem. Vol 60, pp 551-560

Jenny D A, Loferski J J, Rapparort P, 1956, Phys. Rev. Vol 101, pp 1208

Johnson S X, 1993 12th NREL Photovoltaic Program Review, Denver Colarado, Eds R Noufi, H S Ullal, AIP New York, pp 227-245

Jordan J F, Albright S P, 1988 Solar Cells Vol 23, pp 107-113

Kampmann A, Cowache P, Mokili B, Lincot D, Vedel J, 1995 J. Crystal Growth Vol 146, pp 256-261

Kim D S, Kim S Y, Ahn H B 1994 Journal of Materials Science: Materials in Electronics Vol 5 No 1, pp 17-21

Kröger F A, 1964 The Chemistry of Imperfect Crystals, North Holland, Amsterdam

Kröger F A, 1978 J. Electrochem. Soc.Vol 125, No 12, pp 2028-2034

Lee J H, Lee H Y, Park Y K, Shin S H, Park K J, 1998 Jpn. J. Appl. Phys. Vol 37, pp 3357-3362

Lincot D, Kampmann A, Mokili B, Vedel J, Cortes R, Fromet M, 1995 Appl. Phys. Lett. Vol 67 No 16, pp 2355-2357

Loferski J J, 1956 J. Appl. Phys. Vol 27, No 7, pp 777-784

Loginov Y Y, Durose K, Al-Allak, Galloway S A, Oktik S, Brinkman A W, Richter H, Bonnet D, 1996 J. Crystal Growth Vol 161, pp 159-163

Lokhande C D, Pawar S H, 1989 Phys. Stat. Sol. Vol 111, pp 17-40

Lyons L E, Morris G C, Horton D H, Keyes JG, 1984 J. Electroanal.Chem. Vol 168, pp 101-116

Lyons L E, Morris G C, Tandon R K, 1989 Solar Energy Materials, Vol 18, pp 315-331

Ma Y Y, Fahrenbruch A L, Bube R H, 1977 J. Electrochem. Soc.Vol 124 No 9, pp 1430-1435

Ma Y Y, Fahrenbruch A L, Bube R H, 1977a Appl. Phys. Lett. Vol 30, pp 423-424

Matsumoto H, Kuribayashi K, Uda H, Komatsu Y, Nakano A, Ikegami S, 1984 Solar Cells Vol 11, pp 367-373

Mc Candles B E, Birkmire R W, 1991 Solar Cells Vol 31, pp 527-535

McCann J F, Skyllas Kazacos M, 1981 J.Electroanal. Chem. Vol 119, pp 409-412

Meyers P V, 1986 7th Commision of the European Communities Conf. on Photovoltaic Solar Energy (Riedel Dordrecht), pp 1211-1213

Meyers P V, 1988 Solar Cells Vol 23, pp 59-67

Meyers P V, 1988a Solar Cells Vol 24, pp 35-42

Meyers P V, 1989 Solar Cells Vol 27, pp 91-98

Meyers P V, Zhou T, Powell R C, Reiter N, 1993 Proc. 23rd IEEE Photovoltaics Specialists Conference, Louisville Kentucky, pp 400-404

Meyers P V, Sandwisch D W, 1993a 12th NREL Photovoltaic Program Review, Denver Colarado, Eds R Noufi, H S Ullal, AIP New York, pp 265 - 271

Miller B, Heller A, 1976 Nature Vol 262, pp 680-681

Mitchel K W, Farenbruch A L, Bube R H, 1977 J. Appl. Phys. Vol 48 No 2, pp 829-830

Mitchel K W, Farenbruch A L, Bube R H, 1977a J. Appl. Phys. Vol 48 No 10, pp 4365-4371

Monnier R, Bakarat D, 1957 Helv. Chim. Acta Vol 40, pp 204

Monnier R, Giacometti J C, 1964 Helv. Chim. Acta Vol 47, pp 345

Morris G C, Tanner R G, Tottszer A, 1990 Proc. 21st IEEE Photovoltaic Specialists Conf. pp 575-580

Morris G C, Tottszer A, Das S K, 1991 Materials Forum Vol 15, pp 164-170

Morris G C, Das S K, 1992 Int. J. Solar Energy Vol 12, pp 95-108

Morris G C, Vanderveen R J, 1992a Solar Energy Materials and Solar Cells Vol 27, pp 305-319

Morris G C, Vanderveen R J, 1993 Solar Energy Materials and Solar Cells Vol 30, pp 339-351

Morris G C, Vanderveen R J, 1996 Applied Surface Science Vol 92, pp 630-634

Moutinho H R, Al-Jassim M M, Abulfoltuh F A, Dippo P C, Dhere R G, Kazmerski L L,1997 Proc. 26th IEEE Photovoltaic Specialists Conf. Anahiem California.

Moutinho H R, Al-Jassim M M, Levi D H, Dippo P C, Kazmerski L L, 1998 J. Vac. Sci. Technol. A Vol 16 No 3 pp 1251-1257

Nakayama N, Matsumoto H, Yamaguchi K, Ikegami S, Hioki Y, 1976 Jpn. J. Appl. Phys. Vol 15 No 11 pp 2281-2282

National Science Foundation 1975, Proc. Photovoltaic conversion of solar energy for terrestrial applications, Report NSF-RANN74-013, Cherry Hill, NJ, Vols I and II, Washington, DC, NSF-RANN

Nebergall W H, Schmidt F C, Holtzclaw H F, 1963 General Chemistry, DC Heath and Company, pp 358

Niles D W, Rioux D, Höchst H, 1993 J. Appl. Phys. Vol 73 No 9 pp 4586-4590

Nolan J F, 1993 Proc. 23rd IEEE Photovoltaics Specialits Conference Louisville Kentucky pp 34-41

Ohata K, Saraie J, Tanaka T, Japan J. Appl. Phys 1973 Vol 12 No 10 pp1641-1642

Ondris M, Pichler M A, Brownfield R E, 1989 US Patent 4 816 120

Ortega-Borges R, Lincot D, 1993 J. Electrochem Soc. Vol 140, pp 3464-3473

Panicker M P R, Knaster M, Kröger F A, 1978 J. Electrochem. Soc.Vol 125 No 4, pp 566-572

Park J W, Ahn B T, Im H B, Kim C S, 1992 J.Electrochem. Soc. Vol 139 No 11, pp 3351-3356

Peter L, 1978 Electrochim. Acta Vol 23, pp165-174

Pourbaix M, 1963 Atlas d'Equilibres Electrochimiques, Gauthiers-Villars et Cle

Power G P, Peggs D R, Parker A J, 1981 J. Electrochemica Acta, 1981 Vol 26 No 5, pp 681-682

Rajeshwar K, 1992 Advanced Materials Vol 4 No 1, pp 23-29

Ramanathan K, Dhere R G, Coutts T J, Chu T L, Chu S, 1993 Proc. 23rd IEEE Photovoltaics Specialits Conference Louisville Kentucky, pp 466-468

Rappaport P, RCA Rev. 1959 Vol 20, pp 373

Reynolds D C, Leies G, Antes L L Marburger R E, 1954, Phys. Rev. Vol 96, pp 533

Ringel S A, Smith A W, MacDoughal M H, Rohatgi A, 1991 J. Appl. Phys. Vol 70 No 2, pp 881-889

Rohatgi A, Ringel S A, Sudharasan R, Meyers P V, Liu C H, Ramanathan V, 1989 Solar Cells Vol 27, pp 219-230

Rohatgi A, 1992 Int. J. Solar Energy Vol 12, pp 37-49

Saraby-Reintjes A, Peter LM, Özsan ME, Dennison S, Webster S, 1993 J.Electrochem. Soc. Vol 140 No 10, pp 2880-2888

Sasala R A, Liu X X, Sites J R, 1992 Int. J. Solar Energy Vol 12, pp 17-24

Schmidt M, 1957 Z. Anorg. Allg. Chem. Vol 289, pp 147

Sella C, Boncorps P, Vedel J, 1986 J.Electrochem. Soc. Vol 133 No 10, pp 2043-2047

Seol Y S, Im H B, 1989 9th European Photovoltaic Solar Energy Conference (Frieberg, Germany, November 25-29 1989), pp 294-297

Shafarman W N, Birkmire R W, Fardig D A, Mc Candless B E, Mondal A, Phillips J E, Varrin R D, 1991 Solar Cells Vol 30, pp 61-67

Shkedi Z, Rod R L, 1980 Proc.14th IEEE Photovoltaic Specialists Conf. IEEE New York pp 472-475

Sites J R, 1988 Proc. 21st IEEE Photovoltaic Specialists Conf. Las Vegas, IEEE New York pp 1604-1607

Skarp J, Anttila E, Rautiainen A, Suntola T, 1992 Int. J. Solar Energy Vol 12, pp 137-142

Smith W, 1873, Nature, Vol 7, pp 303

So S M, Hwang W, Meyers P V, Liu C H, 1984 J. Appl. Phys. Vol 55 No 1, pp 253-261

St. Claire De Ville, 1854, Compt. Rend. Acad. Sci. Paris Vol 39, pp 323

Strauss A J, 1977 Revue De Physique Aplliquée Vol 12, pp 167-184

Sudharsanan R, Rohatgi A, 1991 Solar Cells Vol 31, pp 143-150

Sunyama N, Arita T, Nishiyama Y, Ueno N, Kitamura S, Murozono M, 1990 Proc. 21st IEEE Photovoltaic Specialists Conf. pp 498-503

Sunyama N, Arita T, Nishiyama Y, Ueno N, Kitamura S, Murozono M, 1990a Optoelectronics - Devices and Technologies Vol 5 No 2, pp 259-274

Sze S M, 1985, "Semiconductor Devices. Physics and Technology", John Wiley & Sons New York, pp 291

Takahashi M, Uosaki K, Kita H, 1984 J. Electrochem. Soc. Vol 131 No10, pp 2304-2307

Takahashi M, Uosaki K, Kita H, 1984a J. Appl. Phys. Vol 55 No 10, pp 3879-3881

Takamoto T, Agui T, Kurita H, Ohmori M, 1997 Solar Energy Materials and Solar Cells Vol 49 pp 219-225

Talasek R T, Ohlson M J, Syllaios A J, 1986 J. Electrochem. Soc. Vol 133 No 1, pp 230- 232

Touskova J, Kindle D, Kovanda J, 1992 Thin Solid Films Vol 214, pp 92-98

Toyama T, Yamamoto T, Okamoto, 1997 Solar Energy Materials and Solar Cells Vol 49 pp 213-218

Tyan Y S, 1982 US Patent 4 207 119

Tyan Y S, Perez-Albuerne E A, 1982 Proc. 16 th IEEE Photovoltaic Specialis Conf. San Diego, IEEE New York, pp 794-800

Qi B, Kim D, Williamson D L, Trefny J U, 1996 J. Electrochem. Soc. Vol 143 No 2, pp 517-523

Uda H, Matsumoto H, Komatsu Y, Nakano A, Ikegami S, 1982 Proc. 16 th IEEE Photovoltaic Specialists Conf. IEEE New York, pp 801

Ullik F, 1865, Ber. Akad. Wien. Vol 52, pp 1115

U.S. Department of Energy, 1987, National Photovoltaics Program 5 year research plan 1987-1991 DOE/CH 10095-7 NTIS, U.S. Department of Commerce

U.S. Department of Energy, 1989, Photovoltaic Energy program summary Vol 1 overview 1988 DOE/CH 10093-40 NTIS, U.S. Department of Commerce.

Valvoda V, Touskova J, Kindle D, 1986 Crystal Research and Technology Vol 21 No 8, pp 975-981

Von Windheim J, Renaud I, Cocivera M, 1990 J. Appl. Phys. Vol 67 No 9, pp 4167-4172

Wald F V, 1977 Revue De Physique Aplliquée Vol 12, pp 277-290

Werthen J G, Farenbruch A L, Bube R H, Zesch J C,1983 J. Appl. Phys. Vol 54 No 5, pp 2750-2756

Woodcock J M, Turner A K, Özsan M E, Summers J G, 1991 Proc. 22nd IEEE Photovoltaic Specialists Conf. pp 842-847

Woodcock J M, Özsan M E, Turner A K, Cunningham D, Johnson D, Marshall R, Mason N, Oktik S, Patterson M H, Ransome S, Roberts S, Sadeghi M, Sherbourne J, Sivapathasundaram, Walls I A, 1994 12th European Photovoltaic Solar Energy Conference 1994 pp 948-950.

Yamaguchi K, Nakayama N, Matsumoto H, Hioki Y, Ikegami S, 1975 Jpn. J. Appl. Phys. Vol 14 No 9, pp 1397-1398

Yamaguchi K, Matsumoto H, Nakayama N, Ikegami S, 1976 Jpn. J. Appl. Phys. Vol 15, pp 1575-1576

Yamaguchi K, Nakayama N, Matsumoto H, Ikegami S, 1977 Jpn. J. Appl. Phys. Vol 16 No 7, pp 1203-1211

Yoshida T, 1992 J. Electrochem. Soc. Vol 139 No 8, pp 2353-2357

Zanio K, 1978, Semiconductors and Semimetals, Volume 13, "Cadmium Telluride" Willardson R K, Beer A C, eds., Academic Press Inc London.

Zweibel K, Ullal S, Von Roedern B G, Noufi R, Coutts T J, Al-Jassim M M, 1993 Proc. 23rd IEEE Photovoltaics Specialits Conference Louisville Kentucky pp, 379-388

Appendix

Published Refereed Papers Relating To This Work

"Growth of CdS and CdTe by Electrochemical Techniques For Utilisation in Thin Film Solar Cells", S M Mc Gregor, I M Dharmadasa, I Wadsworth, C M Care, Optical Materials 6 (1996) 75-81

"Glow discharge optical emission spectroscopy; A new technique for characterisation of thin film solar cells" I M Dharmadasa, S M McGregor, M Ives, K Premaratne, S N Akurantillake, C. Vithana and O Ileperuma. Proc. of the workshop on "Low cost electronic materials and solar cells", Colombo, Sri Lanka, 5-6 March 1997.

"Comparison of CdS Thin Films Prepared By Different Techniques For Apllication In Solar Cells As A Window Material", O A Ileperuma, C Vithana, K Premaratne, S N Akuranthilaka, S M Mc Gregor, I M Dharmadasa, Journal of Materials Science: Materials In Electronics 9 (1998) 367-372

Other Published Refereed Papers

"Photoemission study of the formation of intimate In-InGaAs (100) contacts at room and cryogenic temperatures", D S Cammack, S M McGregor, J J McChesney, I M Dharmadasa, S A Clark, P R Dunstan, S R Burgess, S P Wilks and M Elliott. J. Appl. Phys. 81 (12), 1997, pp7876-7879

Papers in Preparation

"Photovoltaic Devices Based on Electrodeposited CdS and CdTe Thin Films", I M Dharmadasa, S M Mc Gregor

"The Effect of Chlorine Treatment on CdS/CdTe Solar Cells", S M Mc Gregor, I M Dharmadasa